Fall 12-2013

Hydrochemical Investigation of a Transient Parafluvial Zone Under Drought Conditions, Platte River, Nebraska

Audrey R. Boerner
University of Nebraska-Lincoln, aboerner@huskers.unl.edu

HYDROCHEMICAL INVESTIGATION OF A TRANSIENT PARAFLUVIAL ZONE UNDER DROUGHT CONDITIONS, PLATTE RIVER, NEBRASKA

by

Audrey R. Boerner

A THESIS

Presented to the Faculty of

The Graduate College at the University of Nebraska

In Partial Fulfillment of Requirements

For the Degree of Master of Science

Major: Earth and Atmospheric Sciences

Under the Supervision of Professor John B. Gates

Lincoln, Nebraska

December, 2013

HYDROCHEMICAL INVESTIGATION OF A TRANSIENT PARAFLUVIAL ZONE UNDER DROUGHT CONDITIONS, PLATTE RIVER, NEBRASKA

Audrey R. Boerner, M.S.

University of Nebraska, 2013

Adviser: John B. Gates

Shallow groundwater (0.5 m -1.2 m deep) beneath a vegetated and non-vegetated fluvial island was observed in the lower Platte River, Nebraska, USA during exceptional summer drought. Over the course of three months, sub-hourly measurements of hydraulic head, and weekly measurements of redox indicators, $\delta^{2}H$, $\delta^{18}O$, and dissolved gases were analyzed together with nitrogen and carbon species from an array of shallow piezometers in the river bed and islands. These data were compared with the same parameters collected from a 15 m-deep riparian borehole.

Vertical hydraulic gradients in the island piezometers indicated the vertical component to groundwater flow was downward over the observation period. Despite high nitrate concentrations in regional groundwater, shallow groundwater and river water contained very low nitrate. Sediment microcosm lab experiments indicated that the island sediment denitrification potential was high, but that carbon-limitation likely limited denitrification within the islands. Redox indicators and dissolved gas data suggest that denitrification of regional groundwater occurred outside of the shallow groundwater monitoring zone.

Shallow groundwater also exhibited a positive correlation between water temperature and alkalinity. Analysis of conservative ions, stable isotopes, and carbonate mineral saturation indices indicate that the alkalinity increase is most likely attributed to soil PCO_2 over the observation

period. Thermodynamic equilibrium modeling indicated that shallow groundwater was supersaturated with respect to carbonate minerals and in equilibrium with soil PCO_2 of $10^{-2.9}$ atm to $10^{-1.7}$ atm throughout the study period.

The results suggest that the spring/summer seasonal transition and drought impacted shallow groundwater nitrogen and carbon chemistry: Low-flow conditions in the river decreased delivery of dissolved organic carbon to streambed and island pore water, reducing the denitrification potential. It is also plausible that low-flow conditions in the river facilitated upgradient denitrification by increasing groundwater residence times. Additionally, soil respiration likely increased as a result of increasing air temperatures and the drought-induced water table decline. This increase of soil CO_2 led to increased mineral dissolution and dissociation of carbonic acid, evident from the carbonate saturation and temporal trends in alkalinity, Ca^{2+}, and Mg^{2+}.

ACKNOWLEDGMENTS

This material is based upon work supported by the National Science Foundation Graduate Research Fellowship under Grant No. 25-0514-0142-001. This research was supported by additional grants from the Geological Society of America, University of Nebraska (UNL) Department of Earth and Atmospheric Sciences, UNL Office of Graduate Studies, UNL Layman Fund, Nebraska Geological Society, American Association of Petroleum Geologists, and Phi Kappa Phi honor society.

I owe great thanks to Duane Woodward of Central Platte Natural Resources District, and Dr. Hong Chen of UNL for their early assistance in experimental design and study site selection. I am also thankful to the Mary Lanning Hospital Trust, Crane Trust, and Kevin Kauffman for allowing unrestricted access to the field site. This project would not have been possible with volunteers who helped with the field work, often in extreme temperatures: Zablon Adane, Leilani Arthurs, Lindsey Bobak, Justin Gibson, Nathan Rossman, and JP Traylor. I am also thankful to Matt Marxson, UNL Conservation and Survey Division, for drilling and logistical assistance, as well as Dr. Mary Harner and Mark Morten, both of Crane Trust, for their support of this work and field assistance.

Dan Miller and Ryan McGhee of the UNL USDA Agricultural Research Service Lab and Aaron Schultis of the UNL Water Sciences Lab provided invaluable insight regarding sample collection, analysis, and data interpretation. I am also appreciative of their time in the lab analyzing samples for this work. Bryan Miller also provided technical support

I am grateful for the support and patience of my committee members, Dr. Daniel Snow and Dr. Vitaly Zlotnik, as well as my advisor, Dr. John Gates. Their interest in this project translated to no shortage of ideas on how to improve and deepen the scope and meaning of this

work, which challenged me as a student and scientist. I am especially thankful for the opportunity to work with Dr. Gates, who provided the initial framework for this project and continued optimism despite technical hiccups along the way.

Dr. Kent Syverson and Dr. Katherine Grote, both of University of Wisconsin-Eau Claire, originally piqued my interested in geology, encouraged me to apply to graduate school, and offered sound guidance throughout the application process. Without their encouragement, I would not have had this opportunity.

Finally, I am thankful for the constant support, love, and encouragement of my husband Zach. I am also grateful for the support, inspiration, and example from my parents Ron and Penny. My family is a continual reminder to have faith and persevere.

TABLE OF CONTENTS

TABLE OF FIGURES

TABLE OF TABLES

LIST OF PARAMETERS AND ABBREVIATIONS

Parameter/abbreviation	Description
a	Represents relationship between thermal properties and groundwater velocity
A_{z0}	Amplitude of surface temperature oscillation
A_z	Amplitude of temperature fluctuation about the mean at depth z
ANCOVA	Analysis of covariance
C	Measured tritium in sample
Co	Tritium input function (concentration prior to radioactive decay)
c_0	Heat capacity of water
$c\rho$	Volumetric heat capacity of aquifer materials
DIC	Dissolved inorganic carbon
DNP	Denitrification potential
GND	Groundwater monitoring well
HZ	Hyporheic zone
IAP	Ion activity product
k	Aquifer thermal conductivity
K_{a1}	Thermodynamic dissociation constant for carbonic acid
K_{CO2}	Henry's Law coefficient for CO_2
K_{sp}	Solubility constant
LMWL	Local meteoric water line
NPP	Net primary productivity
OM	Organic matter
ORP	Oxidation-reduction potential
ρ_0	Density of water
PCO_2	Partial pressure of CO_2
$pPCO_2$	Negative logarithm of the partial pressure of CO_2
q	Fluid flux
R_{sample}	Ratio of Ar/N_2 or $^{15}N/^{14}N$ in the sample
$R_{standard}$	Ratio of Ar/N_2 or $^{15}N/^{14}N$ in air
SI	Saturation index
τ	Period of surface temperature oscillation
T_m	Mean surface water temperature
T_z	Ground water temperature at depth z
$T_{1/2}$	Half life
TDS	Total dissolved solids
TU	Tritium units
VHG	Vertical hydraulic gradient
VSMOW	Vienna Standard Mean Ocean Water

PREFACE

Awareness of regional and global water scarcity has increased as excessive groundwater pumping, in many circumstances, has depleted surface and groundwater reservoirs. Furthermore, agriculture, industry, and urbanization, through point- and non-point source pollution, have led to drinking water degradation, amplifying the difficulty for some to access clean water. Through the lens of climate change, these underlying water quality and quantity issues are exacerbated by a forecasted increase in global temperatures and regional decreases in groundwater recharge.

This study investigates water quality and quantity changes during the confluence of seasonal transition and historic drought in the lower Platte River, Nebraska, USA. This location serves as a microcosm of the water issues being faced on a global scale: non-point source agricultural pollution has affected groundwater quality, while increased demand for high crop yields has led to over-pumping of irrigation wells and river diversions to canals. These uses commonly draw down the water table such that the river channel seasonally becomes dry.

An extensive amount of research has been conducted in the Platte River basin regarding water quality degradation, groundwater age, geomorphology, and sedimentary characteristics of the river bed and alluvial aquifer. One of the most prominent features of the river is its anastomosing and braided nature. However, the hydrochemical functioning of these features remains largely unexplored. This hydrochemical investigation focuses on pore water chemistry of parafluvial zone (the portion of the river channel which is dry during low-flow conditions) islands and hydrogeologic response to seasonal changes, as well as the impact of exceptional drought during summer 2012. The results of this investigation are organized into three chapters respectively focusing on hydrogeologic response to seasonal transition in a flow regime exacerbated by the drought; nitrogen-cycling hydrochemistry and potential for denitrification in the island sediments; and inorganic carbon cycling in response to elevated summer temperatures and drought-induced water table decline. Each chapter specifically accomplishes the following:

Chapter 1:

- Analyzes “losing” nature of the Platte River using water table decline and vertical hydraulic gradient data
- Quantifies water table decline beneath the river bed and river bed seepage rates
- Estimates vertical component to groundwater flow using a modified groundwater temperature-tracer method
- Constrains absolute groundwater age in the study reach using the tritium decay method

Chapter 2:

- Discusses denitrification systematics in context of hyporheic zones and in comparison with aquifers
- Presents evidence for groundwater denitrification prior to discharge to river through dissolved gas and N-isotope concentrations, as well as redox indicators
- Quantifies denitrification potential of fluvial island sediments under lab conditions

Chapter 3:

- Discusses relevance of carbon cycle to groundwater chemistry and global carbon budget
- Analyzes theoretical relationship between ambient air temperature and groundwater carbon cycling
- Quantifies thermodynamic equilibrium between soil gas and groundwater alkalinity
- Argues that increasing seasonal temperatures increased groundwater PCO_2, and discusses likely mechanisms for the observed increase.

Chapter 1

Streambed Groundwater Seepage Rates and Water Table Dynamics

1.0 INTRODUCTION

The goal of the physical hydrogeological investigation presented in this chapter is to gain a conceptual understanding of surface and subsurface flow regimes in the study reach during summer 2012. Two methods—piezometry and seepage meter—were used to directly measure water table fluctuations and quantify groundwater flux through the streambed, respectively. Modeling of groundwater seepage based on a vertical groundwater temperature profile also added to the conceptual model of the magnitude and direction of flow in the riparian zone. Finally, groundwater age dates using tritium (^3H) as a groundwater tracer constrain absolute groundwater ages and the uppermost rate of downward groundwater flow. These tools inform the conceptual model of groundwater flow throughout the May to August 2012 study period, as well as the impact of a severe to exceptional regional drought on the groundwater levels in the study area. This conceptual understanding is called on in subsequent chapters to interpret hydrochemical data collected at the same location, as well as determine the potential for interactions between groundwater and surface water that may impact shallow groundwater chemistry.

1.1 Geomorphology and Physical Hydrology

This study took place within the Platte River basin of central Nebraska, USA. The Platte River carries the combined flow of the North and South Platte rivers from the eastern Rocky

Mountains prior to discharging into the Missouri River (Fig. 1). Downstream of the North and South Platte confluence, tributaries from the Nebraska Sandhills and agricultural regions drain into the Platte. The entire Platte basin is approximately 222,740 km^2 (Eschner et al., 1983).

The Platte River is a well-known example of a braided river system, though the 556 km length also includes significant anastomosing and meandering reaches. Braided streams generally represent unstable channel conditions in which the channel bottom is under active construction (Piégay et al., 2006) and the river planform can be subject to significant morphologic change during high-flow regimes (Lane, 1995; Eaton et al., 2010). A braided river pattern develops under high sediment load and high streambed slope conditions, in which the river carrying capacity does not match the volume of sediment load (Leopold and Wolman, 1957; Piégay et al., 2006). Braided features develop by the initial deposition of a submerged, central bar during high flow. As more sediment is deposited, stream velocity in the middle of the channel declines, further lowering the stream carrying capacity and increasing sediment load on the bar. Once the bar breaks the water surface, the channel is forced to bifurcate and flow around it. The diverted channels will be successively divided in the same manner (Leopold and Wolman, 1957). This model of active construction and the unstable nature of the channel bed can lead to co-existing stable, vegetated islands and younger, actively-expanding barren gravel bars within a single channel (Piégay et al., 2006).

Braided streams are sensitive to changes in channel width, sediment influx, flood regime, and slope (Leopold and Wolman, 1957; Piégay et al., 2006). Alterations to any of these factors may be natural or occur as a result of anthropogenic influence on the river channel. In example, sediment load increases from poor land management has been shown to increase braiding intensity in some rivers (Piégay et al., 2006). Conversely, dam construction along a river reach can decrease sediment load and reduce the relative braiding intensity. In this case, where there is a sediment deficit given the stream carrying capacity, a braided stream may stabilize into one or

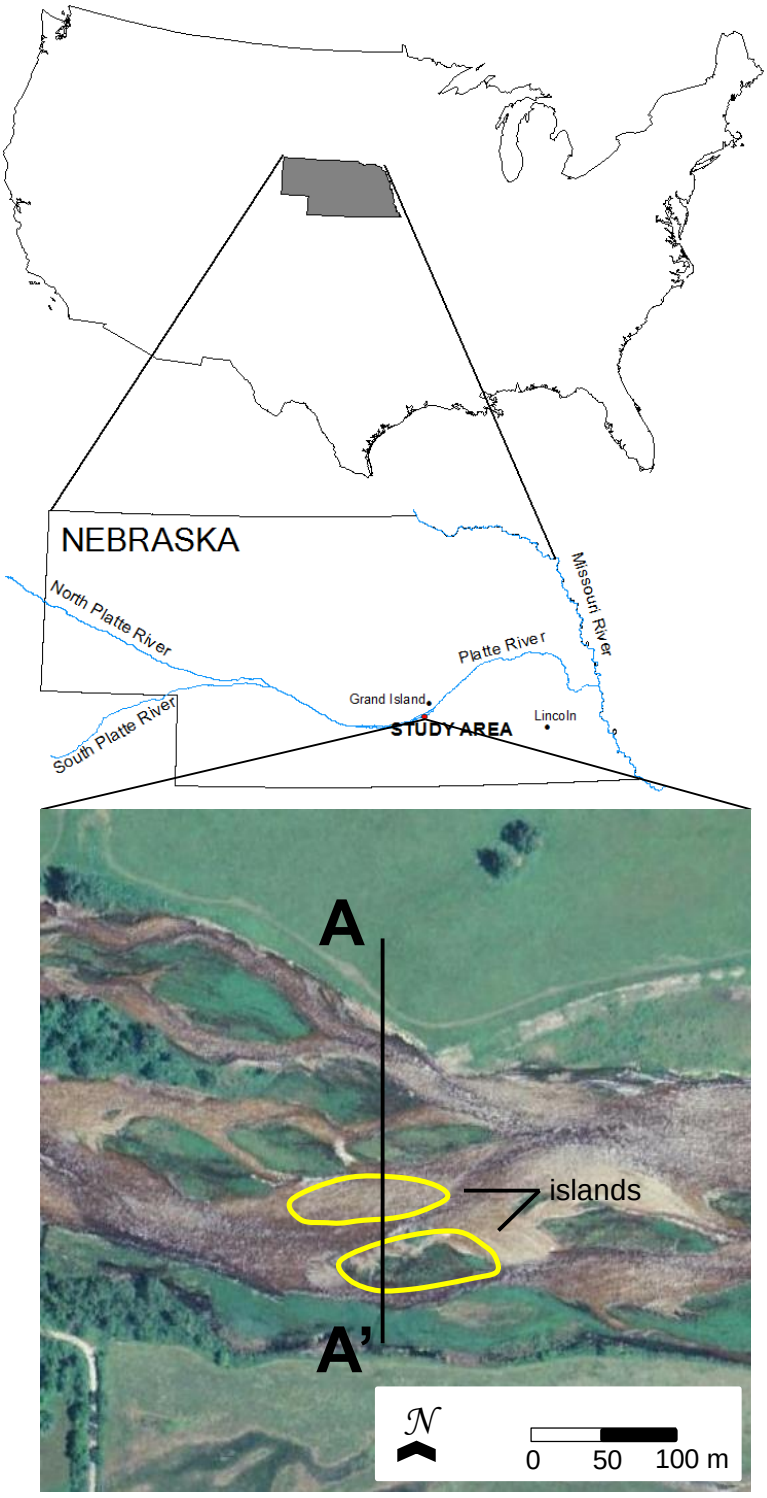

Figure 1. Study location on the central Platte River, Nebraska, USA. Two piezometer nests were installed on a vegetated and non-vegetated island. Only the south channel is shown; the north bank of the north channel is approximately 3200 m to the north. The cross-section line correlates to Fig. 3. Image source: Google Earth: USDA Farm Service Agency, 12/31/2009.

two channels, subsequently leading to vegetation colonization, bank stabilization, and valley incision (Eaton et al., 2010). The latter case describes the changes occurring in the central Platte River (Eschner et al., 1983). Decreased maximum flows and sediment load in the central Platte River have led to the development of an anastomosing channel pattern throughout much of the valley, in which flows are diverted between two or three individual channel threads that rejoin downstream (Fotherby, 2009). However, in many of the individual channel threads the sediment load and bed slope are sufficient to support a braided pattern, evidenced by vegetated and non-vegetated islands and bars within the channels (Smith, 1971). The islands and bars vary greatly in size, ranging from 7 m to 405 m long and 3 m to 91 m wide (Horn et al., 2012). Stable, vegetated islands are a ubiquitous feature of Platte River geomorphology, noted as early as the 19th century by pioneers who traveled in the Platte Valley (Eschner et al., 1983).

The bankfull width of the river is highly variable between the confluence of the North and South Platte Rivers, and the Platte River mouth at the Missouri River. Historically, the Platte River channel width has exceeded 1000 m in south-central Nebraska. Presently, the river channel rarely exceeds 300 m in width (Eschner, 1983). The river is also characteristically shallow (< 1m), with banks and high flows of only a few meters (Williams, 1978). Dense vegetation is present along the banks of the river, ranging from scrub brush to willows and cottonwoods. Trees and dense brush are also present on many of the islands within the channels. The surrounding area is primarily agricultural and heavily irrigated.

Anthropogenic influences in the Platte basin have greatly influenced the geomorphology and discharge regime of the river. In the central Platte basin, the river has become increasingly incised in its banks (Williams, 1978) and channel width has decreased by as much as 65% (Eschner et al., 1983; Joeckel and Henebry, 2008; Horn et al., 2012). These changes are in part a result of dams built on the North and South Platte rivers for hydroelectric power that have decreased the sediment load downstream. Annual river discharge has been impacted by

diversions from the river channel to supply irrigation and hydroelectric canals, beginning upstream in the North Platte River with the Interstate and Tri State Canals, which supply 80% of irrigation water for the area (Böhlke et al., 2007). An additional eight canals divert water for irrigation along the ~200 km distance between the North and South Platte confluence, and the study area. Many of the canals are unlined and locally recharge the alluvial aquifer (Harvey and Sibray, 2001; Böhlke et al., 2007).

The high density of irrigation wells in the valley and near the river have also led to decreased river discharge. The central Platte River valley is one of the most heavily irrigated areas of the state, with an average irrigation well density of three wells per km^2 (Chen, 2007), though there can be as many as nearly one well per km^2 (Chen and Shu, 2006). The river is hydraulically connected to the alluvial aquifer (Chen, 2007); responses in the aquifer at distances up to 750 m from the river channel can be detected within 24 hours of a change in river stage (Hurr, 1983). Therefore, irrigation wells (with pumping rates upwards of 4500 $m^3 d^{-1}$) in the alluvial aquifer can lead to stream depletion and reduced baseflow during the peak irrigation season of May/June through September (Chen and Shu, 2002). Reaches in the most heavily irrigated areas regularly become dry during this time (Hurr, 1983; Chen, 2007). The alluvial aquifer adjacent to the north and south banks of the Platte is comprised of Pliocene and Pleistocene alluvial sediments deposited as the Platte River migrated across south central Nebraska prior to settling in its present-day course. In the Grand Island area, where this study took place, these unconsolidated gravels, sands, silts, and clay are approximately 45 m thick and laterally continuous (Chen, 2007; Chen, 2011). The Pleistocene sediments are capped by Holocene loess, approximately 8 m thick (Condon, 2005).

Streambed sediments are poorly sorted sand and gravel, with fines present in low-energy pools and on stable islands. The vertical hydraulic conductivity of the streambed sediments decreases with depth, as fines clog sediments at depth (Chen, 2011), and are estimated to range

from 25 to 45 m d^{-1} (Cheng et al., 2011; Chen, 2011; Chen et al., 2013). The sediments also have a high horizontal hydraulic conductivity of 100-120 m d^{-1} at the surface (Chen and Shu, 2006), which facilitates rapid response by the river to changes in groundwater levels, as well as the reverse. Groundwater flow is approximately parallel to the river channel (Chen and Shu, 2006), and the reach in this study is neither exclusively gaining nor losing, but varies seasonally and possibly over the reach scale (Peckenpaugh and Dugan, 1983; Kilpatrick, 1996).

Tertiary strata in the area are consolidated sands and gravels of the Ogallala group, 30 to 40 m thick. Paleovalleys have incised the Tertiary bedrock surface across much of Nebraska, lending to a spatially variable thickness of Tertiary and Quaternary deposits. The water-bearing units of the Tertiary and Quaternary rocks together make up the High Plains Aquifer, the primary water producing aquifer for Nebraska and large portions of the Great Plains (Korus and Joeckel, 2011). The Tertiary units overlie the Late Cretaceous Pierre Shale, and chalk and limestone of the Niobrara formation. These units are considered the bottom of the Aquifer (Hurr, 1983).

1.2 Study Area

The study site is within a 180 m-wide, 100 m-long reach of the central Platte River. For this study, two adjacent islands (one vegetated, ~70 m long, ~40 m wide; one non-vegetated, ~50 m long, ~20 m wide) of comparable size were selected for intensive sampling and monitoring over the study period (40°47’ 9” N, 98°25’57”W; 40°47’10.5”N, 98°25’55.8”W, approximately 14 km southwest of Grand Island, NE; Fig. 1). The Platte River along this reach is separated into three small channels (anabranches, referred to as North, Middle, and South Channels). At the study area, the distance between the North and South channels is 3200 m, though the total width of the three individual channels at this location is ~300m. The South and Middle channels border Mormon Island, a large (approximately 16 km long, 2 km wide, Hurr, 1983), stable island used primarily for grazing. The islands selected for this study were within the South Channel.

The 30-year average annual precipitation for the area is 650 mm (NCDC, 2013), recorded by the Grand Island Weather Station. However, during 2012 much of Nebraska experienced an exceptional drought and extended high-temperature period. In the 12-month period beginning from September 2011 to the conclusion of this study in August 2012, only 390 mm of precipitation was recorded, a 40% decrease from average annual precipitation. The Palmer Drought Severity Index (PDSI) indicated mild drought conditions in May (-1.90) which became extreme in July (-4.60) and August (-5.48), after which the study concluded (NCDC, 2013). Daily stream discharge over the study period averaged in the 23rd percentile of daily flows for the 78-year discharge record, as measured by a USGS gaging station approximately 16 km downstream from the study area, near Grand Island.

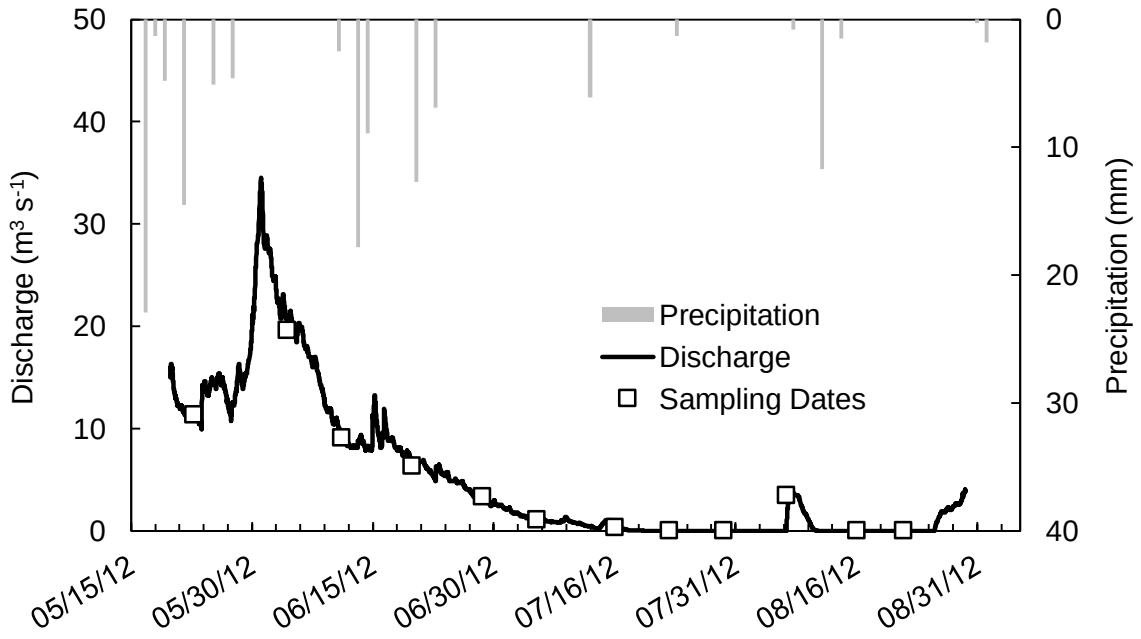

Figure 2. Streamflow recorded at the USGS gaging station at Grand Island. Precipitation data from the National Climatic Data Center, recorded in Grand Island. Following a period of high flow in early June, river stage declined steadily until the channel became dry in mid-July. The brief flow in early August represents an upstream dam release.

Realtime and historical discharge data collected at this station can be obtained at http://waterdata.usgs.gov/nwis. Average daily discharge from May through August 2012 at the gaging station was 5.3 $m^3 s^{-1}$ with 28 days of zero flow recorded (Fig. 2; Appx B Fig. I). Average daily maximum air temperature during the study was 32 °C.

2.0 METHODS

Nine piezometers constructed of Schedule 40 threaded, 6 cm i.d. PVC with a 0.2 m long slotted screen were installed in a north-south transect perpendicular to river flow to collect weekly shallow groundwater samples and field parameters, as well as monitor sub-hourly water table fluctuations (Fig. 3). Piezometer boreholes were hand-augured to the water table and the piezometers were driven to the desired depth. One piezometer was installed in the river bed, and four piezometers were installed in each island. Each island contained two "nests" of two piezometers screened at a shallow and deep interval. Shallow and deep piezometers were screened ~0.5 m and ~1 m below the surface, respectively. Both islands contained one nest in the center of the island, and one at the edge. This experimental design was conceived in order to determine the hydraulic similarities and differences between the vegetated and non-vegetated island. The nested design permitted determination of vertical hydraulic gradients, which indicate the intensity of upward or downward flow at that location. Only one nest was installed on the edge of the islands with the assumption that at this scale, symmetry would allow for conclusions to be drawn for the island hydrogeology as a whole. All piezometers except AV2 were initially screened below the water table, though select piezometers became temporarily dry throughout the sampling period due to water table decline.

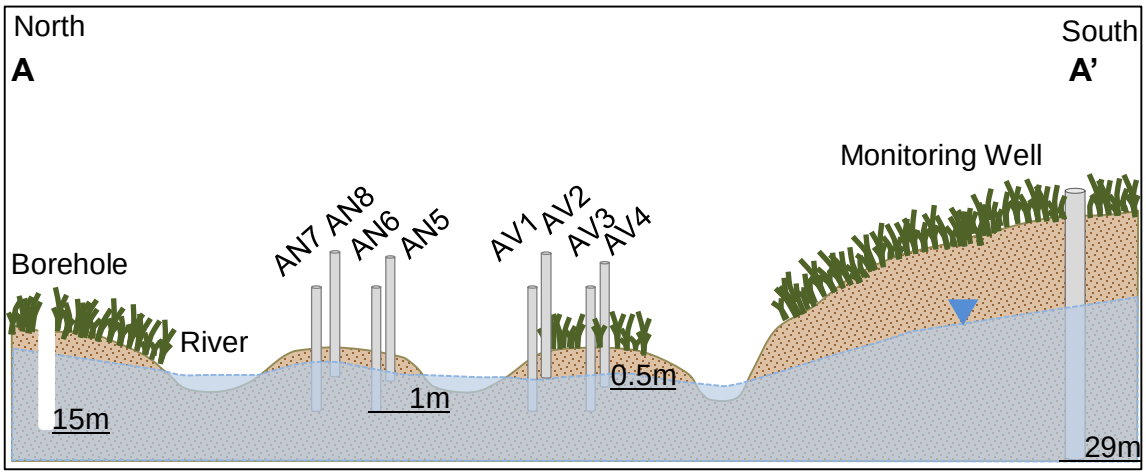

Figure 3. Schematic cross section following the line A-A' shown on Fig. 1, looking east. Relative locations of piezometers and islands are shown. Note piezometers AV1-4 are installed on a vegetated island, AN5-8 in the non-vegetated island. Depths of piezometers, borehole and monitoring well are given. Cross section is not to scale.

Sampling was conducted over a 12 week period in summer 2012. Prior to sampling, each piezometer was purged for approximately two minutes with a portable peristaltic pump (Geopump™ Series I, Geotech Environmental Equipment, Denver, Colorado, USA) or until dissolved oxygen, temperature, and conductivity (measured by YSI ProPlus meter with Quatro sonde, Yellow Springs, Ohio, USA) in a flow cell, stabilized (Appx B Fig. II). Oxidation-reduction potential (ORP) and pH were also measured by the YSI meter. Calibration of the YSI occurred once per day of each sampling event. ORP was calibrated by Zobell solution, pH by three buffer solutions of pH equal to 4, 7, and 10, conductivity by a 10,000 µS/cm solution, and dissolved oxygen by an enclosed, wetted sponge to produce water-saturated air. The same methods were used to collect samples from the river channel and a groundwater monitoring well, approximately 1 km south of the study site with a screen depth ~30 m below the surface.

A 15 m deep borehole was drilled below the water table (located approximately 3 m below surface) during sampling with a 17-cm hollow-stem auger. Upon reaching the final boring

depth, a PVC casing with a 1.5 m screen was lowered into the borehole. A submersible pump was used for sample collection. Field parameters were monitored until stable and recorded, after which the screen was lifted 1.5 m and the process repeated.

2.1 Water Level Monitoring

Each piezometer was outfitted with an unvented pressure transducer (Solinst Levelogger Edge 3001 F5/M15) suspended by Kevlar cord to monitor water level and temperature fluctuations at two minute increments. One barometric pressure transducer (Solinst Barologger Edge 3001) was also deployed in piezometer AV4 to compensate water level data for barometric pressure fluctuations. Vertical hydraulic gradients (VHG) were calculated for three piezometer pairs; two pairs were located on the non-vegetated island and one pair was located on the vegetated island. VHGs were calculated as $\Delta h/\Delta L$, in which Δh represents the difference in total hydraulic head, and ΔL represents the difference in screen-top elevation above an arbitrary datum (Fig. 4). Throughout the course of removing the pressure transducers for data download and inserting the peristaltic pump tubing, pressure transducers were occasionally replaced at a slightly different depth within the piezometer than originally deployed. These occasions were apparent from the compensated water level data and manually corrected. Erratic water level and temperature measurements were recorded by some pressure transducers as they collected readings while outside of the well. These data were also manually removed from the final pressure transducer dataset.

2.2 Seepage Meter

A seepage meter serves to isolate a small area of river or lake bed, depending on its application, with the purpose of determining the rate at which water is being gained or lost

through the sediment-water interface (Landon et al., 2001; Rosenberry et al., 2008). Simple seepage meters can be constructed from an inverted cylinder inserted into the river or lake bed, effectively isolating flow through those sediments (Fig. 5). In gaining streams or lake beds, vertical flux that enters the seepage meter displaces fluid into a seepage bag, through flexible plastic tubing. Seepage meters can also be used in losing systems, and require a known volume of fluid in the seepage bag, which will be depleted at the rate of downward seepage through the sediment-water interface. The accumulated volume in the seepage bag is the seepage flux, and is considered to be within 10% of true seepage, if adjustments are made for errors and inefficiencies (Rosenberry, 2008). Rosenberry (2008) found the standard deviation in seepage measurements ranged from 15 mm d^{-1} to 32 mm d^{-1} in laboratory experiments. Rosenberry et al. (2008) concluded from previous experiments that seepage velocities less than 0.8 mm d^{-1} may be too

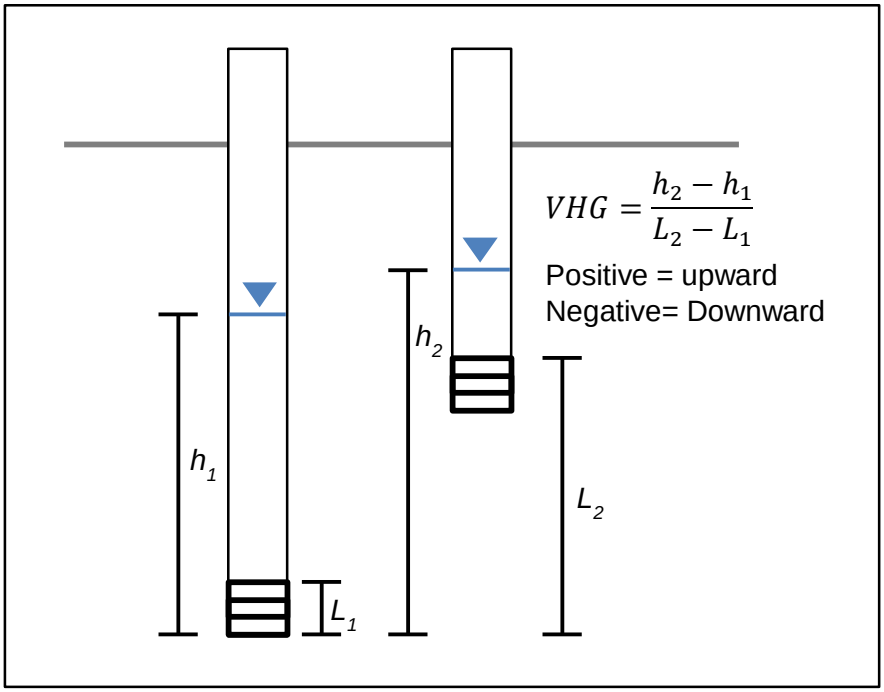

Figure 4. Schematic for measurement of vertical hydraulic gradient (VHG) in a piezometer nest, where h_1-h_2 represents the difference in hydraulic head and L_1-L_2 represents the difference in elevation of the screen top above an arbitrary datum.

small to measure accurately. The use of seepage meters in flowing water requires additional steps relative to seepage meters used in stagnant water, such as a lake, in order to reduce the effects of the hydraulic gradient between the inside and outside of the seepage bag (Rosenberry, 2008). Rosenberry et al. (2008) suggest pre-wetting and adding a small, known volume to the seepage bag, in order to reduce errors from bag relaxation or resistance during filling. Additional steps to reduce error include valves placed at the connection between the seepage bag and tubing, a minimum equilibration time to determine whether the seepage cylinder greatly disturbs the natural flow along the streambed, and a seepage bag shelter box to prevent the flowing water from disturbing the hydraulic head within the seepage bag (Rosenberry et al., 2008).

A seepage meter was designed and constructed for this study from the upper third of a 208-liter (55 gallon) steel drum after Rosenberry (2008) and Landon et al. (2001). Clear plastic tubing was threaded through a rubber stopper, which plugged the access hole in the top of the

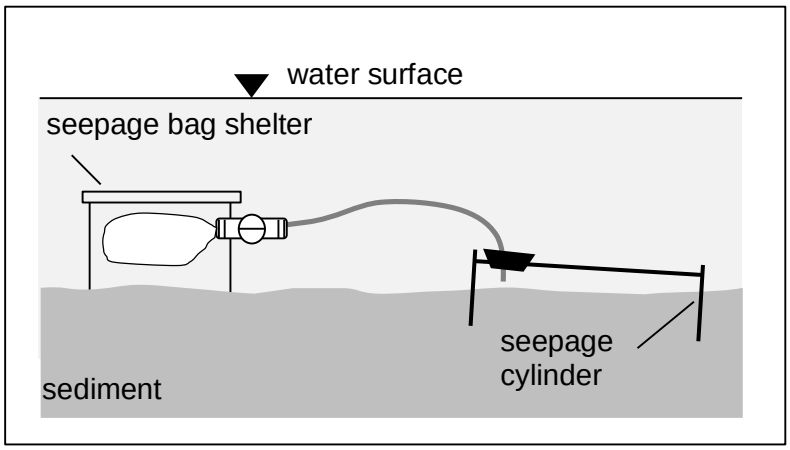

Figure 5. Schematic showing the construction and installation of a seepage meter and bag shelter. Note the seepage cylinder is installed at an angle to allow air to escape the access hole in the cylinder top. The bag shelter must be submerged so that the hydraulic head on the seepage bag is equivalent to the hydraulic head on the sediment surface. Modified from Rosenberry, 2008.

barrel. A PVC ball valve joined the plastic tubing and plastic bag, used as the seepage bag. The seepage bag resided in a lidded clear plastic box. Holes in the box allowed for the water inside the box to be displaced as the bag filled with fluid. To determine volume gained or lost, the bag contents were emptied into a graduated cylinder and recorded. Three seepage meter tests (May 23, June 4, June 29) were conducted over the study period as follows: The seepage cylinder was inserted into the riverbed sediments and angled such that the access hole was slightly elevated, ensuring no trapped air within the cylinder. The cylinder was inserted to a sufficient depth such that water flowing over the meter did not appear disturbed, and that no "scouring" of bed sediments was observed on the upstream side of the cylinder. The seepage cylinder was allowed to equilibrate for approximately 20 minutes. 500 mL water was added to the bag to coat the inside. All air was eliminated from the bag and flexible tubing by submerging under water, while maintaining the initial 500 mL inside the bag. The shelter box was also filled with water, submerged, and secured in the bed sediments to maintain the appropriate head on the seepage bag throughout the test. After installing the bag and shelter box, the tubing was connected to the shelter box, and the ball valve opened to allow water to flow between the seepage meter and bag.

2.3 Temperature Envelope and Seepage Flux Model

Heat has been used as a natural and inexpensive groundwater tracer in numerous hydrogeological environments (Anderson, 2005). The heat tracer method is based on Fourier's law, in which heat flow is dependent on the temperature gradient and thermal conductivity of the geologic material (Constantz and Stonestrom, 2003). Heat tracer investigations have involved either the geothermal gradient of the earth or a thermal gradient resulting from surface water seepage into a shallow aquifer (Constantz and Thomas, 1996; Anderson, 2005). Suzuki (1960) presented an analytical solution for a groundwater temperature profile underlying a sinusoidal temperature fluctuation at the surface:

$$T(z) = T_m + Ae^{-az}\sin\left(\frac{2\pi t}{\tau} - bz\right) \quad (1.1)$$

Where T_m is the mean temperature at depth z, A is the amplitude of temperature fluctuation about the mean at depth z, τ is the period of surface temperature fluctuations, and a and b are constants including thermal properties of the aquifer.

Stallman (1965) described the general response of temperature of an incompressible fluid moving though a porous homogeneous medium as a result of one-dimensional anisothermal flow:

$$\frac{c\rho\partial T}{\partial t} = \frac{k\partial^2 T}{\partial z^2} - qc_0\rho_0\frac{\partial T}{\partial z} \quad (1.2)$$

Parameters c_0 and ρ_0 are the specific heat and density of water, respectively, $c\rho$ is the heat capacity of the soil/water matrix, T is temperature, k represents the fluid/solid mixture thermal conductivity, and q is the fluid flux with dimensions of [L T^{-1}].

Bredehoeft and Papdopulos (1965) built on this general simultaneous heat and water transfer equation and presented an analytical solution for steady-state, advective, anisothermal heat flow through a semi-confining layer. The authors demonstrated the use of temperature profiles to find vertical groundwater flux and hydraulic conductivity. Temperature profiles are an attractive tool for calculating hydraulic conductivity, given the inherent difficulty and inaccuracy of measuring the hydraulic parameter directly (Lapham, 1989). More recently, the numerical code VS2DH (Variably Saturated 2-Dimensional Heat Transport) has been successfully used to determine vertical flux beneath losing areas of streams and lakes (Bartolino and Niswonger, 1999; Anibas et al., 2009). Numerical solutions lend more flexibility in determining groundwater seepage from variable hydrogeologic parameters and boundary conditions (Anderson, 2005).

This study followed the method of Taniguchi (1993), in which the analytical solution presented by Suzuki (1960) is simplified for the case of the surface temperature oscillation at its maximum, which leaves $sin(2\pi\tau/t\text{-}bz)$ equal to +1. This simplification can be used to determine

the temperature envelope in which all temperature profiles throughout the period of surface temperature fluctuation are encompassed (Constantz and Stonestrom, 2003). The solution for the temperature envelope at depth *z* is (Taniguchi, 1993):

$$A_z = A_{z0} e^{-az} \tag{1.3}$$

where the amplitude of temperature fluctuation about the mean at the surface, A_{z0}, and the extinction coefficient *a* largely determine the shape of the envelope. The amplitude of temperature fluctuation about the mean at some depth *z* is A_z. The parameter *a* is dependent on the thermal properties of the aquifer as well as the groundwater flux:

$$a = \left[\left(K^2 + \frac{V^4}{4} \right)^{\frac{1}{2}} + \left(\frac{V^2}{2} \right) \right]^{\frac{1}{2}} - V \tag{1.4}$$

where

$$K = \frac{c\rho\pi}{k\tau} \tag{1.5}$$

and

$$V = \frac{q c_0 \rho_0}{2k} \tag{1.6}$$

In this investigation, one temperature profile was collected in the borehole drilled through the stream bank adjacent to the river channel. Temperature measurements were recorded after temperature and dissolved oxygen measurements stabilized in an overflowing bucket collecting borehole water from a submersible pump. The temperature profile collected in the borehole was used to develop a temperature envelope assumed to encompass annual temperature fluctuations in the borehole. Also assuming the collected profile represents the warmest temperatures for the entire season, the envelope was fit such that it was tangent to the borehole profile. The temperature input for the upper bound of the temperature envelope was within 1 °C of the

maximum surface temperature measured at the USGS gaging station at Overton, NE, approximately 96 km upstream from the study area. The mean surface water temperature is 13.7 °C, measured at the Overton station, by a USGS gaging station. This value was used as a fitting parameter and modifed slightly from that measured at the gaging station. The lower bound of the envelope was the temperature of the deepest profile measurement, which was within 1 °C of the average groundwater temperature measurements in the monitoring well (Fig. 3). This is slightly above the 30-year mean annual air temperature near Grand Island of 9.9 °C (NCDC, 2013). A_{z0} was calculated as the difference between the upperbound of the temperature envelope (28.5 ºC) and the modified mean surface water temperature, 12.5. The parameters used in groundwater flux estimation are given in Table 1.1. Lapham (1989) provides a range of volumetric heat capacities, dependent on the dry bulk sediment density. The volumetric heat capacity used in the model assumes a dry bulk density of approximately 1.6 g cm^{-3}. This value agrees closely with the volumetric heat capacity value used by Taniguchi (1993) for sand and gravel, and recommended by Stonestrom and Blasch (2003) for sandy aquifer materials. Thermal conductivity values for saturated, coarse-grained aquifer materials are dependent on grain size distribution and dry bulk density, and generally range between 1.2 $Wm^{-1}C^{-1}$ and 2.5 $Wm^{-1}C^{-1}$ (Lapham, 1989). We estimated a thermal conductivity value of 2.2 $Wm^{-1}C^{-1}$, which is similar to the value found by Taniguchi (1993) for a coarse-grained saturated alluvial aquifer.

2.4 Tritium

Tritium was collected from the borehole described above, in order to determine groundwater ages at depth below the riverbank. The radioactive hydrogen isotope tritium (^3H) is a naturally occurring isotope produced by the interaction of nitrogen and cosmic rays in the upper atmosphere. ^3H is commonly reported in tritium units (TU), in which one TU is equivalent to one

^{3}H atom in 10^{18} hydrogen atoms. The half-life of the tritium isotope is approximately 12.3 years, making it useful for dating groundwater less than 50 years old (Solomon and Sudicky, 1991; Michel, 2005). Human activities began influencing background atmospheric levels of ^{3}H in the mid-twentieth century as a result of thermonuclear weapon testing. Through atmospheric mixing, elevated levels of historic atmospheric ^{3}H occurred around the world, with a maximum atmospheric ^{3}H in 1962, also known as the "bomb peak". Through equilibration with the atmosphere, ^{3}H concentrations in rainfall match the atmospheric concentration, leading to detection of the bomb peak in groundwater recharged in the early 1960's. The bomb peak was a useful groundwater tracer for approximately 50 years, until radioactive decay diminished the peak below analytical detection limits. Background atmospheric ^{3}H concentrations increased by over two orders of magnitude in Lincoln, NE during the height of thermonuclear testing (Fig. 6).

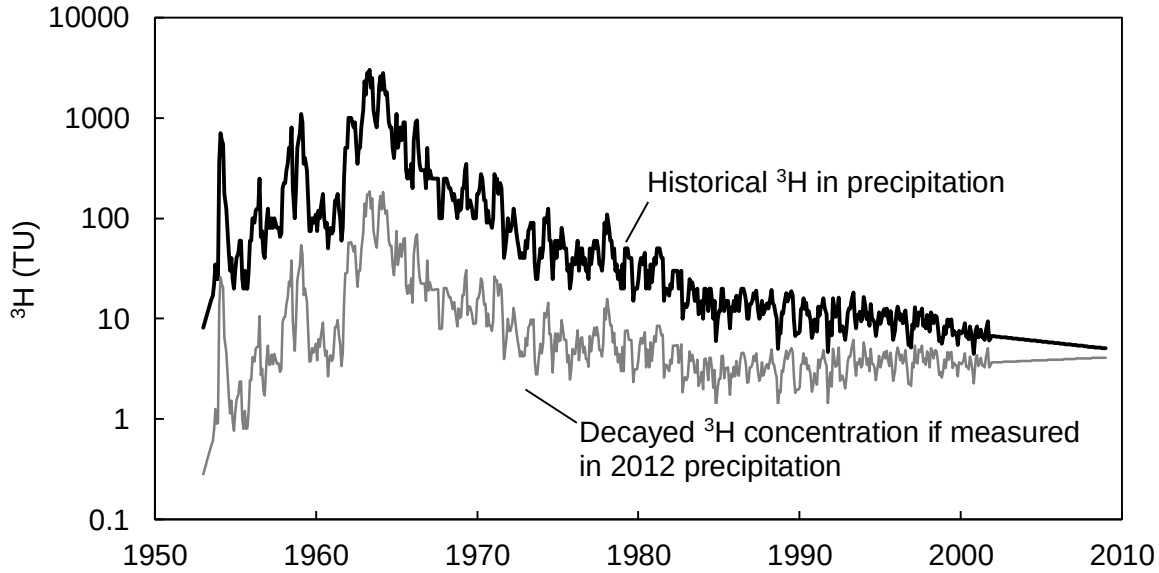

Figure 6. Hisotorical tritium concentration in precipitation measured in Lincoln, NE from 1962-1986. Data from 1953-1962 and 1987-2009 are based on correlation of measured data with concurrent ^{3}H measurements from Vienna. Maximum ^{3}H in precipitation correlates with the 1962 "bomb peak", or atmospheric maximum ^{3}H as a result of thermonuclear testing (International Atomic Energy Agency, Michel 2005). Also shown is the decayed ^{3}H concentration that would be detected in groundwater of the given age and analyzed in 2012.

In addition to the bomb peak marker, ^{3}H can be used to calculate groundwater ages as a function of radioactive decay when the historical atmospheric ^{3}H concentration is known. Using known initial ^{3}H concentrations, absolute groundwater ages can be calculated using the following formula:

$$t = \frac{1}{-\lambda} \ln \frac{C}{C_0} \tag{1.5}$$

in which

$$\lambda = \frac{\ln(2)}{T_{1/2}} \tag{1.6}$$

C is equivalent to the measured ^{3}H concentration, C_0 is equivalent to the initial ^{3}H, or tritium "input function", and $T_{1/2}$ equals the half-life. ^{3}H samples were collected from the borehole after temperature and O_2 measurements stabilized. Unfiltered water samples were contained in 1 L plastic bottles and analyzed at the University of Miami Tritium Laboratory. Groundwater ages were calculated using the ^{3}H concentration measured in the river at the study area, 8.02 TU, assuming that this measurement reasonably represents "modern" rainfall (^{3}H concentration near that in precipitation in the study area).

Tritium concentrations were recorded in Lincoln, Nebraska precipitation on a monthly basis from 1962 to 1986 (Fig. 6). This data was correlated with ^{3}H measurements from Vienna and this correlation was used to estimate ^{3}H in precipitation for Lincoln from the periods 1953 to 1962 and 1987 to 2009 when precipitation data is not available (International Atomic Energy Agency Global Network of Isotopes in Precipitation; Michel, 2005).

3.0 RESULTS

3.1 River and Shallow Groundwater Data

The water level data from all piezometers indicate a steady decrease in the water table elevation over the study period, beginning in the first week of June (Fig. 7a-f). The maximum measured vertical hydraulic head decline of 1.04 m occurred in AN6. Vertical hydraulic head decline may have been as great or greater in other locations, but in all other piezometers, the minimum hydraulic head was at or below the bottom of the piezometer. The average rate of water table decline in AN6 was approximately 17 mm d^{-1}. The range of water table levels collected by the pressure transducers is given in Table 1.2. In August, a release from an upstream dam created a brief "pulse flow" or temporary increase in river discharge following several weeks of no flow in the river channel. This pulse was indicated by concurrent head increases in each of the piezometers. In addition to these overall trends, the pressure transducers in all piezometers indicated diurnal fluctuations in the water table as a result of evapotranspiration. The water table fluctuation for each of the pressure transducers was relatively similar, with a daily average fluctuation in individual piezometers between 20 and 30 mm.

Analysis of the vertical hydraulic head gradients indicate the islands were dominated by downward groundwater flow for the entire summer (Fig. 8a-c). The magnitude of downward flow and rate of water table decline varied spatially and temporally, but no upward flow occurred in any of the piezometers according to the VHG data. Table 1.3 shows the minimum, maximum, and average VHGs from the three piezometer pairs (see Fig. 3 for piezometer locations).

The VHGs indicate that the center of the vegetated and non-vegetated island experienced a greater average VHG over the course of the study period (0.97 m/m, 1.00 m/m respectively) compared to the piezometer pair on the edge of the island (0.36 m/m). In addition, the greatest

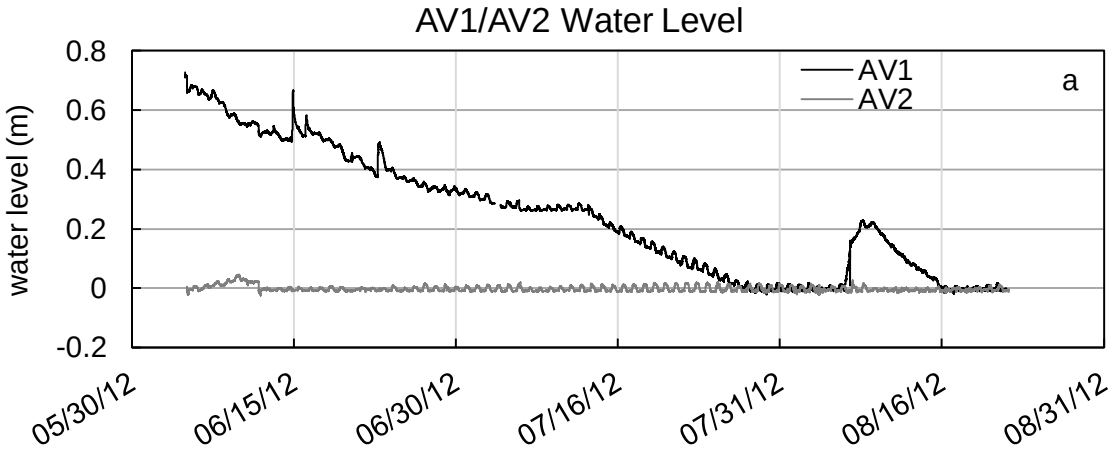
AV1/AV2 Water Level
water level (m)
0.8
0.6
0.4
0.2
0
-0.2
AV1
AV2
a
05/30/12
06/15/12
06/30/12
07/16/12
07/31/12
08/16/12
08/31/12

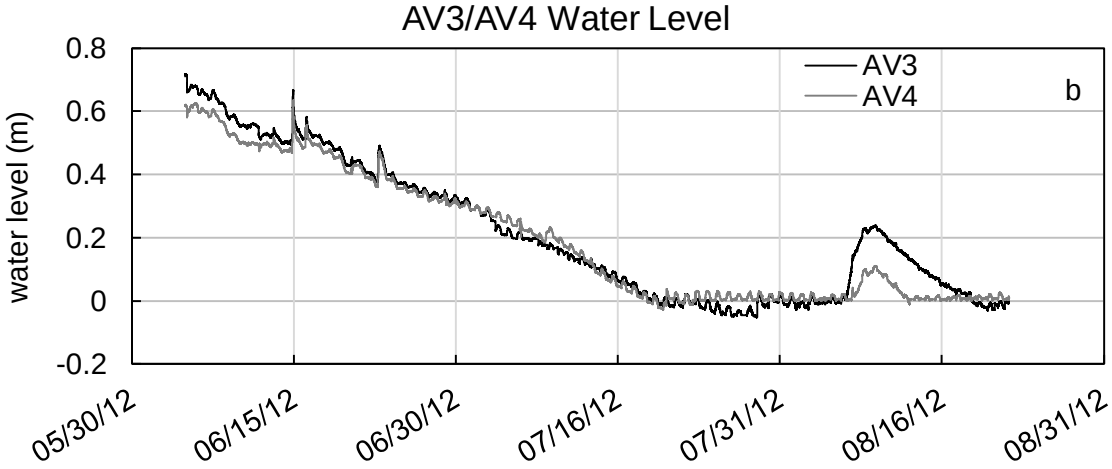
AV3/AV4 Water Level
water level (m)
0.8
0.6
0.4
0.2
0
-0.2
AV3
AV4
b
05/30/12
06/15/12
06/30/12
07/16/12
07/31/12
08/16/12
08/31/12

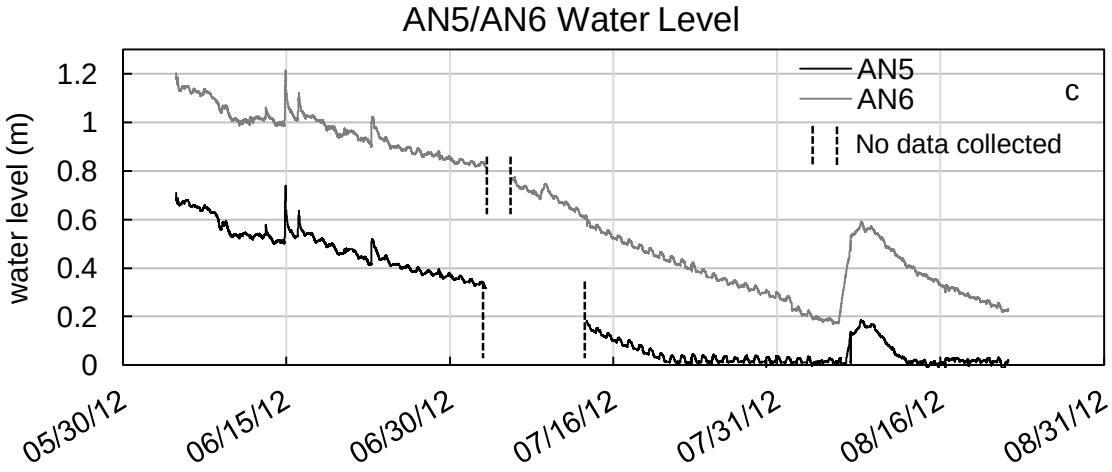
AN5/AN6 Water Level
water level (m)
1.2
1
0.8
0.6
0.4
0.2
0
AN5
AN6
No data collected
c
05/30/12
06/15/12
06/30/12
07/16/12
07/31/12
08/16/12
08/31/12

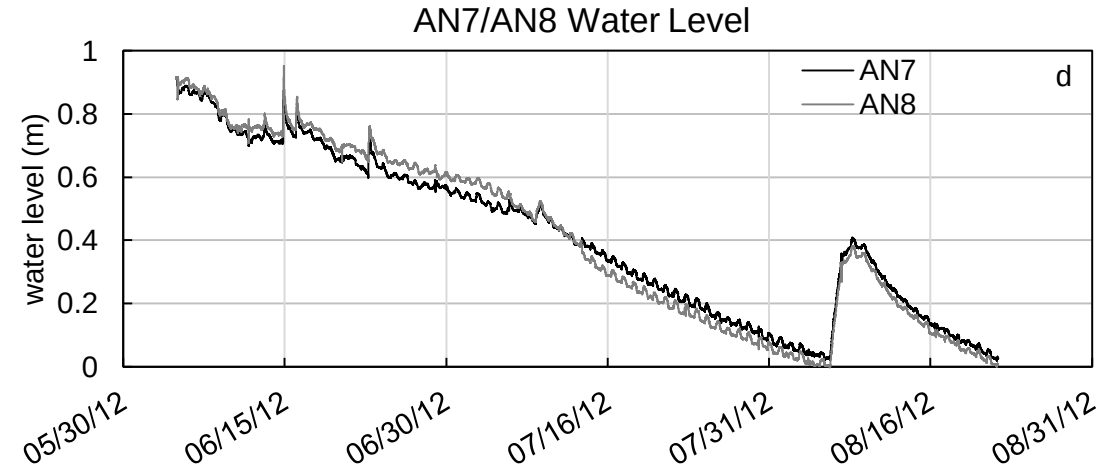
AN7/AN8 Water Level
water level (m)
1
0.8
0.6
0.4
0.2
0
AN7
AN8
d
05/30/12
06/15/12
06/30/12
07/16/12
07/31/12
08/16/12
08/31/12

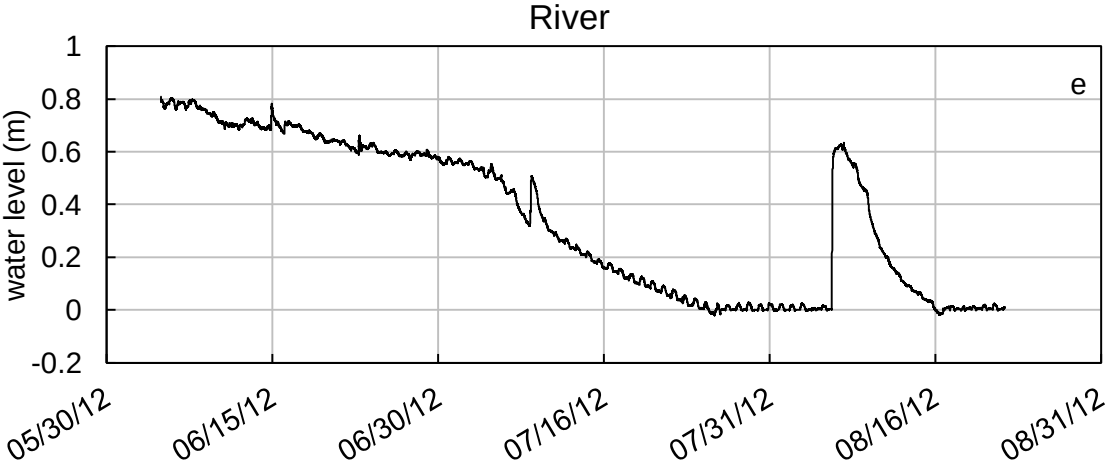
River
water level (m)
1
0.8
0.6
0.4
0.2
0
-0.2
e
05/30/12
06/15/12
06/30/12
07/16/12
07/31/12
08/16/12
08/31/12

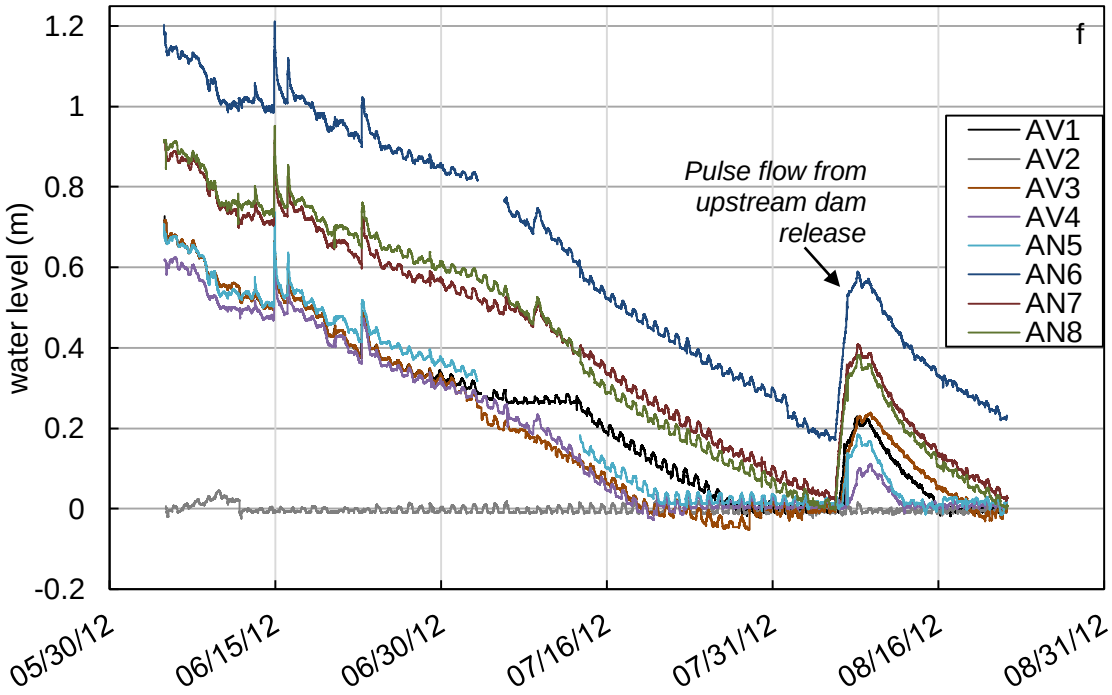

Figure 7. a-d) Water level measured by pressure transducers in the island piezometers; e) water level measured in the river bed piezometer; f) combined data from all island transducers. Data gaps in 'c' represent the period of time the transducer was not submerged due to external disturbance of the piezometer. All piezometers indicate diurnal fluctuations in the water table. The early August peak recorded in all piezometers was due to an upstream dam release. Piezometer AV2 (a) was installed dry and remained dry throughout the study. The water level fluctuation in this piezometer is likely due to diurnal fluctuations in the capillary fringe.

VHG occurred in the center of the non-vegetated island (1.11 m/m). However, the greatest change in VHG over the study period, an increase of 0.54 m/m, occurred at the piezometer pair on the edge of the non-vegetated island. The August pulse impacted the VHG in piezometer pairs 3/4 and 5/6. In both piezometers, the VHG decreased in magnitude, but remained downward. In both pairs, the VHG also returned to pre-pulse magnitude as head levels in the transducer returned to pre-pulse levels.

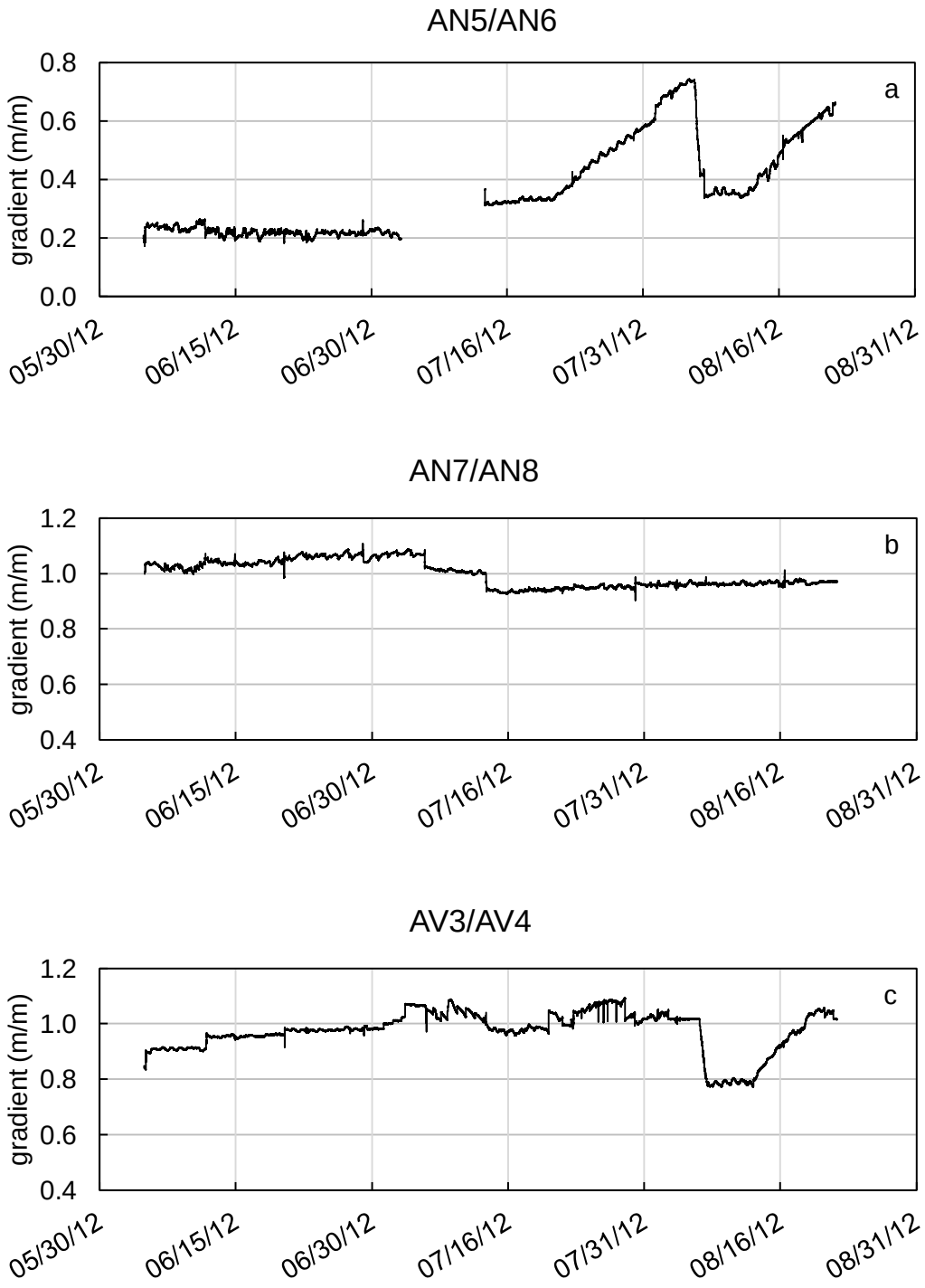

Figure 8a-c. Vertical hydraulic gradients for piezometers on the vegetated and non-vegetated islands. Positive VHG indicates downward flow in all piezometer pairs. The pulse flow from an upstream dam release temporarily decreased the magnitude of downward flow at the center of the vegetated island and the edge of the non-vegetated.

3.2 Seepage Meter

Seepage meter tests were conducted on three occasions throughout the study period. The first seepage meter test occurred on May 23rd, and resulted in a gain of 62 mm d^{-1}. The second seepage meter test occurred on June 4, with a gain of 2 mm d^{-1}. On June 29th, the third seepage meter test was conducted. By the end of the test, a small fraction of the initial 500 mL added to the bag had been lost, indicating losing conditions in the test location. The calculated seepage rate was -1 mm d^{-1}. The seepage meter tests indicated that through the first week of June, upward flow was occurring in the shallow river sediments. However, the last test at the end of June indicated very slight downward flow in the river sediments.

3.3 Temperature Envelope and Seepage Flux Model

Temperature profiles beneath streambeds can be seasonally transient or steady-state (Anibas et al., 2009), and a steady-state approach by Bredehoeft and Papadopulos (1965) may result in accurate estimation of groundwater flux for seasonally transient profiles. However, the findings of Anibas et al. (2009) were not applicable to our field data, as the collected curve exhibits one inflection point, indicative of typical transient characteristics, rather than a profile without, characterizing steady state conditions (Fig. 9). Therefore, application of the steady-state approach is not appropriate in this case. The technique of Taniguchi (1993) described above provided an alternative method for interpretation of the temperature profile, though the accuracy of the solution would increase with a greater number of temperature profiles. However, temperature fluctuations at the surface, and the depth at which groundwater temperatures become stable were acquired in the field. These were used to constrain the minimum and maximum values in the temperature envelope. Yet, fitting the envelope to the single profile and assuming this represents the warmest profile for the annual thermal cycle is a somewhat crude means of fitting of parameter *'a'* that introduces uncertainty. The temperature envelope and temperature

profile are shown in Fig. 10. The estimated downward seepage flux from this method was equivalent to 8 mm d^{-1}.

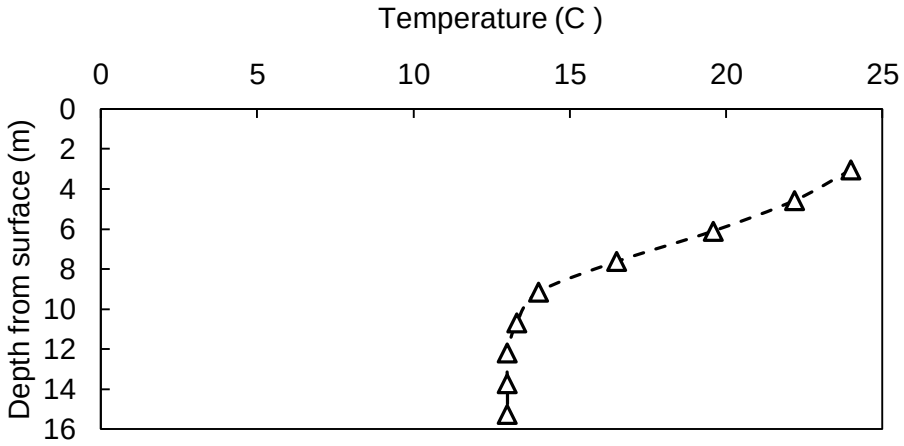

Figure 9. Temperature in the borehole. The profile indicates that groundwater up to 11 m deep is impacted by surface temperature fluctuations. Below this depth, groundwater temperatures are relatively stable and are within a few degrees of the mean annual air temperature.

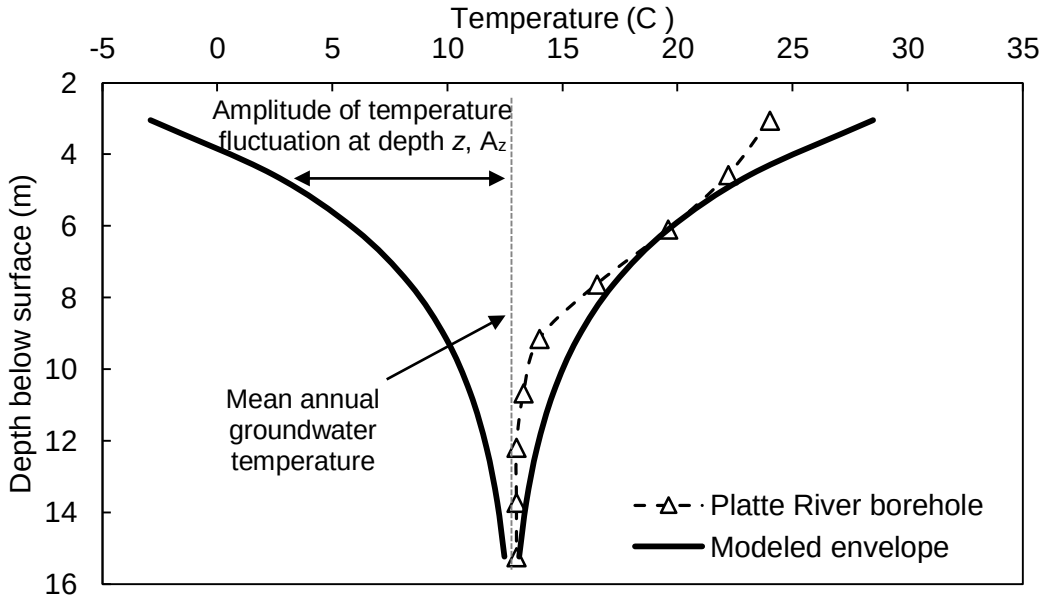

Figure 10. The modeled envelope is calculated using the solution by Taniguchi (1993), and illustrates the maximum annual temperature oscillation at each depth, based on the surface temperature fluctuation and extinction coefficient (rate at which the surface temperature fluctuation is attenuated). Traditional temperature modeling bases the envelope dimensions on several temperature profiles collected over at least one year. This study assumed the profile collected represented a groundwater temperature maximum, and the envelope was modeled to be tangential to this profile.

3.4 Tritium

Results of ^{3}H concentrations in the borehole are shown in Fig. 11. The highest ^{3}H concentration was present in the river, and generally decreased with depth. The 20-year average of atmospheric ^{3}H at Lincoln is ~8 TU, which is similar to the ^{3}H concentration in the river. Assuming that river water is representative of initial ^{3}H, absolute ages were calculated and show that the oldest groundwater is at the bottom of the profile, approximately six years older than that in the river. The shallowest samples, collected from 0-6 m below the surface are all less than two years old. The "bulge" in groundwater age at 9 m below the surface is an indication that groundwater flow in the area may include a horizontal flow component. Errors for groundwater age were calculated from one standard deviation of the 1998-2001 precipitation ^{3}H concentrations (the last three years of unextrapolated data). Tritium concentrations and groundwater age are shown in Table 1.4.

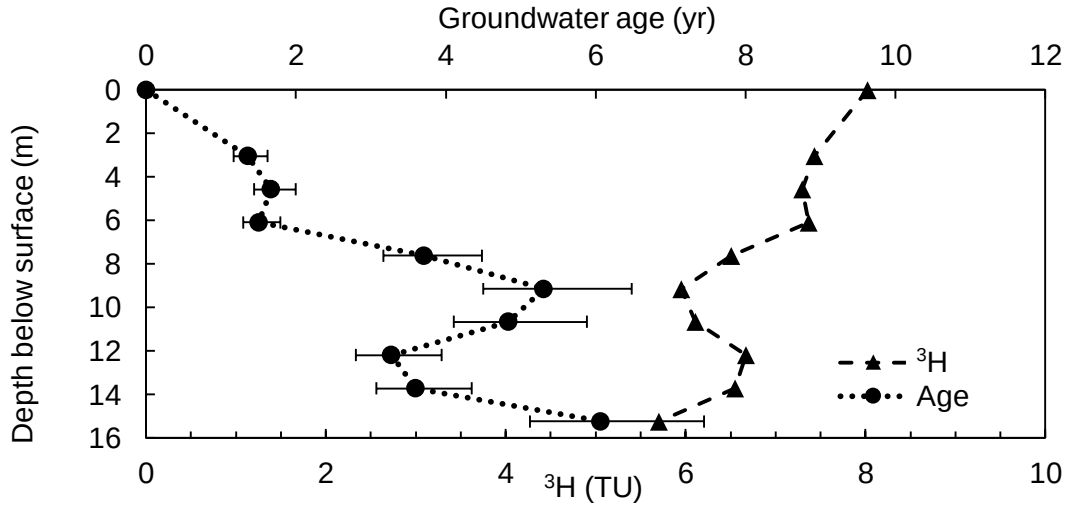

Figure 11. Tritium concentration and interpreted groundwater age in the riparian borehole. Samples collected at the surface are from the river channel. The non-monotonic age trend with depth indicates that groundwater flow in the region likely contains a large component of horizontal flow, rather than purely vertical. Error bars represent the error propagation in groundwater age from one standard deviation in the precipitation tritium concentrations for 1998 to 2001.

4.0 DISCUSSION

4.1 Conceptual Model

The methods and results described above provide a relatively consistent interpretation of the nature of groundwater flow and response of shallow groundwater to the drought in the study area. Combined, the piezometer, ^{3}H, and temperature profile data provide a conceptual model in which shallow groundwater levels declined at a steady rate over the summer, except for a temporary increase due to an upstream dam release. Thus, the reach was losing (stream water infiltrating into the aquifer) over the summer. Though the alluvial aquifer seasonally recharges the river, the dry weather conditions and onset of irrigation in the early weeks of the study likely drew down the alluvial aquifer to the point that the river began recharging the aquifer until the river channel became dry by mid-July (Fig. 2). However, this data does not indicate exclusively vertical downward flow; groundwater flow contained components of both vertical downward, and horizontal flow.

4.2 Uncertainty and Possible Sources of Error

Each of the methods contains some inherent uncertainty. The pressure transducers have a manufacturer-reported accuracy of ± 3 mm, and relative to the other methods presented, exhibit the least uncertainty. The transducers collected essentially continuous water level data for the entire study, and are representative of groundwater levels up to 1 m below the surface over an approximately 65 m-long transect. Using the vertical hydraulic gradients calculated for three piezometer nests and the range of vertical hydraulic conductivities estimated by Cheng et al., (2011), Chen (2011), and Chen et al. (2013), a Darcy velocity for each well nest can be calculated. Vertical hydraulic gradients ranged from approximately 0.2 m m^{-1} to 1.1 m m^{-1}. With an estimated riverbed vertical hydraulic conductivity of 25 m d^{-1} to 45 m d^{-1}, the estimated Darcy

velocity ranges from 5 m d^{-1} to 50 m d^{-1}. This estimate is not directly comparable to any of the other methods described here because of the different process that each method measures. However, this estimated velocity is likely considerably higher than the actual Darcy velocity in the field.

The obvious weakness of the temperature profile method is the assumption that the measured temperature profile represents the warmest temperature profile. This assumption was made to establish an upper bound of vertical seepage based on available data, and was reasonable considering the profile was collected shortly after the warmest groundwater temperatures were collected in August. In order to use a single temperature profile for groundwater seepage estimates, steady-state conditions must prevail. With our field evidence suggesting non-steady state at this location (two inflection points in the temperature profile curve), the temperature envelope method is most appropriate. However, without several temperature profiles at this location spanning an annual cycle, there is high uncertainty as to whether the temperature envelope developed in this exercise is truly representative of the annual temperature envelope. If the temperature envelope underestimates the maximum temperature oscillation at any depth, the seepage velocity has also been underestimated.

A sensitivity analysis was conducted to determine the magnitude by which this assumption may underestimate seepage. A 3 ºC increase in temperature measured at 6 m below the surface (at which the envelope is tangent to the profile) results in a seepage increase by approximately an order of magnitude. There is also some reasonable variability in the volumetric heat capacity estimation of the aquifer materials, as this parameter is dependent on bulk density data and this data was not collected in the field. Over the range of estimated volumetric heat capacities for the borehole sediments (2.3×10^6 to 2.8×10^6 J m^{-3} C^{-1}), seepage velocities are downward between 6 mm d^{-1} and 9 mm d^{-1}. There is a greater possible range of thermal conductivity values for coarse aquifer materials. Thermal conductivity values of 1.2 W m^{-1} C^{-1} to

2.5 W m^{-1} C^{-1} result in a downward seepage estimate of 6 mm d^{-1} to a very slight upward seepage (<1 mm d^{-1}). It should be noted that this velocity represents the velocity based on this temperature profile and calculated envelope only, and that it does not represent a constant seepage velocity over an extended period as groundwater velocity is sensitive to the hydraulic gradient, which may fluctuate with changes in river stage.

The lab-reported error for the ^{3}H measurements are up to ±0.26 TU, which is equivalent to an uncertainty in groundwater age of less than one year. Though groundwater age in the borehole is well constrained by the tritium data, this data does not indicate the magnitude of the vertical groundwater component. Assuming purely vertical flow and a linear infiltration rate, the groundwater age data indicates a maximum infiltration rate of 7 mm d^{-1} over the length of the borehole. However, it is unlikely that purely vertical flow exists in the riparian zone, but that a horizontal flow component also exists, likely leading seepage rates estimated by ^{3}H to overestimate actual seepage in the study area. This is also suggested by the non-monotonic increase in groundwater age with depth (profile shows a 3 m interval in the middle of the borehole with older groundwater than that of the intervals directly above or below it, Fig. 11). A purely vertical downward flow would exhibit a monotonic age increase with depth. Though it is possible that groundwater mixing in the borehole vicinity may have led to the ^{3}H profile shown, the temperature profile from the borehole does not indicate groundwater mixing. Another possible explanation is that a low-hydraulic conductivity layer at depth could exhibit higher groundwater ages compared to the surrounding depths. There was no lithological evidence during drilling of the borehole to indicate a low-conductivity layer at depth, though the streambed and alluvial sediments are known to contain lenses of silt and clay at depths ranging from 3 m to 7 m within the area (Chen, 2011). It should also be noted that the presence of age stratification in the riparian zone is possible without any vertical component to groundwater flow in the area. Similar to the results of Puckett et al. (2002), purely horizontal flow paths may demonstrate the same age

stratification. Deeper flow paths represent older groundwater that has traveled relatively farther than the shallow, younger flow path.

The estimated maximum vertical flux rate indicated by ^{3}H is within 1 mm d^{-1} of that indicated by the temperature profile method, and within an order of magnitude of estimated groundwater seepage given the uncertainty in aquifer thermal properties, as described above. It is reasonable to conclude that, despite the uncertainties in the temperature profile method introduced by calculating the temperature envelope based on a single temperature profile, the temperature profile method may also provide an estimate of the maximum downward flow component to groundwater flow in the riparian zone.

The seepage meter results contrast with the transducer, ^{3}H, and temperature profile results. Uncertainty in the seepage flux from the seepage meter can be a result of the limited lateral and vertical extent covered by the seepage cylinder during the test. The seepage meter is only representative of the depth and area over which the seepage cylinder is inserted. Therefore, it is representative of the shallowest flux conditions relative to the piezometers and data collected in the borehole. Additionally, it is possible that trapped air, friction within the seepage meter or tubing, or disturbance of the bed sediments may lead to errors in the fluid gained or lost from the seepage bag relative to actual seepage. Certainty in the seepage meter measurements could increase by collecting at least three measurements on a single day at different locations within the river bed for comparison.

One reasonable explanation for the contrast with the seepage meter data compared to the other methods at the beginning of the study is that the seepage meter was under the influence of hyporheic flow though the overall regime was downward flow (Kalbus et al., 2006). That is, riffles and pools along the streambed can induce hyporheic flow in which surface water cycles through the streambed, infiltrating into the shallow sediments and discharging back to the surface at a short distance downstream (Hill et al., 1998; Cardenas et al., 2004). As the seepage cylinder

is representative of the uppermost ~0.2 m depth, it is possible that hyporheic flow was occurring in these sediments, leading to an upward flux into the seepage meter despite the overall water table decline. In addition, the seepage meter also gives the shortest temporal representation relative to the other methods in this study. Seepage meter tests generally lasted 1.5 hours, and ceased when the river channel became dry. This is in contrast to the high-temporal resolution of the piezometers, which are more useful for drawing conclusions over the entire study period.

The conclusion that primarily horizontal flow paths exist near the river are consistent with the conceptual model for shallow flow systems in which the river and aquifer are hydraulically connected; flow toward or away from the river is expected to have a greater component of horizontal rather than vertical flow (Winter et al., 1999). This conclusion is strongly a result of ^{3}H and NO_3^- (presented in Chapter 2) concentrations measured in the borehole. An additional interpretation of the non-monotonic increase in groundwater age with depth is that cyclicity in the gaining/losing regime of groundwater near the river. It is plausible that variability in the vertical flow component (seasonally, or less frequent) may have disrupted groundwater flow and subsequently groundwater ages in the riparian zone.

It is outside the scope of this study to determine the cause for groundwater decline over the period. However, the area experienced a severe to exceptional drought during summer 2012, and it is likely that groundwater pumping for irrigation purposes was compounded by the lack of precipitation, causing groundwater levels to decline up to a meter in the study area (Fig. 7). Following water table decline, water flowing in the river channel would begin recharging the alluvial aquifer, as indicated by the June 29th seepage meter test. Within a week following this seepage meter test, there was zero flow in the river channel. Overall, these results are useful for interpretation of the hydrochemistry presented in the following chapters. Understanding of the physical hydrology of the study site is important for determining the potential impact of

groundwater mixing or unsaturated zone processes on shallow groundwater chemistry, as well as general groundwater flow within the study reach.

5.0 CONCLUSION

Four methods were employed to estimate the magnitude and direction of vertical groundwater flow in the central Platte River channel during an exceptional drought in summer 2012. This data was used to develop a conceptual model about the overall groundwater flow regime, and the interaction between groundwater and surface water in the study area during the study period. High temporal resolution water level data from the river and eight island piezometers exhibited downward vertical hydraulic gradients, indicating that the Platte River was recharging the alluvial aquifer through the 2012 summer, as a result of groundwater table decline, possibly induced by groundwater pumping for irrigation. Diurnal water table fluctuations of 20-30 mm resulting from evapotranspiration were apparent from water level data in both the vegetated and non-vegetated islands. A seepage meter for use in flowing water was constructed and used to estimate seepage in the shallow river sediments. The meter indicated net upward flow in shallow hyporheic zone sediments early in the study, likely a result of transient hyporheic flow.

Temperature and ^{3}H data were collected from a riparian zone borehole at intervals up to 15 m deep. Temperature was used as a tracer to develop a temperature envelope and estimate vertical groundwater seepage. Tritium concentrations indicated older groundwater (~ 6 years) at 15 m below the surface, and younger groundwater (<2 years) at the water table approximately 3 m below the surface. The temperature and ^{3}H methods, similar to the water level data, indicated a vertical downward flow component to groundwater flow of < 10 mm d^{-1}. This conceptual model is useful for the interpretation of geochemical data and temporal variations in groundwater geochemistry described in the following chapters.

Table 1.1. Parameters and respective values used in modeling of the temperature envelope.

Parameter	Description	Value	Dimension
c_0	Heat capacity of water	4.18×10^3	J Kg^{-1} C^{-1}
ρ_0	Density of water	1×10^3	Kg m^{-3}
$c\,\rho$	Volumetric heat capacity of aquifer materials	2.6×10^6	J m^{-3} C^{-1}
k	Aquifer thermal conductivity	2.2	W m^{-1} C^{-1}
τ	Period of surface temperature oscillation	3.15×10^7	s
T_z	Ground water temperature	13	°C
T_m	Mean surface water temperature	12.5	°C
A_{z0}	Amplitude of surface oscillation	16	°C
A_z	Amplitude of temperature fluctuation about the mean at depth z	varies	°C
q	Fluid flux	varies	L T^{-1}
a	Parameter characterizing thermal properties and groundwater velocity	0.266	--

Table 1.2. Range of water level data collected by the pressure transducers in the island and riverbed piezometers

Piezometer	Max water level (m)	Min water level (m)	Pulse flow peak (m)
AV1	0.727	-0.022	0.229
AV2	0.046	-0.024	--
AV3	0.719	-0.053	0.238
AV4	0.636	-0.029	0.111
AN5	0.737	-0.016	0.185
AN6	1.211	0.169	0.589
AN7	0.917	0.019	0.409
AN8	0.952	-0.003	0.381
River	0.81	-0.020	0.635

Table 1.3. Range of data for vertical hydraulic gradients, calculated from water level data from three piezometer nests. No vertical hydraulic gradient data was available for piezometer nest 1 & 2, as piezometer AV2 was installed above the water table.

Piezometer Pair	**Minimum VHG (m/m)**	**Maximum VHG (m/m)**	**Average VHG (m/m)**	**Range**
Vegetated: 3 & 4	0.77	1.09	0.97	0.32
Non-vegetated 5 & 6	0.20	0.74	0.36	0.54
Non-vegetated 7 & 8	0.90	1.11	1.00	0.21

Table 1.4. Temperature, tritium, and groundwater age data for multi-level sampling in the riparian zone borehole. eTU represents one standard deviation.

Sample Name	Sample Date	Depth below surface (m)	Temperature (C)	^{3}H (TU)	eTU	Age (yr)
River	13-Sep-12	0	23.4	8.02	0.26	0
PR 10	13-Sep-12	3.1	24.1	7.43	0.25	1.4
PR 15	13-Sep-12	4.6	22.2	7.30	0.24	1.7
PR 20	13-Sep-12	6.1	19.6	7.37	0.24	1.5
PR 25	13-Sep-12	7.6	16.5	6.51	0.21	3.7
PR 30	13-Sep-12	9.1	14.0	5.95	0.20	5.3
PR 35	13-Sep-12	10.7	13.3	6.11	0.20	4.8
PR 40	12-Sep-12	12.2	13.0	6.67	0.22	3.3
PR 45	12-Sep-12	13.7	13.0	6.55	0.19	3.6
PR 50	12-Sep-12	15.2	13.0	6.07	0.26	6.1

6.0 REFERENCES

Anderson, M.P., 2005, Heat as a ground water tracer: Ground Water, v. 43, p. 951-968.

Anibas, C., Fleckenstein, J.H., Volze, N., Buis, K., Verhoeven, R., Meire, P., and Batelaan, O., 2009, Transient or steady-state? Using vertical temperature profiles to quantify groundwater–surface water exchange: Hydrological Processes, v. 23, p. 2165-2177.

Bartolino, J.R., and Niswonger, R.G., 1999, Numerical simulation of vertical ground-water flux of the Rio Grande from ground-water temperature profiles: U.S. Geological Survey Water-Resources Investigation Report 99-4212.

Böhlke, J.K., Verstraeten, I.M., and Kraemer, T.F., 2007, Effects of surface-water irrigation on sources, fluxes, and residence times of water, nitrate, and uranium in an alluvial aquifer: Applied Geochemistry, v. 22, p. 152-174.

Bredehoeft, J.D., and Papadopulos, I.S., 1965, Rates of vertical groundwater movement estimated from the earth's thermal profile: Water Resources Research, v. 1, p. 325-328.

Cardenas, M.B., Wilson, J.L., and Zlotnik, V.A., 2004, Impact of heterogeneity, bed forms, and stream curvature on subchannel hyporheic exchange: Water Resources Research, v. 40.

Chen, X., Dong, W., Ou, G., Wang, Z., and Liu, C., 2013, Gaining and losing stream reaches have opposite hydraulic conductivity distribution patterns: Hydrology and Earth System Sciences, v. 17, p. 2569-2579.

Chen, X., 2011, Depth-dependent hydraulic conductivity distribution patterns of a streambed: Hydrological Processes, v. 25, p. 278-287.

Chen, X., 2007, Hydrologic connections of a stream-aquifer-vegetation zone in south-central Platte River valley, Nebraska: Journal of Hydrology, v. 333, p. 554-568.

Chen, X., and Shu, L., 2006, Groundwater evapotranspiration captured by seasonally pumped wells in river valleys: Journal of Hydrology, v. 318, p. 334-347.

Chen, X., and Shu, L., 2002, Stream-aquifer interactions: Evaluation of depletion volume and residual effects from ground water pumping: Ground Water, v. 40, p. 284-290.

Cheng, C., Song, J., Chen, X., and Wang, D., 2011, Statistical distribution of streambed vertical hydraulic conductivity along the Platte River, Nebraska: Papers in Natural Resources, Paper 362.

Condon, S.M., 2005, Geologic studies of the Platte River, south-central Nebraska and adjacent areas, geologic maps, subsurface study, and geologic history: Publications of the US Geological Survey, Paper 1706.

Constantz, J.E., and Stonestrom, D.A., 2003, Heat as a tracer of water movement near streams, *in* Stonestrom, D.A. and Constantz, J.E., eds., Heat as a tool for studying the movement of ground water near streams: USA, U.S. Geological Survey Circular 1260, p.1-6.

Constantz, J.E., and Thomas, C.L., 1996, The use of streambed temperature profiles to estimate the depth, duration, and rate of percolation beneath arroyos: Water Resources Research, v. 32, p. 3597-3602.

Eaton, B.C., Millar, R.G., and Davidson, S., 2010, Channel patterns: Braided, anabranching, and single-thread: Geomorphology, v. 120, p. 353-364.

Eschner, T.R., 1983, Hydraulic Geometry of the Platte River near Overton, south-central Nebraska, *in* Eschner, T.R., Hadley, R.F. and Crowley, K.D., eds., Hydrologic and geomorphic studies of the Platte River basin: Washington, D.C., U.S. Geological Survey Professional Paper 1277.

Eschner, T.R., Hadley, R.F., and Crowley, K.D., 1983, Hydrologic and morphologic changes in channels of the Platte River basin in Colorado, Wyoming, and Nebraska: A historical perspective, *in* Eschner, T.R., Hadley, R.F. and Crowley, K.D., eds., Hydrologic and geomorphic studies of the Platte River basin: Washington, D.C., U.S. Dept. of the Interior, Geological Survey Professional Paper 1277.

Fotherby, L.M., 2009, Valley confinement as a factor of braided river pattern for the Platte River: Geomorphology, v. 103, no. 4, p. 562-576.

Harvey, F.E., and Sibray, S.S., 2001, Delineating ground water recharge from leaking irrigation canals using water chemistry and isotopes: Ground Water, v. 39, p. 408-421.

Hill, A.R., Labadia, C.F., and Sanmugadas, K., 1998, Hyporheic zone hydrology and nitrogen dynamics in relation to the streambed topography of a N-rich stream: Biogeochemistry, v. 42, no. 3, p. 285-310.

Horn, J.D., Joeckel, R.M., and Fielding, C.R., 2012, Progressive abandonment and planform changes of the central Platte River in Nebraska, central USA, over historical timeframes: Geomorphology, v. 139, p. 372-383.

Hurr, T.E., 1983, Groundwater hydrology of the Mormon Island Crane Meadows Wildlife Area near Grand Island, Hall County, Nebraska: U.S. Geological Survey Professional Paper 1277-H.

Joeckel, R.M., and Henebry, G.M., 2008, Channel and island change in the lower Platte River, Eastern Nebraska, USA: 1855-2005: Geomorphology, v. 102, p. 407-418.

Kalbus, E., Reinstrof, F., and Schirmer, M., 2006, Measuring methods for groundwater-surface water interactions: a review: Hydrology and Earth System Sciences, v. 10, p. 873-887.

Kilpatrick, J.M., 1996, Temporal changes in the configuration of the water table in the vicinity of the management systems evaluation area site, central Nebraska: USGS Water-Resources Investigations Report: 94-4173.

Korus, J.T., and Joeckel, R.M., 2011, Generalized geologic and hydrostratigraphic framework of Nebraska 2011, ver. 2: Conservation and Survey Division, School for Natural Resources, Institute of Agriculture and Natural Resources, University of Nebraska-Lincoln. Geologic Maps and Charts (GMC) 38.

Landon, M.K., Rus, D.L., and Harvey, F.E., 2001, Comparison of instream methods for measuring hydraulic conductivity in sandy streambeds: Ground Water, v. 39, p. 870-885.

Lane, S., 1995, The dynamics of dynamic river channels: Geography, v. 80, p. 147-162.

Lapham, W.W., 1989, Use of temperature profiles beneath streams to determine rates of vertical ground-water flow and vertical hydraulic conductivity: U.S. Geological Survey Water-Supply Paper 2337.

Leopold, L.B., and Wolman, M.G., 1957, River channel patterns: Braided, Meandering and straight: Washington, DC, US Geological Survey Professional Paper 282-B, 49 p.

Michel, R.L., 2005, Tritium in the hydrologic cycle, *in* Aggarwal, P.K., Gat, J. and Froehlich, K.F.O., eds., Isotopes in the water cycle: Past, present and future of a developing science: Dordrecht, The Netherlands, International Atomic Energy Agency, p. 53-66.

National Climatic Data Center (NCDC), 2013, National Climatic Data Center Global Historical Climatology Network-Grand Island Weather Station: http://www.ncdc.noaa.gov/.

Peckenpaugh, J.M., and Dugan, J.T., 1983, Hydrogeology of parts of the Central Platte and Lower Loup Natural Resources Districts, Nebraska: Lincoln, Nebraska, U.S. Geological Survey Water-Resources Investigations Report 83-4219, 110 p.

Piégay, H., Grant, G., Nakamura, F., and Trustrum, N., 2006, Braided river management: from assessment of river behavior to improved sustainable development, *in* Sambrook-Smith, G.H., Best, J.L., Bristow, C.S. and Petts, G.E., eds., Braided Rivers: Process, deposits, ecology, and management: USA, Special Publication 36 of the International Association of Sedimentologists, p.257-275.

Puckett, L.J., Cowdery, T.K., McMahon, P.B., Tornes, L.H., and Stoner, J.D., 2002, Using chemical, hydrologic, and age dating analysis to delineate redox processes and flow paths in the riparian zone of a glacial outwash aquifer-stream system: Water Resources Research, v. 38.

Rosenberry, D.O., 2008, A seepage meter designed for use in flowing water: Journal of Hydrology, v. 359, p. 118-130.

Rosenberry, D.O., LaBaugh, J.W., and Hunt, R.J., 2008, Use of monitoring wells, portable piezometers, and seepage meters to quantify flow between surface water and ground water, *in* Rosenberry, D.O. and LaBaugh, J.W., eds., Field techniques for estimating water fluxes between surface water and ground water, US Geological Survey Techniques and Methods Chapter 4-D2, p.43 - 70.

Smith, N.D., 1971, Transverse bars and braiding in the Lower Platte River, Nebraska: Geological Society of America Bulletin, v. 82, no. 12, p. 3407-3420.

Solomon, D.K., and Sudicky, E.A., 1991, Tritium and He-3 isotope ratios for direct estimation of spatial variations in groundwater recharge: Water Resources Research, v. 27, no. 9, p. 2309-2319.

Stallman, R.W., 1965, Steady one-dimensional fluid flow in a semi-infinite porous medium with sinusoidal surface temperature: Journal of Geophysical Research, v. 70, p. 2821-2827.

Stonestrom, D.A., and Blasch, K.A., 2003, Determining temperature and thermal properties for heat-based studies of surface-water ground-water interactions, *in* Constantz, J.E. and Stonestrom, D.A., eds., Heat as a tool for studying the movement of groundwater near streams, U.S. Geological Survey Circular 1260, p.73-80.

Suzuki, S., 1960, Percolation measurements based on heat flow through soil with special reference to paddy fields: Journal of Geophysical Research, v. 65, p. 2883-2885.

Taniguchi, M., 1993, Evaluation of vertical groundwater fluxes and thermal properties of aquifers based on transient temperature-depth profiles: Water Resources Research, v. 29, p. 2021-2026.

Williams, G.P., 1978, The case of the shrinking channels--the North Platte and Platte Rivers in Nebraska: Geological Survey Circular 781.

Winter, T.C., Harvey, J.W., Franke, O.L., and Alley, W.M., 1999, Ground water and surface water a single resource: Denver, CO, US Geological Survey, Circular 1139, 79 p.

Chapter 2

Potential for and Evidence of Denitrification in Riparian and Transient Parafluvial Zones

1.0 INTRODUCTION

1.1 Environmental Impact of Nitrate Contamination

Human impact on the nitrogen cycle through application of nitrogen fertilizers has led to increased NO_3^- in groundwater and surface water due to leaching and runoff, with implications for ecosystem health and groundwater quality (Galloway et al., 2004; Schlesinger et al., 2006). Non-point source NO_3^- pollution is one of the most common agricultural contaminants in the Midwestern U.S. (Schlesinger et al., 2006), including Nebraska (Exner and Spalding, 1990; Exner and Spalding, 1994). Excess N in surface water can cause eutrophication in lakes and coastal zones (McIsaac et al., 2001), and often exceeds drinking water standards (10 mg L^{-1} NO_3-N) in groundwater (McMahon et al., 2008). Excessive NO_3^- in drinking water can lead to methemoglobinemia in children (an impairment of the body's ability to transport oxygen through the bloodstream). Additionally, the widespread nature of groundwater NO_3^- contamination and the relatively high costs of treatment complicate remediation efforts. However, as part of the global nitrogen cycle, several processes such as denitrification can serve locally as a sink for environmental NO_3^-.

1.2 Denitrification in Groundwater

Denitrification is the microbially-mediated chemical reduction of NO_3^- (the most oxidized form of nitrogen) to N_2 through a series of oxidation-reduction reactions. When oxygen becomes depleted in groundwater (usually less than 2 mg L^{-1}, Bates and Spalding, 1998; Böhlke et al., 2002; McMahon et al., 2004; Tesoriero and Puckett, 2011; Liao et al., 2012), NO_3^- may serve as the electron acceptor in the oxidation of organic matter. The general denitrification reactions, including intermediate reactions, take the general form (Istok et al., 1997):

$$\begin{aligned} CH_2O + NO_3^- &\rightarrow NO_2^- + H_2O + CO_2 \\ CH_2O + NO_2^- &\rightarrow NO + H_2O + CO_2 \\ CH_2O + NO &\rightarrow N_2O + H_2O + CO_2 \\ CH_2O + N_2O &\rightarrow N_2 + H_2O + CO_2 \end{aligned} \qquad (2.1)$$

(Note that these equations are for illustration and not balanced). As water becomes increasingly depleted in O_2, NO_3^- is typically the next thermodynamically favored electron acceptor. (Following denitrification of available NO_3^-, MnO_2, $Fe(OH)_3$, and SO_4^- will subsequently serve as electron acceptors as the water becomes increasingly reducing, assuming that none of these compounds are a limiting oxidant.) Though the most common electron donor in denitrification is organic carbon, other reduced species may also serve as donors, such as FeS_2 (Böhlke et al., 2002). Denitrification is the only permanent sink for reactive N in groundwater, as opposed to temporary restriction such as plant uptake or microbial immobilization (Mariotti et al., 1988; Grimm and Fisher, 1984; Ranalli and Macalady, 2010; Tesoriero and Puckett, 2011).

1.3 Controls on Aquifer Denitrification

Denitrification rates in aquifers depend primarily on the concentrations of O_2 and available electron donors. Aquifers have been shown to be effective sinks for NO_3^- (Böttcher et al., 1990; Wilson et al., 1990), if residence times are sufficient for O_2 reduction and there is a supply of organic carbon. Tesoriero and Puckett (2011) found a range of denitrification rates of 0.21 to >3.9 mg N L^{-1} yr^{-1} throughout coastal plain, alluvial and glacial outwash aquifers. These rates are similar to those found by Liao et al. (2012) in a vertical transport model based on measured aquifer characteristics from 14 United States locations. However, many aquifers may be limited in organic carbon or other suitable electron donors (Starr and Gillham, 1993; Tesoriero and Puckett, 2011; Krause et al., 2013), preventing the reduction of NO_3^-, and eventually causing groundwater to serve as a source of NO_3^- to surface water (Puckett et al., 2002; Krause et al., 2009).

1.4 Controls on Riverbed and Riparian Denitrification

Riverbeds and the riparian zone often experience relatively high denitrification rates because of the comparably higher organic carbon quantity and quality in these zones, compared to aquifers, leading to greater redox potential (Hill, 1996; Boulton et al., 1998; Hill et al., 1998; Ostrom et al., 2002; Hill and Cardaci, 2004; Mulholland et al., 2004; Puckett and Hughes, 2005; Tesoriero and Puckett, 2011; Zarnetske et al., 2011; Krause et al., 2013). Sources of organic carbon in riverbed and riparian zones may include buried organic layers among fluvial sediments (Krause et al., 2013), or densely vegetated zones. Mulholland et al. (2004) found published denitrification rates in streams and rivers ranged from 0 to 1400 μmol m^{-2} h^{-1}, with generally higher rates in agricultural watersheds. Specifically in riverbeds, exchange processes in the zone where groundwater and surface water mix (hyporheic zone, HZ) are strongly driven by

geomorphology and related hydraulic head gradients (Brunke and Gonser, 1997; Cardenas et al., 2004; Shope et al., 2012). This exchange can lead to the development of physiochemical gradients at the exchange interface (Brunke and Gonser, 1997), or chemical transformation "hotspots" (Boulton et al., 1998; Zarnetske et al., 2011). Krause et al. (2013) found the upper 1.5 m of streambed sediments to be a denitrification hotspot due to buried organic layers; the NO_3^- concentration of upwelling groundwater decreased by 15 mg NO_3-N L^{-1} in the upper 15 cm, and 24 mg NO_3-N L^{-1} in the 15-150 cm depth (River Tern sands and gravels, Central United Kingdom).

1.5 Methods for Denitrification Quantification

The denitrification process is difficult to measure in the field, and numerous techniques have been developed to determine denitrification potential and calculate denitrification rates in-situ and in the lab (Groffman et al., 2006). Given inherent uncertainty with many methods, multiple approaches are generally preferred in order to reduce uncertainty of individual methods. Hyporheic and riparian denitrification studies have been performed using both in-situ and laboratory methods to measure denitrification rates and potential. In-situ methods commonly utilize shallow piezometers in the river bed, river bank, or both, in order to compare water quality and field parameters at different depths and locations. Some studies have analyzed water evolution along a flow path in the shallow subsurface (Hill et al., 1998; Puckett et al., 2002). Others have used an array of shallow piezometers to investigate nitrogen dynamics as they relate to river bed geomorphology (Holmes et al., 1996; Krause et al., 2009). Tracer tests have also been utilized in single well injection/extraction experiments (Istok et al., 1997) or along a stream reach to determine denitrification in a hydraulically-connected gravel bar (Zarnetske et al., 2011).

Laboratory experiments have been used independently and coupled with field experiments to determine sediment denitrification potential (Starr and Gillham, 1993; Holmes et al., 1996; Puckett et al., 2002). The acetylene block technique is a common lab method to measure denitrification potential. Sediments are collected and saturated with NO_3^--spiked water (Yoshinari and Knowles, 1976; Smith et al., 1978). The headspace above the sediment matrix must be evacuated, commonly with nitrogen (Smith et al., 1991; Holmes et al., 1996; Woodbury et al., 2001) or argon gas (Hill and Cardaci, 2004) to ensure anaerobic conditions. Finally, acetylene gas (C_2H_2), which blocks the reduction of N_2O to N_2 in the final step of the denitrification process, is added at approximately 0.1 atm. N_2O, the production of which is linear within 3-10 hours following anaerobisis (Smith and Tiedje, 1979), can then be measured by gas chromatography to determine denitrification rates.

There are a number of diverse applications for the acetylene block method. Hill and Cardaci (2004) and Puckett et al. (2002) used soil microcosm studies to investigate potentially carbon-limited zones along a ground water flow path. Smith et al. (1991) similarly relied on microcosm experiments to delineate redox-reactive zones from non-reactive zones in the vicinity of a NO_3^- plume. Smith and Tiedje (1979) utilized the isolation of discrete areas within the soil zone allowed by microcosm experiments for investigation into how heterogeneities, such as roots, may impact soil denitrification. Microcosm experiments also allow for determination of potential limiting factors such as organic carbon or NO_3^- concentration (Starr and Gillham, 1993; Hill and Cardaci, 2004).

The method is limited, however, to providing insight to denitrification potential and rate-limiting steps only, and cannot be relied on for the occurrence of in situ denitrification or in situ denitrification rates. Overestimation of in situ rates can occur if field conditions are typically oxic rather than reducing, NO_3^- removal is dominated by biotic uptake rather than denitrification

(Grimm and Fisher, 1984), or NO_3^- is a limiting oxidant in the study area. Underestimation may occur due to the disturbed nature of the samples, or the fact that C_2H_2 inhibits NO_3^- production through nitrification (Groffman et al., 2006).

1.6 Objectives

This study was undertaken to determine whether the HZ and riparian sediments of a braided river serve as a NO_3^- sink in an agricultural watershed with high- NO_3^- groundwater. Specifically, this study investigated the pore-water of river islands in the Platte River, where river and groundwater may mix during high-flow periods. Brunke and Gonser (1997) found that braided-type rivers held the most potential for vertical and lateral exchange processes resulting from high sediment porosity and rapid channel migration, compared to meandering, anastomosing, or straight channels. It is these lateral and vertical exchange processes that we anticipate may serve to juxtapose high-NO_3^- groundwater and organic carbon present in shallowly buried organic-rich layers, and result in potentially high rates of denitrification in the islands. This study differs from much of the previous work by the high temporal resolution (weekly) at which full major ion chemistry and field parameters were measured, as well as focusing specifically on nitrogen cycling within fluvial islands, rather than riverbed sediments. Our experimental design served to investigate these research questions:

1) Do the island sediments, similar to river bed sediments, exhibit reducing conditions and sufficient organic carbon to potentially serve as a NO_3^- sink?

2) Is there any evidence (low NO_3^-, low Ar/N_2 ratios) for in-situ denitrification in the saturated island sediments in the study area?

We hypothesize that low O_2 and high-NO_3^- groundwater discharges to the river through the islands, which supply sufficient organic carbon for denitrification to occur, and that stream NO_3^- concentrations are low as a result of this process. In addition, we hypothesize that controlled tests of island sediment denitrification potential as well as intermediate denitrification N-compounds (NO_2^-, N_2O) will indicate ongoing denitrification in the islands.

2.0 METHODS

2.1 Study Area

Please refer to Chapter 1, Sections 1.1 and 1.2 for a detailed description of the regional geology and study area. In addition, NO_3^- is a pervasive contaminant in many shallow Nebraska aquifers, particularly in southern Nebraska and the lower Platte basin where heavy agriculture and extensive irrigation are present (Fig. 12).

2.2 Field Methods

2.2.1 Riverbed and Islands

Please refer to Chapter 1, Section 2.0 for a detailed description of the experimental setup. In addition, total alkalinity (approximated by HCO_3^-) was measured in the field by titration to approximately pH 4.5 with H_2SO_4. Nitrite was measured in 71 samples with a CHEMetrics VACUettes colorimetric test kit. Samples collected for major ion and stable isotope analyses were filtered through a 0.45 μm nylon filter and field cooled in 8 mL plastic bottles. Cation samples were preserved by addition of nitric acid in the field to pH <2. Select piezometers were also sampled for dissolved organic carbon. Samples were filtered into 40 mL clear glass vials and preserved with H_2SO_4.

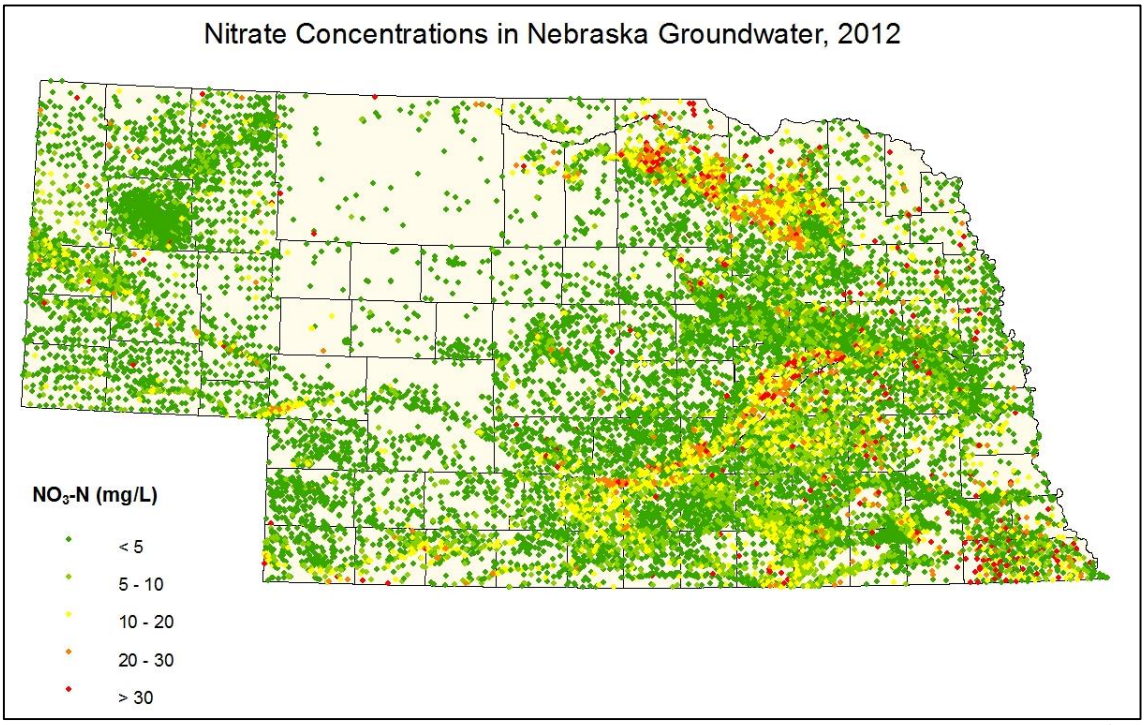

Figure 12. Nitrate concentrations in groundwater, 2012. Measurements are as NO_3-N in mg L^{-1}. The federal drinking standard is 10 mg L^{-1}. The highest concentrations are found in the Platte (south-central) and Elkhorn (north-east) river basins. Nitrate data is from the Nebraska Department of Environmental Quality.

Two dissolved argon and nitrogen gas samples were collected from two non-vegetated island piezometers in 100 mL air-tight glass syringes fitted with a syringe valve. After temperature and dissolved oxygen readings stabilized, back-pressure was maintained on the pump to prevent sample degassing and the syringe was connected to the pump tubing with a luer lock fitting. All syringes were field-cooled on ice and stored at 4 ºC. Only two dissolved gas samples were collected because of the drought condition; many of the island piezometers were partially dry or dry during the second half of the study period and these conditions were not favorable for sampling of dissolved gases in groundwater. All of the above methods were also used for water and dissolved gas sampling at the river and a groundwater monitoring well, approximately 1 km south of the study site with a screen depth 30 m below the surface (Fig. 3).

Sediment for a microcosm test was collected from the vegetated island in two locations, both near piezometer AV1 and approximately 50 cm from the surface. The sampled depth was targeted due to fine-grained, dark, organic-rich characteristics.

2.2.2 Riparian Zone Borehole

A 15 m deep borehole was drilled below the water table (approximately 3 m below surface during sampling) and adjacent to the stream channel with a 17 cm hollow-stem auger. Upon reaching the final boring depth, a PVC casing with a 1.5 m screen was lowered into the borehole. A submersible pump was used for sample collection. Field parameters were monitored until stable, in the same manner as in the islands. The screen was then lifted 1.5 m, and the process was repeated. Dissolved gas, ion, isotope samples, and field parameters were collected from multiple intervals in the borehole using the methods described above.

2.3 Laboratory Methods

All samples were refrigerated in the laboratory and analyzed at the University of Nebraska—Lincoln. Anions (Cl^-, SO_4^{2-}, NO_3^-) and cations (Ca^{2+}, Mg^{2+}, Na^+, K^+) were analyzed via ion chromatography (Dionex ICS-2100 five and four-standard calibration respectively; detection limit = 0.1 mg L^{-1}). Calibration standards were analyzed for every ten unknown samples, and a method blank included in every analytical batch. Charge balance error was within 10% for most samples (exceptions noted in Appendix A). Stable isotopes of water ($\delta^{18}O$, δ^2H) were analyzed by a Picarro Cavity Ringdown Spectrometer (analytical precision= ±0.2 $\delta^{18}O$‰, ±2 δ^2H‰ VSMOW). Dissolved gas samples were analyzed by Micromass Optima Dual Inlet IRMS following the methods of Martin et al. (1995) at the University of Nebraska Water Sciences Laboratory, within three days of collection. Dissolved organic carbon samples were

analyzed via persulfate oxidation (SM 5310 C) using an OI 1010 Organic Carbon Analyzer at the University of Nebraska Water Sciences Laboratory.

2.3.1 N_2O

Twenty-five samples were collected from the borehole and select piezometers for analysis of nitrous oxide (N_2O). Water samples were injected into stoppered, helium-flushed clear glass serum bottles. Prior to gas analysis, samples equilibrated in a 20 °C water bath. Headspace analysis was completed by gas chromatography (model SRI 8610C) at the University of Nebraska USDA Agricultural Research Service Laboratory.

2.3.2 Microcosm Tests

In order to evaluate denitrification potential of sediments in islands during high flow periods, sediment samples were collected for laboratory-controlled microcosm tests, similar to those previously described. Three tests (Microcosm I, II, and Control) were conducted using stoppered serum bottles, with four replicates each. Microcosms I & II contained 10 g of island sediment. Pore water from the study area was amended with $NaNO_3$ to create an approximate 5 mM $NaNO_3$ solution. Microcosm I was slurried with the 5 mM $NaNO_3$ solution only. Microcosm II was slurried with a solution of 5 mM NO_3^- and 2.5 mM glucose ($C_6H_{12}O_6$). The control serum bottles contained only the NO_3^- + glucose solution and no sediments. No antibiotic was added to prevent the growth of denitrifiers. All twelve serum bottles were sealed with a rubber septa, and made anaerobic by purging with helium for approximately two minutes.

Seven 1 mL aliquots were collected from each jar over a 48 hour period and immediately frozen for later analysis. NO_3^- + NO_2^- was determined in each sample colorimetrically by the Griess-Illosvay method using a Lachat flow injection ion analyzer (Zellweger Analytics, Lachat

Instruments Div., Milwaukee, WI) equipped with a copperized cadmium reduction column at the University of Nebraska USDA Agricultural Research Service Laboratory. In between sampling events, the stoppered serum bottles were stored at 25 °C.

2.4 Denitrification Systematics and Hydrochemistry

2.4.1 Ar/N_2

The presence of excess of N_2 compared to that expected in water equilibrated with the atmosphere can be an indicator of denitrification (Wilson et al., 1990; Puckett et al., 2002; Groffman et al., 2006; Green et al., 2010). The only sources for N_2 in groundwater are microbial denitrification and the atmosphere (p_{N2} = 0.78). Sources for Ar include the atmosphere (p_{Ar} = 0.009) and radiogenic Ar from the potassium decay series, though this source is very small (estimated 8 x 10^{-4} ml Ar L^{-1} H_2O per 10^6 yr for sedimentary aquifers, Almon and Magaritz, 1990). Using Henry's Law, Ar/N_2 gas in air-saturated water (ASW) can be calculated for any given recharge temperature, and then compared with the measured gas ratio. Because the Ar source in groundwater is minimal, denitrification is the main process that can change the Ar/N_2 from that expected in ASW. Therefore, Ar/N_2 estimates are a useful indicator of whether, and to what extent, denitrification has occurred. Ar/N_2 is often reported using δ-notation with units of per mil (‰), calculated as:

$$\left(\frac{R_{sample}}{R_{standard}} - 1\right) * 1000 \qquad (2.2)$$

where R is equivalent to Ar/N_2 and the reference standard is atmospheric Ar/N_2. By definition, the δAr/N_2 of the standard "air" is 0.0‰. δAr/N_2 for ASW at the study area was calculated after

Benson and Krauss (1976); at an estimated recharge temperature of 20 °C, $\delta Ar/N_2$ in air-saturated water at 500 m above sea level is approximately 1180‰.

2.4.2 $\delta^{15}N$-N_2

Nitrogen isotopes are frequently used to indicate that denitrification has occurred (Smith et al., 1991; Böhlke and Denver, 1995; Böhlke et al., 2002; Fukada et al., 2003; Böhlke et al., 2004; Green et al., 2010; Zarnetske et al., 2011), track denitrification progress along a flow path (Mariotti et al., 1988; Böttcher et al., 1990; Zarnetske et al., 2011), or to determine sources of NO_3^- contamination in groundwater (Wilson et al., 1994). ^{15}N-NO_3^- is one of the most common isotopes analyzed for these purposes (Groffman et al., 2006). Similar to other natural isotopes, $\delta^{15}N$-N_2 is computed by Eqn. 2.2, in which R is equivalent to $^{15}N_2/^{14}N_2$, $R_{standard}$ is atmospheric $^{15}N_2/^{14}N_2$, and the $\delta^{15}N$-N_2 of the standard "air" is 0.0‰.

In a single-step, theoretical reaction from NO_3^- to N_2, $\delta^{15}N$-N_2 increases from its initial value through fractionation, as ^{14}N-NO_3 is preferentially reduced to N_2 according to a Rayleigh distillation (Eqn. 2.3). As denitrification progresses, $\delta^{15}N$-N_2 will increase as the residual NO_3^- becomes depleted and ^{15}N-NO_3 is denitrified (Bates et al., 1998). If the entire NO_3^- substrate is reduced via denitrification, the product (N_2) will have the same isotopic composition as the initial $\delta^{15}N$-NO_3 composition. The $\delta^{15}N$-N_2 of a given sample, like any other fractionation process, depends entirely on the initial N-isotopic composition of the substrate, the enrichment factor ε, and the fraction of the substrate remaining, *f*, as given in Wilson et al. (1990):

$$\delta^{15}N_{2\,denit} = \delta^{15}NO_{3\,initial}^{-} - \varepsilon[(f \ln f)/(1-f)] \qquad (2.3)$$

Smith et al. (1991) found a good fit between $\delta^{15}N$-N_2 field data and a Rayleigh-type distillation curve following the form of Eqn. 2.3. However, mixing of multiple flowpaths,

multiple NO_3^- sources, or degassing can cause the isotopic composition of the final product to deviate from that predicted by Eqn. 2.3. Additionally, because the denitrification process is mediated by microbes, discrimination by the organisms against heavier isotopes can also prevent the reaction from following a Rayleigh fractionation pathway (Wilson et al., 1990). Citing these reasons and the multi-step nature of the denitrification process, Wilson et al., (1990) explained why $\delta^{15}N\text{-}N_2$ in a limestone aquifer was not consistent with a Rayleigh-type distillation.

3.0 RESULTS

3.1 NO_3^- and $\delta Ar/N_2$

Results of the gas sampling for the piezometers and groundwater monitoring well are shown in Table 2.1. $\delta Ar/N_2$ results for the borehole are shown graphically with NO_3^- in Fig. 13. NO_3^- and $\delta Ar/N_2$ in the borehole are similar to the range of concentrations measured in the islands shown in Fig. 14. NO_3^- concentration in the borehole was the highest of all sampling locations, but did not exceed 1.3 mg NO_3-N L^{-1}.

At each depth interval, $\delta Ar/N_2$ is below the estimated range of $\delta Ar/N_2$ in ASW for reasonable recharge temperatures. These low $\delta Ar/N_2$ values indicate "excess" N_2 present in the samples compared to the expected Ar/N_2 in air-saturated water. Because N_2 is a product of denitrification, it is reasonable to infer that denitrification contributed to the excess N_2 in these samples.

3.2 $\delta^{15}N\text{-}N_2$

The $\delta^{15}N\text{-}N_2$ composition in the borehole and piezometers are given in Table 2.1. $\delta^{15}N\text{-}N_2$ in the borehole is shown graphically in Figure 13 and was close to atmospheric $\delta^{15}N\text{-}N_2$ at depths

of 1.5 m to 3 m below the water table, as well as 9 m and 12 m below the water table. The isotopic composition of N_2 was the lightest (-7.7 ‰) at the same depth where NO_3^- concentrations were the highest, near 7.5 m below the water table. The overall $\delta^{15}N\text{-}N_2$ composition in the piezometers and monitoring well are similar to that of the borehole.

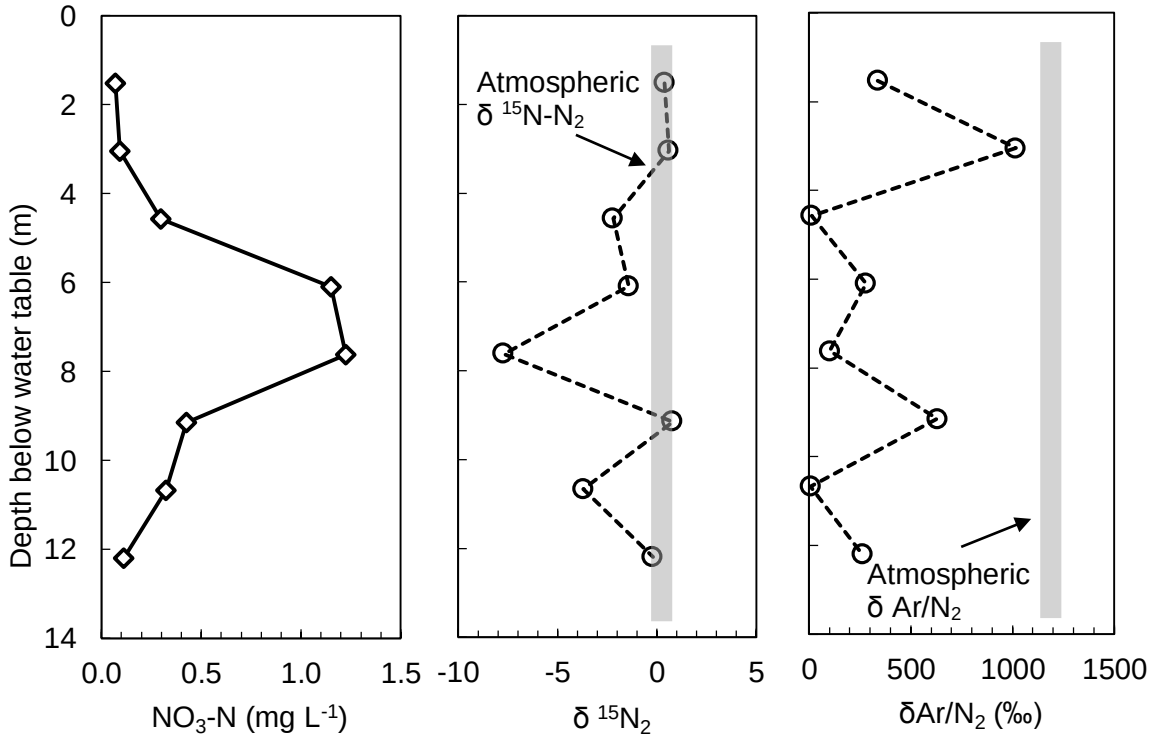

Figure 13. $\delta Ar/N_2$, $\delta^{15}N\text{-}N_2$, and nitrate in the riparian zone borehole. Nitrate concentrations in the borehole were comparable to those measured in the islands. The highest nitrate concentrations were measured between 6 and 8 m below the water table in the borehole, as shown. $\delta Ar/N_2$ are all below $\delta Ar/N_2$ in air-saturated water, indicating that excess N_2 is present in the samples collected from all depths. Despite the variability in nitrate concentrations with depth, $\delta Ar/N_2$ reasonably indicates that denitrification has occurred up to 12 m depth in the riparian pore water. $\delta^{15}N\text{-}N_2$ data indicate that many of the samples are similar to atmospheric $\delta^{15}N\text{-}N_2$, and that all except for one sample (~8 m deep) is within the range of values expected for complete denitrification of synthetic fertilizer NO_3. Data is given in Table 2.1.

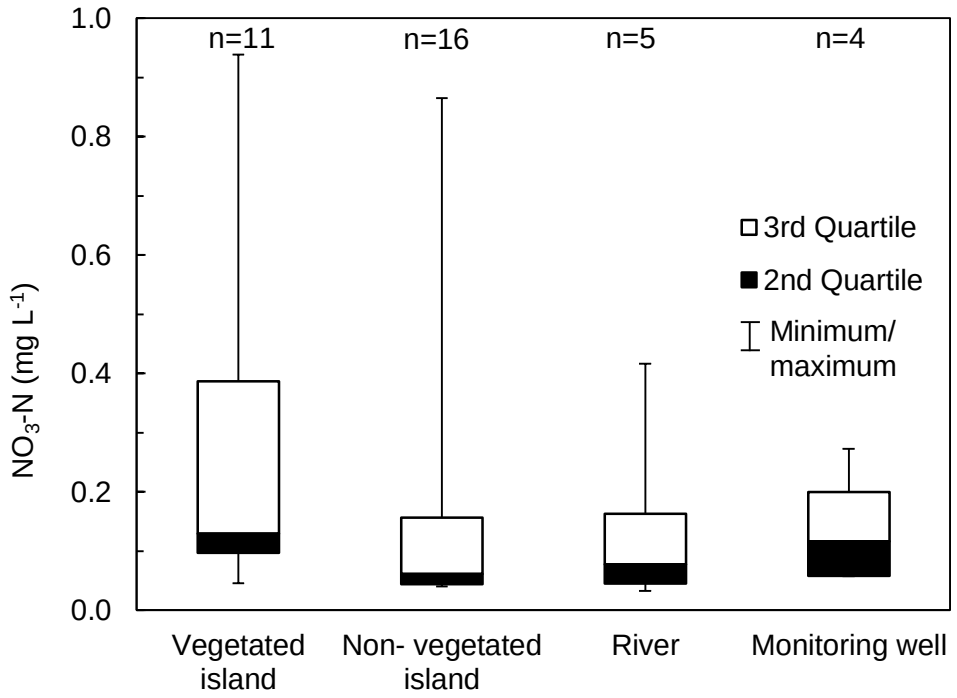

Figure 14. Nitrate concentrations in island piezometers, river, and monitoring well. Upper and lower bars indicate maximum and minimum nitrate concentrations measured over the study, respectively. The shaded box represents the 25th to 50th percentile of all data collected at the given location, hollow box represents 50th to 75th percentile of data collected at the given location. Over half of the samples collected for nitrate analysis were below detection limits (0.025 mg L^{-1} NO_3-N). Data are given in Appendix A.

3.3 Redox Indicators

3.3.1 Piezometers

Below 2 mg L^{-1} O_2, denitrifying microbes will generally begin to reduce NO_3^-, and with the exception of the river, dissolved oxygen was below this level for all of the sample locations during most sampling events (Fig. 15). ORP in the islands indicated reducing (<-100 mV) to moderately oxidizing (50 to 100 mV) conditions for the first half of the study (Fig. 16). However, beginning in mid-July, there was a notable change in the islands from a slightly reducing (-50 to 0 mV) to highly oxidizing (>100 mV) environment. This shift in ORP in the islands correlates with the timing of river discharge reaching zero. As anticipated, the ORP of the river remained

oxidizing throughout the study period, and the groundwater monitoring well ORP remained relatively stable with slightly reducing conditions.

Oxidation-reduction potential and O_2 together indicated that reducing conditions were present in the islands for the first half of summer 2012. Dissolved organic matter was also present in the island pore water at concentrations ranging from 2 to 4.5 mg C L^{-1} (data not shown). There was no N_2O or NO_2^- above detection limits in any of the piezometers throughout the study period.

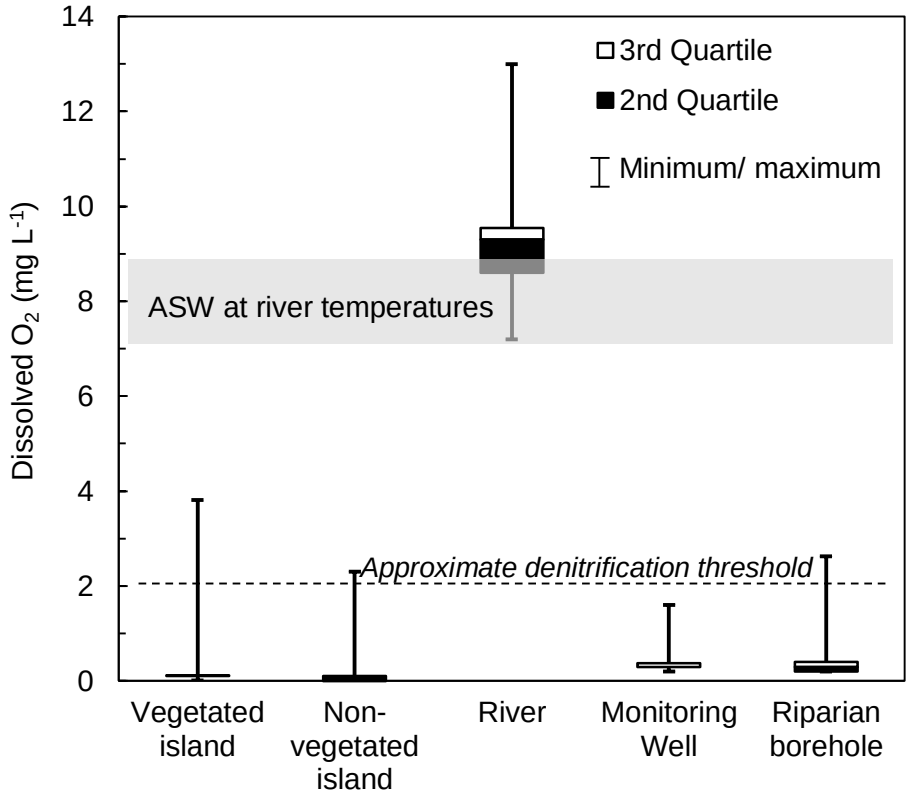

Figure 15. Dissolved oxygen in island piezometers, river, and monitoring well. Upper and lower bars indicate maximum and minimum O_2 concentrations measured over the study, respectively. The shaded box represents the 25th to 50th percentile of all data collected at the given location, hollow box represents 50th to 75th percentile of data collected at the given location. Dissolved oxygen in the river is significantly higher than groundwater or pore water samples due to contact with the atmosphere and turbulent flow. River O_2 is equivalent to or exceeds dissolved oxygen in air-saturated water at the temperatures measured in the field. Most groundwater and porewater samples were below the general denitrification threshold of 2 mg L^{-1}.

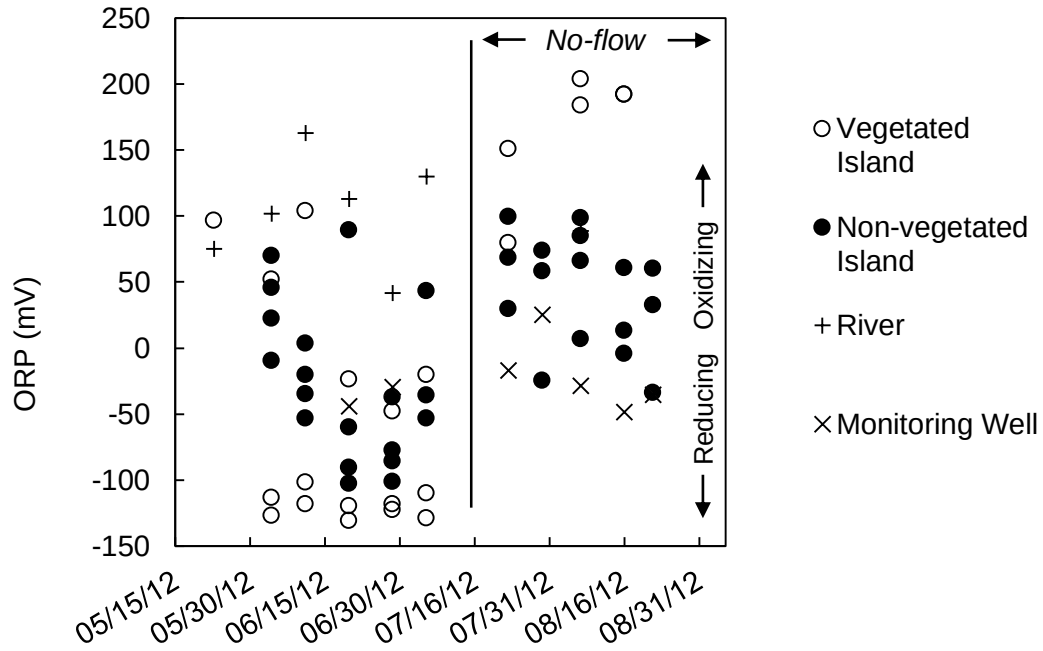

Figure 16. Oxidation reduction potential in island piezometers, river, and monitoring well. Positive ORP indicates oxidizing conditions; negative ORP indicates reducing conditions. Flow in the river channel ceased in mid-July. Concurrently, ORP in the islands increased from strongly reducing to slightly reducing or oxidizing. There is no clear temporal trend in the river or monitoring well ORP. Data are given in Appendix A.

3.3.2 Borehole

Similar to the piezometers, O_2 in the borehole was less than 2 mg L^{-1} at all depths (Fig. 17). In contrast, ORP in the borehole increased with depth. At this location, similar to the islands, O_2 and ORP conflict as to whether conditions are generally oxidizing or reducing. However, the measurements of O_2 and ORP in the borehole are consistent with those also collected from the islands near the end of the study period. Samples from the borehole did not contain any detectable concentration of NO_2^- or N_2O.

3.4 Microcosm Tests

The microcosm tests indicated that the vegetated island sediments had potential for significant denitrification, but that the sediments were generally carbon-limited (Fig. 18). In the control microcosm (NO_3^- + glucose), denitrification rates were not significantly greater than zero. In Microcosm I (sediment + NO_3^-), denitrification rates over the first 24 hours were low, averaging 49 µmol NO_3^- + NO_2^- kg^{-1} h^{-1}, but were significant compared to the control ($p < 0.05$). Denitrification rates in Microcosm I increased to an average 102 µmol NO_3^- + NO_2^- kg^{-1} h^{-1} in the 24-48 hour period. In Microcosm II (sediment + NO_3^- + glucose), denitrification rates were significant during both the first 8- and 24-hour periods ($p < 0.05$). With the glucose amendment, organisms capable of using NO_3^- and glucose flourish within the first 24 hours, and utilize all NO_3^- by the end of the 48-hour period. The rate of denitrification in Microcosm II averaged 74 µmol NO_3^- + NO_2^- kg^{-1} h^{-1} over the 0-8 hour period, and increased to an average of 1002 µmol NO_3^- + NO_2^- kg^{-1} h^{-1} over the 24-48 hour period.

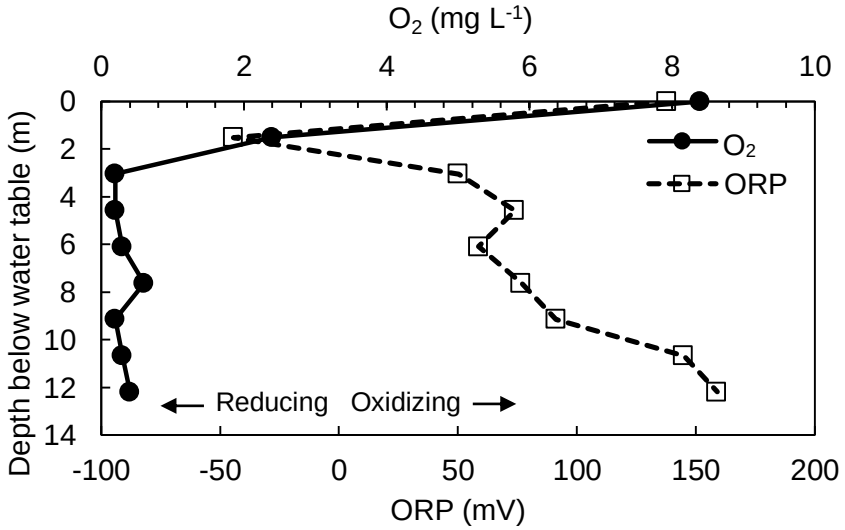

Figure 17. Dissolved oxygen and oxidation reduction potential in the riparian borehole. Samples shown at 0 m were collected from the river adjacent to the borehole. Dissolved oxygen concentrations below 2 m below the water table generally indicate reducing conditions. This contrasts with ORP, which may indicate decreasing microbial activity with depth.

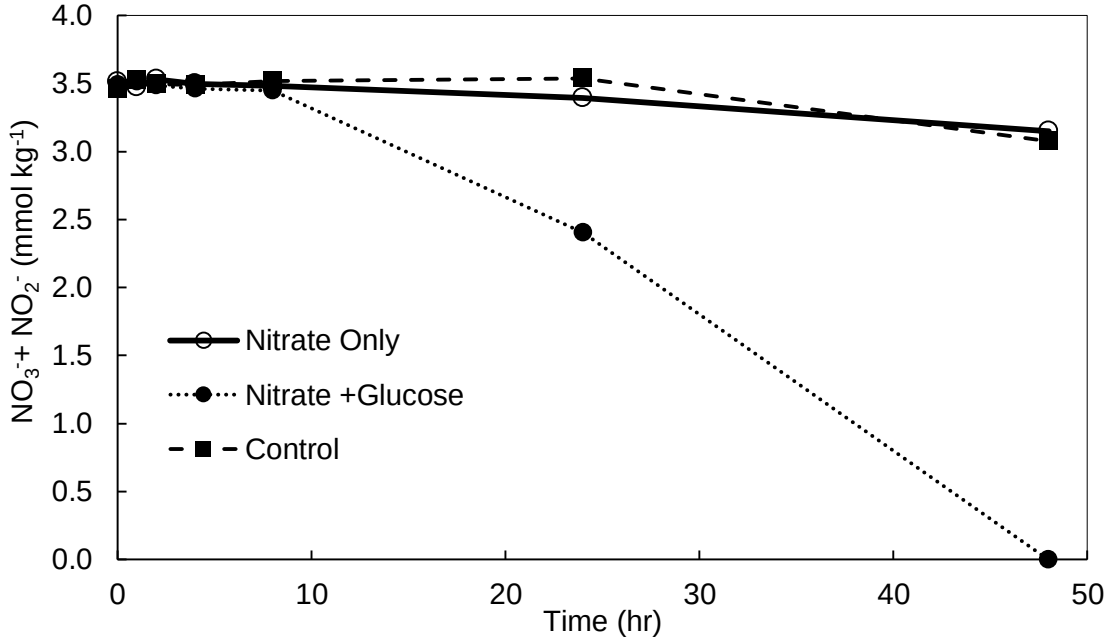

Figure 18. Consumption of NO_3^- + NO_2^- in the microcosm experiments. No significant denitrification occurred in the control microcosm. Very low rates of denitrification occurred in the nitrate-only amended microcosm over the first 24-hour period. Denitrification rates were significant in the first 8 and 24-hour periods in the nitrate+glucose amended microcosm ($p < 0.05$), and reduced NO_3^- + NO_2^- concentration to below detection limits in the first 48 hours.

4.0 DISCUSSION

4.1 Local and Regional Measured NO_3^- in Recharge and Groundwater

The island piezometers and riparian borehole indicated low (<1.3 mg NO_3-N L^{-1}) NO_3^- in shallow groundwater beneath the river bed, as well as in the riparian zone up to a depth of 12 m below the water table. Concentrations in the deep monitoring well and river were also, like the islands, mostly below 0.7 mg NO_3-N L^{-1}, with over half of the NO_3^- samples below detection limits. The highest NO_3^- concentration throughout the study was measured at approximately the mid-depth of the borehole, at 1.2 mg NO_3-N L^{-1}. The cause of this NO_3^- "bulge" between 6 and 8 m below the water table is unclear. It is plausible that in this area, the main component of groundwater flow is horizontal, and that a thin NO_3^- plume exists at this depth, and migrates

beneath the river, preventing detection in the island piezometers. This hypothesis is supported by comparing the temperature and NO_3^- data from the borehole. The highest NO_3^- concentrations are at approximately the same depth at which groundwater temperatures approach the minimum temperatures in the borehole. It is expected that groundwater migrating from upgradient of the borehole would be close to average groundwater temperatures measured at the borehole. The fact that this lower-temperature water is also contains high NO_3^- suggests that the NO_3^- is also migrating from an upgradient source. However, measured NO_3^- concentrations in the study area, even beneath the river, are significantly lower than the NO_3^- concentration in regional wells (Fig. 12), the occurrence of which has been shown to largely be a result of leaching of agricultural fertilizers and animal waste (Exner and Spalding, 1990; Exner and Spalding, 1994; Tarkalson et al., 2006). The contrasting concentration ranges between the local streambed groundwater and regional groundwater may be considered to be indirect evidence of the local streambed groundwater having undergone denitrification, provided that regional groundwater is the source of the streambed groundwater outside of the May-September irrigation season (as discussed in Chapter 1; Peckenpaugh and Dugan, 1983; Kilpatrick, 1996).

4.2 Chemical and Isotopic Evidence for Denitrification

The hypothesis that local streambed groundwater NO_3^- concentrations have been affected by denitrification can be tested using the chemical and isotopic dataset. $\delta Ar/N_2$ was higher than the equilibrium value for air, suggesting that "excess" N_2 gas is present in the groundwater at all sample locations and in samples collected from the water table to 12 m below the water table. The most likely source of this excess N_2 is from denitrification. Consider, for example, a closed system in which the initial mole fraction of Ar and N_2 in groundwater is equivalent to that predicted by Henry's Law at 500 m elevation and 20 ºC (2.43×10^{-7} mol Ar mol H_2O^{-1}; 9.23 x

10^{-6} mol N_2 mol H_2O^{-1}). If 10 mg L^{-1} of NO_3- in groundwater are completely denitrified to N_2, 8.06 x 10^{-5} mol N_2 L^{-1} (1.45 x 10^{-6} mol N_2 mol H_2O^{-1}) would be formed. Assuming all N_2 formed during denitrification goes into solution, $\delta Ar/N_2$ can be calculated using Eqn. 2.2:

$$\left[\frac{\left(\frac{2.43\ x\ 10^{-7}}{1.45\ x\ 10^{-6}\ +\ 9.23\ x\ 10^{-6}}\right)}{\left(\frac{2.43\ x\ 10^{-7}}{9.23\ x\ 10^{-6}}\right)}\right] * 1000 = 884‰ \quad (2.4)$$

This is higher than the $\delta Ar/N_2$ measured at most depths in the borehole, indicating that more than 10 mg L^{-1} NO_3^- may have been denitrified in groundwater. Assuming closed system denitrification in the borehole groundwater as well as the temperature and elevation specified above, $\delta Ar/N_2$ indicates that complete denitrification of approximately 1 mg NO_3-N L^{-1} to 17 mg NO_3-N L^{-1} may have occurred. These concentrations are consistent with NO_3^- concentrations measured in the Platte River basin (Fig. 12).

The sensitivity of $\delta Ar/N_2$ to equilibrium temperature and "excess air" was examined because these factors can also affect dissolved gas ratios in groundwater. $\delta Ar/N_2$ for the range of theoretical recharge temperatures from 10 °C to 25 °C at 500 m is equivalent to 1215‰ to 1166‰, demonstrating the lower solubility of dissolved gasses at higher water temperatures (Benson and Krause, 1976). "Excess air" refers to dissolved gases in groundwater attributable to trapped atmospheric gas bubbles that partially or fully dissolve into groundwater under increased hydrostatic pressure and/or by water table fluctuations, leading to dissolved gas concentrations that exceed those predicted by Henry's Law. In the absence of neon gas measurements that are commonly used to quantify excess air (Wilson et al., 1994), the amount of excess air that may be present in the samples collected for this study can not be quantified. In the case that excess air—in which $\delta Ar/N_2$ resembled atmospheric—was trapped in groundwater, the effect on $\delta Ar/N_2$

would be negligible. For example, assume that 0.1 cc STP kg H_2O^{-1} of unfractionated air is forced into solution. The conversion factor for the molar fraction of gas per mole H_2O from cc STP kg^{-1} is 1.24339 x 10^6. Therefore, the moles of gas in solution are calculated by:

$$\frac{0.1 \text{ cc} \frac{\text{STP}}{\text{kg}} \text{ air}}{1.24339 \text{ x } 10^6} = 8.04 \text{ x } 10^{-8} \frac{\text{mol gas}}{\text{mol } H_2O} \tag{2.5}$$

Argon gas will comprise 0.9% of the added moles, and nitrogen 78%, according to their atmospheric partial pressures. Therefore, the addition of 0.1 ccSTP kg^{-1} unfractionated air would add 7.56 x 10^{-10} mol Ar, and 6.27 x 10^{-8} mol N_2. The gas ratio of the sample can be found by rearranging Eqn. 1:

$$R_{\text{sample}} = \left(\frac{\delta \frac{\text{Ar}}{\text{N}_2}}{1000} + 1 \right) * R_{\text{standard}} \tag{2.6}$$

If we assume a $\delta Ar/N_2$ of 400‰ (near the average for samples collected in this study), and an atmospheric molar ratio of 1.21 x 10^{-2} for the standard, the molar ratio of Ar/N_2 in the sample is

$$R_{\text{sample}} = \left(\frac{400‰}{1000} + 1 \right) * 1.21 \text{ x } 10^{-2} = \ 1.69 \text{ x } 10^{-2} \tag{2.7}$$

Using Henry's Law, assuming a recharge temperature of 20 ºC and elevation of 500 m, the mole fraction of Ar in solution is 2.43 x 10^{-7}. Assuming also that this is the mole fraction of Ar present in groundwater at the study site, the mole fraction of N_2 in solution with a $\delta Ar/N_2$ of 400‰ is 1.44 x 10^{-5}. Adding the moles of Ar and N_2 from unfractionated excess air, the new molar ratio of the sample would be:

$$\frac{2.43 \text{ x } 10^{-7} \text{ mol Ar} + 7.56 \text{ x } 10^{-10} \text{ mol Ar}}{1.44 \text{ x } 10^{-5} \text{ mol } N_2 + 6.27 \text{ x } 10^{-8} \text{ mol } N_2} = 1.69 \text{ x } 10^{-2} \tag{2.8}$$

Using this value as the new gas ratio in the sample, a new $\delta Ar/N_2$ is calculated using Eqn 1:

$$\left(\frac{1.69 \text{ x } 10^{-2}}{1.21 \text{ x } 10^{-2}} - 1\right) * 1000 = 398.3 \text{ ‰} \quad (2.9)$$

Therefore, a reasonable amount of excess air, if present, would lead to only a slight underestimation of $\delta Ar/N_2$.

Over half of the samples collected from the borehole have $\delta^{15}N\text{-}N_2$ values within 1.5‰ of atmospheric $\delta^{15}N\text{-}N_2$, and these values also closely resemble the initial isotopic composition of synthetic fertilizers, which have a $\delta^{15}N\text{-}NO_3^-$ between -5‰ and +5‰ (Exner and Spalding, 1994; Wilson et al., 1994; Bates and Spalding, 1998; Clark and Fritz, 1999). Without knowledge of initial $\delta^{15}N\text{-}NO_3^-$, it is difficult to conclude whether the measured $\delta^{15}N\text{-}N_2$ range is consistent with denitrification. However, the similarity of the $\delta^{15}N\text{-}N_2$ measured in this study to the $\delta^{15}N\text{-}NO_3^-$ of fertilizer may indicate that denitrification has converted the majority of NO_3^- in groundwater to N_2, such that the isotopic composition of the product (N_2) matches the initial isotopic composition of the reacted substrate.

To illustrate this, Eqn. 2.3 was used to determine reasonable $\delta^{15}N\text{-}N_2$ values assuming an initial $\delta^{15}N\text{-}NO_3^-$ between -5‰ and +5‰. According to Kendall (1998), enrichment factors for denitrification may range from -40‰ to -5‰. Böttcher et al. (1990) found an enrichment factor of -15.9‰ for $\delta^{15}N$ in a sandy aquifer beneath a forested and farmed watershed. Böhlke et al. (2002) found a range of denitrification enrichment factors for $\delta^{15}N$ between -21‰ and -7‰ best fit isotopic data collected from a glacial outwash aquifer.

Figure 19 shows the evolution of $\delta^{15}N\text{-}N_2$ from assumed initial $\delta^{15}N\text{-}NO_3^-$ values using two different enrichment factors within the range given by Kendall (1998). The data collected in this study falls within the range of values expected with an initial $\delta^{15}N\text{-}NO_3^-$ of 1‰ and an enrichment factor between -5‰ and -10‰. Though it is possible that initial $\delta^{15}N\text{-}NO_3^-$ varied

between the different sampling locations, this figure demonstrates that measured $\delta^{15}N\text{-}N_2$ can be reasonably explained by denitrification of synthetic fertilizer. Additionally, using the above assumptions of initial $\delta^{15}N\text{-}NO_3^-$ and the published range of enrichment factors, >80% of the substrate is unreacted at locations with very low $\delta^{15}N\text{-}N_2$, such as at 7.6 m depth in the borehole. In the islands and shallow depths of the borehole where $\delta^{15}N\text{-}N_2$ was relatively high (-0.4‰ to +0.6‰), less than ~10% of the original substrate is unreacted. This simple model shows the possible high variability in denitrification progression, which is mirrored in the variability of the $\delta Ar/N_2$ data, as well as the NO_3^- concentrations in the borehole.

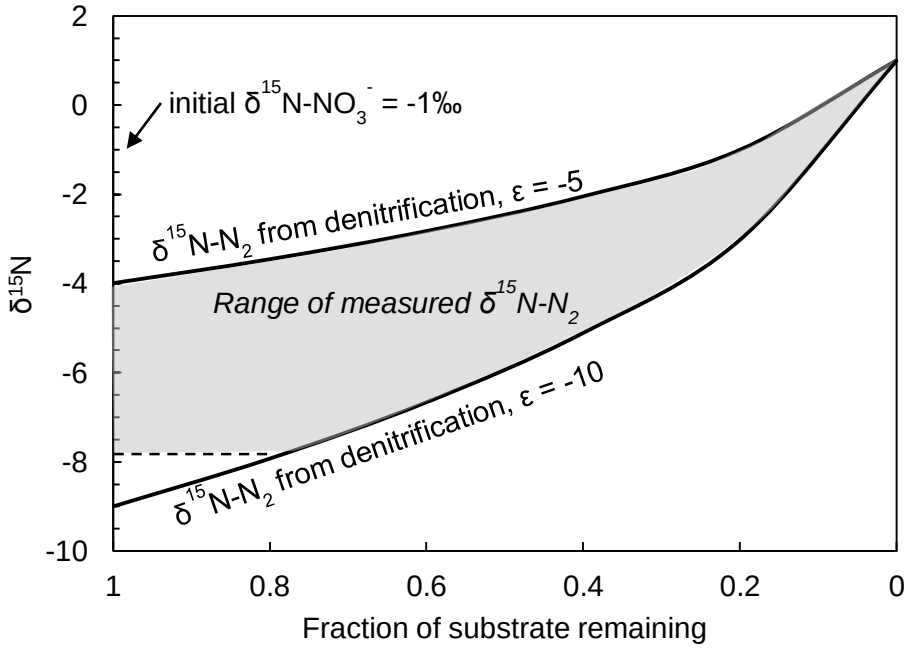

Figure 19. Possible range of $\delta^{15}N\text{-}N_2$ from denitrification of commercial fertilizer. Solid lines indicate the N_2 isotopic composition from denitrification following a Rayleigh distillation, assuming an initial $\delta^{15}N\text{-}N_2$ of 1‰ and the reasonable enrichment factors shown. Shaded area indicates the range of measured $\delta^{15}N\text{-}N_2$ in the borehole and islands. Using these assumptions, measured $\delta^{15}N\text{-}NO_3^-$ indicates no denitrification of the nitrate substrate to complete denitrification (no remaining substrate).

Interestingly, the most depleted $\delta^{15}N\text{-}N_2$ measurement corresponds to the highest NO_3^- concentrations in the borehole (Fig. 13). This may be the result of a NO_3^- plume at this depth that has yet to be completely denitrified. If a large fraction of the substrate remains unreacted, $\delta^{15}N\text{-}N_2$ will be depleted relative to the presumed initial $\delta^{15}N\text{-}NO_3^-$ between -5‰ and +5‰. This scenario would also explain the higher NO_3^- concentrations relative to the other depths. If this flow path could be isolated and sampling were to occur further downgradient, an enriched $\delta^{15}N\text{-}N_2$ and lower NO_3^- compared to those measured between 6 m and 8 m depth in the borehole would be expected.

Because $\delta^{15}N\text{-}N_2$ data from the borehole and island samples are very close to atmospheric, their evidence regarding denitrification is equivocal. However, low O_2 (<2 mg L^{-1} at all borehole depths and most island sites), low NO_3^- (< 1.3 mg NO_3-N L^{-1}), and excess N_2 described above add confidence to the inference that denitrification has decreased NO_3^- concentration in these samples. Therefore, it is reasonable to conclude that groundwater collected in this study originally contained a higher NO_3^- concentration than measured prior to sampling near the Platte River and that low measured NO_3^- in the study area is a result of denitrification.

If denitrification was occurring in the Platte River streambed within the study period, it would be expected that intermediate denitrification products such as NO_2^- or N_2O would be detectable (Appelo and Postma, 1996). Betlach and Tiedje (1981) demonstrated the accumulation of NO_2^- and N_2O following the reduction of NO_3^-. However, NO_2^- is relatively unstable in the denitrification process (Lee et al., 2006), and often is reduced as rapidly as it is formed (Mariotti et al., 1981). N_2O is similarly unstable and infrequently detectable in denitrification field studies or lab experiments. For this reason, the acetylene block method is frequently utilized in denitrification studies. However, in this study, all NO_2^- and N_2O results were below respective detection limits of 0.25 mg L^{-1} NO_2-N and 0.5 mg L^{-1} (headspace N_2O concentration), suggesting

no denitrification was occurring, or that denitrification rates were lower than NO_2^- and N_2O reduction kinetics.

4.3 Denitrification Potential

The denitrification potential of the island sediments (DNP, maximum denitrification rate if the sediments are not N or C-limited) can be determined from the microcosm tests. Denitrification in the islands is unlikely to occur if there is an insufficient carbon substrate to serve as an electron donor in the reduction of NO_3^-, or if there is an insufficient NO_3^- source (generally < 2 mg NO_3-N L^{-1}, Hill and Cardaci, 2004). The experimental setup of Microcosm I tested whether denitrification would occur if NO_3^- was not limited. The results indicated that denitrification did occur in the microcosm sediments, but that denitrification rates were low. Microcosm II tested whether denitrification was inhibited in situ due to carbon-limitation. The results indicated significantly higher rates of denitrification in the carbon-amended sediments, indicating that the islands have high denitrification potential, but are carbon limited, and likely NO_3^- limited, considering all of the vegetated and non-vegetated island pore water samples contained <2 mg NO_3-N L^{-1} (Fig. 14).

The average rates measured in both microcosms are within an order of magnitude of measurements from similar denitrification potential lab experiments (Table 2.2). The highest average denitrification rate in Microcosm I (102 µmol $NO_3^- + NO_2^-$ kg^{-1} h^{-1}, 24-48 hour time period) is similar to rates reported by Komor and Fox (2002) for NO_3^--amended wetland sediments (202-308 µmol $NO_3^- + NO_2^-$ kg^{-1} h^{-1}) and Hill and Cardaci (2004) for marsh, mixed forest, and conifer peat sediments (118.6, 106.4, 94.3 µmol $NO_3^- + NO_2^-$ kg^{-1} h^{-1}, respectively). However, the rates in Microcosm I were up to two orders of magnitude higher than denitrification rates of 5.7 µmol $NO_3^- + NO_2^-$ kg^{-1} h^{-1} and 1.8 µmol $NO_3^- + NO_2^-$ kg^{-1} h^{-1-} for river bank and

hyporheic zone sediments, respectively, reported by Holmes et al. (1996). Average denitrification rates in Microcosm I of 27.6 µmol NO_3^- + NO_2^- kg^{-1} h^{-1} over the first 8 hours more closely resemble those reported by Holmes et al. (1996) and Hill & Cardaci (2004) for peat soils (22.1 µmol NO_3^- + NO_2^- kg^{-1} h^{-1}). Denitrification rates measured in Microcosm II over the first 24 hours averaged 468.8 µmol NO_3^- + NO_2^- kg^{-1} h^{-1}, and were similar to rates reported by Komor and Fox (2002) of 559 µmol NO_3^- + NO_2^- kg^{-1} h^{-1} for carbon-amended wetland sediments. Denitrification rates measured in Microcosm II from the 24-48 hour period averaged 443 µmol NO_3^- + NO_2^- kg^{-1} h^{-1} higher than carbon-amended experiments reported in Komor and Fox (2002). These higher denitrification rates at a longer time interval are likely attributable to the lack of antibiotic in the Microcosm II serum bottles. This promoted the growth of denitrifiers in the 48-hour period.

Low-flow and drought conditions in 2012 may mean that the results from this study are an exception in flow regime and denitrification rates, rather than the seasonal norm. It is plausible that low-flow conditions throughout this study increased groundwater residence times near the river channel compared to average seasonal residence times, and for about one-third of the study period, prevented discharge from groundwater to the river (see discussion in Chapter 1). Higher residence times allow more time for reduction of O_2, NO_3^-, and greater net NO_3^- removal (Zarnetske et al., 2011). For this drought-year study, the lack of precipitation and subsequent lack of surface runoff likely led to below-average NO_3^- loading directly to surface water, and subsequent low NO_3^- in the river and HZ, similar to the results of Morecroft et al. (2000) in a southern England stream during a drought year. Puckett (2005) noted a similar phenomenon, in which the greatest decrease in NO_3^- concentrations in stream water, relative to groundwater, occurred during an August low-flow period in South Carolina, despite groundwater having the greatest impact on stream water chemistry at the time.

It is plausible that during high-flow conditions, infiltration of river water into the islands may increase the available organic carbon, and that concurrent increased baseflow may lead to higher NO_3^- concentrations in the hyporheic zone, ultimately leading to higher denitrification rates in the islands. Higher annual precipitation may also lead to increased leaching and runoff of NO_3^- applied in the early growing season, possibly increasing the concentration of NO_3^- in the river channel. Conversely, high flows may have a net effect of lower net NO_3^- removal, due to decreased groundwater residence times in the HZ or riparian zone.

5.0 CONCLUSION

This study utilized multiple chemical and isotopic methods and weekly sampling to investigate ongoing denitrification and sediment denitrification potential in the lower Platte River, Nebraska. It has been well established that non-point source NO_3^- pollution has contaminated much of the groundwater within the lower Platte basin and led to NO_3^- concentrations exceeding drinking water standards. However, NO_3^- concentrations measured in the riparian zone, river, and shallow (<1.2 m below the surface) groundwater within the fluvial islands are less than 1.3 mg NO_3-N L^{-1}. Shallow groundwater chemistry and isotopes, and sediment lab experiments indicated that though low rates of denitrification are possible in the islands sediments, the islands were N and C-limited, and there was no chemical indication of active denitrification over the summer 2012 study period. Dissolved gas and N_2-isotope results did suggest that denitrification had occurred within shallow groundwater and groundwater sampled from up to 12 m below the water table in the riparian zone. Therefore, our conceptual model is that denitrification occurred within the groundwater beneath the uplands outside of the river channel, before discharge near the Platte River.

Determining the timing and exact location of denitrification was outside the scope of this study. However, it is apparent that during the low flow conditions of the 2012 drought, loading of NO_3^- to surface water in the study area (either through runoff or groundwater discharge) was lower than the denitrification rates along those transport pathways. To better understand these processes, additional sampling along a confirmed flow path toward the Platte River is needed. This would better illuminate the residence time required to achieve denitrification, as well as the location, depth, and water quality near this redox boundary. NO_3^- concentrations were too low in this study to analyze $\delta^{15}N\text{-}NO_3^-$, a common indicator of NO_3^- source (animal waste, synthetic fertilizer, human waste, etc). Analysis of $\delta^{15}N\text{-}NO_3^-$ and additional analysis of dissolved organic carbon would be useful to 1) identify the source of NO_3^- contamination along the groundwater flow pathway, and 2) track denitrifying pathways outside of the river channel. Finally, it would be useful to compare these, and the water quality parameters measured in this study to an average-precipitation summer, or repeat the study in a different season, to better understand denitrification rates during high-flow regimes, as well as possible seasonality of NO_3^- loading through baseflow.

Table 2.1. Major ion and dissolved gas results for the borehole. Dissolved gas results for the piezometers are also shown. The full data table with piezometer major ions, field parameters, and stable isotopes are shown in Appendix A. GND refers to the groundwater monitoring well. Samples labeled PR were collected in the borehole and indicate depth from the surface in feet.

Sample Name	**Sample Date**	**Depth below surface (m)**	**δAr/N_2 (‰)**	**$\delta^{15}N_2$ (‰)**	**Temp (C)**	**NO_3-N**	**O_2**	**ORP**	**pH**	**Total Alkalinity**	**SO_4^{2-}**	**Cl^-**	**Na^+**	**Ca^{2+}**	**K^+**	**Mg^{2+}**
AN7	22-Aug-12	1.2	886.9	-2.5	25.1	See Appendix A for full island water composition										
AN6	22-Aug-12	0.5	375.8	-1.3	24.8											
GND	22-Aug-12	29	379.7	-0.4	12.9											
PR 10	13-Sep-12	3.1	--	--	24.1	n/d	2.4	-44.4	6.9	244	525	43	107	198	20	54
PR 15	13-Sep-12	4.6	338	0.4	22.2	0.07	0.2	50.3	7.57	173	233	40	101	78	14	22
PR 20	13-Sep-12	6.1	1016	0.6	19.6	0.09	0.2	73.9	7.91	183	232	40	93	86	13	20
PR 25	13-Sep-12	7.6	13.1	-2.2	16.5	0.30	0.3	58.8	7.79	175	228	38	96	101	5.5	17
PR 30	13-Sep-12	9.1	280	-1.4	14.0	1.15	0.6	76.6	7.67	172	185	37	78	85	3.3	10
PR 35	13-Sep-12	10.7	102.8	-7.7	13.3	1.22	0.2	91.3	7.72	180	209	38	100	100	4.0	11
PR 40	12-Sep-12	12.2	630.5	-0.8	13.0	0.43	0.3	145	7.64	180	217	37	77	88	3.9	12
PR 45	12-Sep-12	13.7	7.5	-3.7	13.0	0.32	0.4	159	7.7	184	216	36	87	104	5.2	17
PR 50	12-Sep-12	15.2	262.9	-0.2	13.0	0.11	0.3	173.1	7.74	188	192	36	82	75	7.3	14

Table 2.2. Summary of denitrification rates from microcosm experiments

Author	Soil type	Amendment	Method	Average rate µmol/kg/hr	
This study	Vegetated fluvial island	C & N	Nitrate+Nitrite reduction	74.1	(0-8 hr)
				468.8	(0-24 hr)
				1002.1	(24-48 hr)
	Vegetated fluvial island	N		27.6	(0-8 hr)
				48.8	(0-24 hr)
				101.5	(24-48 hr)
		Control		-38.2	(0-8 hr)*
				-21.5	(0-24 hr)*
				194.0	(24-48 hr)
Hill & Cardaci, 2004	Conifer peat	N	Acetylene block	94.3	
	Peat	N		22.1	
	Interbedded riparian sediments	N		1.4	
	Marsh	N		118.6	
	Mixed forest	N		106.4	
Holmes et al., 1996	River bank	C & N	Acetylene block	5.7	
	Hyporheic Zone	C & N		1.8	
Komor & Fox, 2002	Wetland	N	Nitrate+Nitrite reduction	202.4	
	Wetland	N		307.1	
	Wetland	C & N		559.0	

**Negative rates in the control experiment indicate increase in NO_3+NO_2 concentration (net nitrification)*

6.0 REFERENCES

Almon, E., and Magaritz, M., 1990, Dissolved common gases in groundwaters of the Appalachian Region: Journal of Hydrology, v. 121, p. 21-32.

Appelo, C.A.J., and Postma, D., 1996, Geochemistry, groundwater and pollution: Rotterdam, The Netherlands, A.A. Balkema, 536 p.

Bates, H.K., Martin, G.E., and Spalding, R.F., 1998, Kinetic isotope effects in production of nitrite-nitrogen and dinitrogen gas during in situ denitrification: Journal of Environmental Quality, v. 27, p. 183-191.

Bates, H.K., and Spalding, R.F., 1998, Aquifer denitrification as interpreted from in situ microcosm experiments: Journal of Environmental Quality, v. 27, p. 174-182.

Benson, B.B., and Krause, D., 1976, Empirical laws for dilute aqueous solutions of nonpolar gases: Journal of Chemical Physics, v. 64, p. 689-709.

Betlach, M.R., and Tiedje, J.M., 1981, Kinetic explanation for accumulation of nitrite, nitric oxide, and nitrous oxide during bacterial denitrification: Applied and Environmental Microbiology, v. 42, p. 1074-1084.

Böhlke, J.K., and Denver, J.M., 1995, Combined use of groundwater dating, chemical, and isotopic analyses to resolve the history and fate of nitrate contamination in two agricultural watersheds, Atlantic coastal plain, Maryland: Water Resources Research, v. 31, p. 2319-2339.

Böhlke, J.K., Harvey, J.W., and Voytek, M.A., 2004, Reach-scale isotope tracer experiment to quantify denitrification and related processes in a nitrate-rich stream, midcontinent United States: Limnology and Oceanography, v. 49, p. 821-838.

Böhlke, J.K., Wanty, R., Tuttle, M., Delin, G., and Landon, M., 2002, Denitrification in the recharge area and discharge area of a transient agricultural nitrate plume in a glacial outwash sand aquifer, Minnesota: Water Resources Research, v. 38, p. 1105.

Böttcher, J., Strebel, O., Voerkelius, S., and Schmidt, H.L., 1990, Using isotope fractionation of nitrate-nitrogen and nitrate-oxygen for evaluation of microbial denitrification in a sandy aquifer: Journal of Hydrology, v. 114, p. 413-424.

Boulton, A., J., Findlay, S., Marmonier, P., Stanley, E.H., and Valett, H.M., 1998, The functional significance of the hyporheic zone in streams and rivers: Annual Review of Ecology and Systematics, v. 29, p. 59-81.

Brunke, M., and Gonser, T., 1997, The ecological significance of exchange processes between rivers and groundwater: Freshwater Biology, v. 37, p. 1-33.

Cardenas, M.B., Wilson, J.L., and Zlotnik, V.A., 2004, Impact of heterogeneity, bed forms, and stream curvature on subchannel hyporheic exchange: Water Resources Research, v. 40.

Clark, I.D., and Fritz, P., 1999, Environmental Isotopes in Hydrogeology: USA, CRC Press, 328 p.

Exner, M.E., and Spalding, R.F., 1994, N-15 identification of nonpoint sources of nitrate contamination beneath cropland in the Nebraska Panhandle - 2 case studies: Applied Geochemistry, v. 9, p. 73-81.

Exner, M.E., and Spalding, R.F., 1990, Occurrence of pesticides and nitrate in Nebraska's ground water: Water Center, Institute of Agriculture and Natural Resources, The University of Nebraska—Lincoln, 34 p.

Fukada, T., Hiscock, K.M., Dennis, P.F., and Grischek, T., 2003, A dual isotope approach to identify denitrification in groundwater at a river-bank infiltration site: Water Resources Research, v. 37, p. 3070-3078.

Galloway, J.N., Dentener, F.J., Capone, D.G., 2004, Nitrogen cycles: past, present, and future: Biogeochemistry, v. 70, p. 153-226.

Green, C.T., Böhlke, J.K., Bekins, B.A., and Phillips, S.P., 2010, Mixing effects on apparent reaction rates and isotope fractionation during denitrification in a heterogeneous aquifer: Water Resources Research, v. 46.

Grimm, N.B., and Fisher, S.G., 1984, Exchange between interstitial and surface water: Implications for stream metabolism and nutrient cycling: Hydrobiologia, v. 111, p. 219-228.

Groffman, P.M., Altabet, M.A., Böhlke, J.K., et al., 2006, Methods for measuring denitrification: Diverse approaches to a difficult problem: Ecological Applications, v. 16, p. 2091-2122.

Hill, A.R., 1996, Nitrate removal in stream riparian zones: Journal of Environmental Quality, v. 25, p. 743-755.

Hill, A.R., and Cardaci, M., 2004, Denitrification and organic carbon availability in riparian wetland soils and subsurface sediments: Soil Science Society of America Journal, v. 68, p. 320-325.

Hill, A.R., Labadia, C.F., and Sanmugadas, K., 1998, Hyporheic zone hydrology and nitrogen dynamics in relation to the streambed topography of a N-rich stream: Biogeochemistry, v. 42, p. 285-310.

Holmes, R.M., Jones Jr, J.B., Fisher, S.G., and Grimm, N.B., 1996, Denitrification in a nitrogen-limited stream ecosystem: Biogeochemistry, v. 33, p. 125-146.

Istok, J.D., Humphrey, M.D., Schroth, M.H., Hyman, M.R., and OReilly, K.T., 1997, Single-well, "push-pull" test for in situ determination of microbial activities: Ground Water, v. 35, p. 619-631.

Kendall, C., 1998, Tracing Nitrogen Sources and Cycling in Catchments, *in* Kendall, C. and McDonnell, J.J., eds., Isotope Tracers in Catchment Hydrology: Amsterdam, Elsevier Science B.V., 839 p.

Kilpatrick, J.M., 1996, Temporal changes in the configuration of the water table in the vicinity of the management systems evaluation area site, central Nebraska: USGS Water-Resources Investigations Report: 94-4173.

Komor, A., and Fox, P., 2002, Evaluation of Denitrification Rates and Mechanisms in Microcosm Experiments with Sediments and Plants, *in* Water Environmental Federation Technical Exhibition and Conference: Chicago, Ill, Water Environmental Federation, p. 496-514.

Krause, S., Heathwaite, L., Binley, A., and Keenan, P., 2009, Nitrate concentration changes at the groundwater-surface water interface of a small Cumbrian river: Hydrological Processes, v. 23, p. 2103-2107.

Krause, S., Tecklenburg, C., Munz, M., and Naden, E., 2013, Streambed nitrogen cycling beyond the hyporheic zone: Flow controls on horizontal patterns and depth distribution of nitrate and dissolved oxygen in the upwelling groundwater of a lowland river: Journal of Geophysical Research: Biogeosciences, v. 118, p. 1-14.

Lee, M., Lee, K., Hyun, Y., Clement, T.P., and Hamilton, D., 2006, Nitrogen transformation and transport modeling in groundwater aquifers: Ecological Modelling, v. 192, p. 143-159.

Liao, L., Green, C.T., Bekins, B.A., and Bohlke, J.K., 2012, Factors controlling nitrate fluxes in groundwater in agricultural areas: Water Resources Research, v. 48.

Mariotti, A., Germon, J.C., Hubert, P., Kaiser, P., Letolle, R., Tardieux, A., and Tardieux, P., 1981, Experimental determination of nitrogen kinetic isotope fractionation: Some principles; illustration for the denitrification and nitrification processes: Plant and Soil, v. 62, p. 413-430.

Mariotti, A., Landreau, A., and Simon, B., 1988, N-15 isotope biogeochemistry and natural denitrification process in groundwater-Application to the chalk aquifer of northern France: Geochimica et Cosmochimica Acta, v. 52, p. 1869-1878.

Martin, G.E., Snow, D.D., Kim, E., and Spalding, R.F., 1995, Simultaneous Determination of Argon and Nitrogen: Ground Water, v. 33, p. 781-785.

McIsaac, G.F., David, M.B., Gertner, G.Z., and Goolsby, D.A., 2001, Nitrate flux in the Mississippi River: Nature, v. 414, p. 166-167.

McMahon, P., Böhlke, J.K., and Christenson, S.C., 2004, Geochemistry, radiocarbon ages, and paleorecharge conditions along a transect in the central high plains aquifer, southwestern Kansas, USA: Applied Geochemistry, v. 19, p. 1655-1686.

McMahon, P.B., Böhlke, J.K., Kauffman, L.J., et al., 2008, Source and transport controls on the movement of nitrate to public supply wells in selected principal aquifers of the United States: Water Resources Research, v. 44.

Morecroft, M.D., Burt, T.P., Taylor, M.E., and Rowland, A.P., 2000, Effects of the 1995-1997 drought on nitrate leaching in lowland England: Soil Use and Management, v. 16, p. 117-123.

Mulholland, P.J., Valett, H.M., Webster, J.R., Thomas, S.A., Cooper, L.W., Hamilton, S.K., and Peterson, B.J., 2004, Stream denitrification and total nitrate uptake rates measured using a field ^{15}N tracer addition approach: Limnology and Oceanography, v. 43, p. 809-820.

Ostrom, N.E., Hedin, L.O., von Fischer, J.C., and Robertson, G.P., 2002, Nitrogen transformations and NO_3-removal at the soil-stream interface: A stable isotope approach: Ecological Applications, v. 12, p. 1027-1043.

Peckenpaugh, J.M., and Dugan, J.T., 1983, Hydrogeology of parts of the Central Platte and Lower Loup Natural Resources Districts, Nebraska: Lincoln, Nebraska, U.S. Geological Survey Water-Resources Investigations Report 83-4219, 110 p.

Puckett, L.J., Cowdery, T.K., McMahon, P.B., Tornes, L.H., and Stoner, J.D., 2002, Using chemical, hydrologic, and age dating analysis to delineate redox processes and flow paths in the riparian zone of a glacial outwash aquifer-stream system: Water Resources Research, v. 38.

Puckett, L.J., and Hughes, W.B., 2005, Transport and fate of nitrate and pesticides: Hydrogeology and riparian zone processes: Journal of Environmental Quality, v. 34, p. 2278-2292.

Ranalli, A.J., and Macalady, D.L., 2010, The importance of the riparian zone and in-stream processes in nitrate attenuation in undisturbed and agricultural watersheds – A review of the scientific literature: Journal of Hydrology, v. 389, p. 406-415.

Schlesinger, W.H., Reckhow, K.H., and Bernhardt, E.S., 2006, Global change: The nitrogen cycle and rivers: Water Resources Research, v. 42.

Shope, C.L., Constantz, J.E., Cooper, C.A., Reeves, D.M., Pohll, G., and McKay, W.A., 2012, Influence of a large fluvial island, streambed, and stream bank on surface water-groundwater fluxes and water table dynamics: Water Resources Research, v. 48.

Smith, M.S., and Tiedje, J.M., 1979, The Effect of Roots on Soil Denitrification: Soil Science Society of America Journal, v. 43, p. 951-955.

Smith, M.S., Firestone, M.K., and Tiedje, J.M., 1978, The acetylene inhibition method for short-term measurement of soil denitrification and its evaluation using ^{15}N: Soil Science Society of America Journal, v. 42, p. 611-615.

Smith, R.L., Howes, B.L., and Duff, J.H., 1991, Denitrification in nitrate-contaminated groundwater: Occurrence in steep vertical geochemical gradients: Geochimica et Cosmochimica Acta, v. 55, p. 1815-1825.

Starr, R.C., and Gillham, R.W., 1993, Denitrification and organic carbon availability in two aquifers: Ground Water, v. 31, p. 934-947.

Tarkalson, D.D., Payero, J., Ensley, S.M., and Shapiro, C.A., 2006, Nitrate accumulation and movement under deficit irrigation in soil receiving cattle manure and commercial fertilizer: Agronomy & Horticulture--Faculty Publications, Paper 341.

Tesoriero, A.J., and Puckett, L.J., 2011, O_2 reduction and denitrification rates in shallow aquifers: Water Resources Research, v. 47.

Wilson, G.B., Andrews, J.N., and Bath, A.H., 1994, The nitrogen isotope composition of groundwater nitrates from the East Midlands Triassic sandstone aquifer, England: Journal of Hydrology, v. 157, p. 35-46.

Wilson, G.B., Andrews, J.N., and Bath, A.H., 1990, Dissolved-gas evidence for denitrification in the Lincolnshire Limestone groundwaters, eastern England: Journal of Hydrology, v. 113, p. 51-60.

Woodbury, B.L., Miller, D.N., Nienaber, J.A., and Eigenberg, R.A., 2001, Seasonal and spatial variations of denitrifying enzyme activity in feedlot soil: American Society of Agricultural Engineers, v. 44, p. 1635-1642.

Yoshinari, T., and Knowles, R., 1976, Acetylene inhibition of nitrous oxide reduction by denitrifying bacteria: Biochemical and Biophysical Research Communications, v. 69, p. 705-710.

Zarnetske, J.P., Haggerty, R., Wondzell, S.M., and Baker, M.A., 2011, Dynamics of nitrate production and removal as a function of residence time in the hyporheic zone: Journal of Geophysical Research: Biogeosciences, v. 116.

Chapter 3

Temperature-induced Hydrochemical Evolution of Shallow Groundwater Beneath a Transient Parafluvial Zone

1.0 INTRODUCTION

Dissolved inorganic carbon (DIC) in groundwater is a poorly constrained though potentially significant component of the terrestrial carbon budget (Kessler and Harvey, 2001; Cole et al., 2007; Macpherson, 2009). Constraints on groundwater DIC are important for estimation of the carbon budgets of rivers and oceans (Raymond and Cole, 2003; Worrall and Lancaster, 2005; Jahangir et al., 2012; Kaushal et al., 2013; Lauerwald et al., 2013). Groundwater can also be an atmospheric source of carbon through groundwater CO_2 degassing at surface seeps and springs, and as a result of groundwater pumping (Richey et al., 2009). In addition to carbon budget estimation, groundwater DIC cycles are important to consider because of their influence on other water quality parameters including metals and pH (Appelo et al., 2002; Xie et al., 2012).

The degree to which environmental changes affect DIC in aquifers on a global basis is not well-constrained, although several case studies have demonstrated strong links between temperature and groundwater DIC fluctuations (Drake and Wigley, 1975; Andrews and Schlesinger, 2001; Macpherson et al., 2008; Liu et al., 2010; Yan et al., 2011). Longstanding attention has been paid to the indirect links between temperature and groundwater DIC as a result of the temperature dependence of carbonate mineral solubility and CO_2 solubility (Drake and Wigley, 1975; Yan et al., 2011). More recently, as understanding of the temperature dependence of soil respiration has grown, studies have identified potential links between the temperature, soil

gas CO_2, and groundwater DIC. For example, Macpherson et al. (2008) found a 20% increase in groundwater CO_2 over a 15-year study as a result of carbonate mineral weathering. The authors propose the forcing mechanism may be related to increased soil respiration as a result of increased atmospheric temperature. However, the low temporal resolution at which samples were collected (every 4-6 weeks) makes it difficult to discern sub-seasonal patterns in the temperature/groundwater CO_2 relationship. High-resolution sampling for similar groundwater CO_2 studies is infrequent, as illustrated by the monthly to seasonal sampling conducted in the groundwater CO_2 studies by Tsypin and Macpherson (2012) and Liu and Zhao (1999).

CO_2 in soil gas can accumulate at concentrations up to 100 times atmospheric PCO_2 (partial pressure of CO_2; Drake and Wigley, 1975; Reardon et al., 1979; Kiefer and Amey, 1992; Hendry et al., 1999; Jarvie et al., 2001; Neal et al., 2002) through the combination of root (heterotrophic) and microbial (autotrophic) respiration, together referred to as soil respiration. Soil respiration has been found to be positively related to soil temperature (Kiefer and Amey, 1992; Lloyd and Taylor, 1994; Hendry et al., 1999; Karberg et al., 2005) and soil moisture content (Kiefer and Amey, 1992; Hendry et al., 1999). Other major controls on soil respiration include organic C availability (Naganawa et al., 1989; Kirschbaum, 1995; Bond-Lamberty and Thomson, 2010), evapotranspiration, microbial population, ambient CO_2 concentration, and net primary productivity (NPP; Brooke et al., 1983; Lloyd and Taylor, 1994; Karberg et al., 2005). Henry's Law describes the dissolution of CO_2 into groundwater and the formation of H_2CO_3 (carbonic acid) as proportional to the ambient PCO_2:

$$[H_2CO_3] = K_{CO_2} * PCO_2 \tag{3.1}$$

where K_{CO2} is the temperature-dependent Henry's Law coefficient for CO_2. The dissociation of H_2CO_3 is related to the thermodynamic constant K_{a1}:

$$K_{a1} = \frac{[H^+][HCO_3^-]}{[H_2CO_3]} \tag{3.2}$$

Substituting Eqn. 3.1 into Eqn. 3.2 and solving for HCO_3^-, ambient PCO_2 is related to HCO_3^- as:

$$[HCO_3^-] = \frac{pPCO_2 * K_{CO_2} * K_{a1}}{[H^+]} \quad (3.3)$$

where K_{a1} is the temperature-dependent dissociation constant for H_2CO_3. HCO_3^- is the dominant carbonate species in water with a pH between 6.4 and 10.3.

Mineral weathering is also a source of inorganic carbon to groundwater by reaction between carbonate minerals and H_2CO_3:

$$H_2CO_3 + Ca(Mg)CO_3 \leftrightarrow Ca^{2+}(Mg^{2+}) + 2HCO_3^- \leftrightarrow Ca^{2+} + 2H^+ + 2CO_3^{2-} \quad (3.4)$$

Additional sources of CO_2 directly to groundwater include mantle degassing (Crossey et al., 2009), silicate mineral weathering, and anaerobic microbial respiration (i.e. denitrification, methanogenesis). The main sinks for inorganic carbon in groundwater include the precipitation of carbonate minerals (Eqn. 3.4), which, like carbonate mineral dissolution, is sensitive to temperature and pH, as well as degassing of CO_2-saturated groundwater upon reaching the surface.

Improved understanding of links between temperature and groundwater DIC is especially critical given the need to predict impacts of climate change, including the anticipated increase in intensity and frequency of North American heatwaves (Meehl and Tebaldi, 2004) on the carbon cycle. For example, there is ongoing debate as to whether drought and increased temperatures will increase or decrease global CO_2 sinks (Borken et al., 1999; Cornic and Fresneau, 2002; Ciais et al., 2005; Zeng and Qian, 2005; Liu et al., 2010; Zhao and Running, 2010; Medlyn, 2011). This study addresses hydrochemical trends in shallow groundwater during a period of drought-induced groundwater table decline and a concurrent seasonal temperature increase, with a focus on the carbonate system. The objective of this study was to quantify changes in shallow groundwater (upper 1 m of the water table) chemistry in the lower Platte River, Nebraska, USA, during an

extreme drought and extended high-temperature period in summer 2012. The drought and temperature increases offer a potential analog for future climate extremes.

It is hypothesized that increasing air temperature indirectly impacted shallow groundwater chemistry by increasing soil temperature and subsurface CO_2 production. To test this hypothesis, weekly shallow groundwater samples were collected at two depth intervals on a vegetated and non-vegetated fluvial island within the parafluvial zone, and temporal changes in major ions, total dissolved solids (TDS), stable isotopes of water, and water temperature were quantified. We show here that a high positive correlation between water temperature and groundwater alkalinity (approximated by HCO_3^-) exists in both islands, possibly as a result of temperature-stimulated organic matter oxidation in the soil zone.

2.0 METHODS

2.1 Study Area

Please refer to Chapter 1, Sections 1.1 and 1.2 for a detailed description of regional geology and the study site.

2.2 Experimental Infrastructure

Please refer to Chapter 1, Section 2.0 for a detailed description of the experimental setup.

2.3 Laboratory Methods

Please refer to Chapter 2, Section 2.3 for a detailed description of laboratory methods.

2.4 Modeling Procedures

The thermodynamic equilibrium model Phreeqc was used to determine carbon speciation in solution and carbonate mineral saturation indices from temperature, pH, and total alkalinity

measured in the field (Parkhurst and Appelo, 1999). Modeling details are described in section 4.3.1. Briefly, this model uses the Debye-Hückel formula and thermodynamic database Phreeqc.dat to calculate ionic activity coefficients. Charge balance was achieved by adjusting Na^+ or Cl^- concentration for each sample.

3.0 RESULTS

3.1 River and Shallow Groundwater Hydrogeology

Please refer to Chapter 1, Section 3.1 for a detailed discussion of water table dynamics. In addition, as the water table decreased, water temperature increased in all of the piezometers (Fig. 20). Throughout the study period, piezometers on the vegetated island maintained the cooler water temperatures relative to the non-vegetated island. Shallow groundwater temperatures increased in each of the piezometers steadily through much of July, after which shallow groundwater temperatures stabilized or decreased slightly. Temperatures increased in the piezometers at approximately the same rate over the summer; this maintained the same relative temperature distribution among the piezometers throughout the study period. In example, the deepest piezometer of every pair exhibited consistently cooler water temperatures relative to the shallow piezometer of the pair. The river experienced the greatest temperature increase of 12.4 °C over the summer, though there is no clear temporal trend in the river temperature measurements. Groundwater temperatures in the monitoring well increased slightly (1.2 °C). At the warmest point for shallow groundwater (July 23), the average temperature increase for all piezometers was 8.2 °C. The greatest temperature increase occurred in the non-vegetated island piezometers.

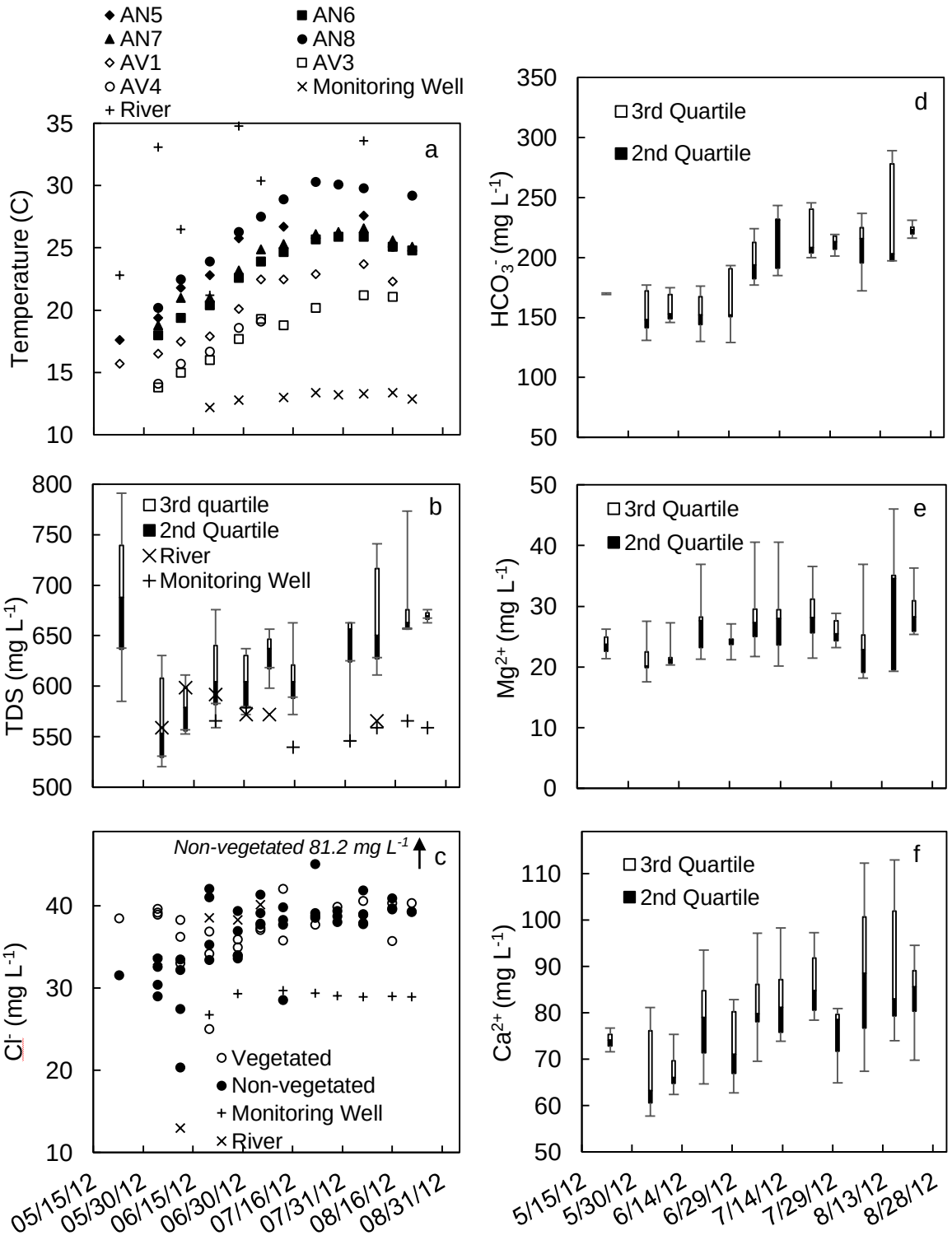
AN5
AN6
AN7
AN8
AV1
AV3
AV4
Monitoring Well
River
a
Temperature (C)
b
3rd quartile
2nd Quartile
River
Monitoring Well
TDS (mg L-1)
c
Non-vegetated 81.2 mg L-1
Vegetated
Non-vegetated
Monitoring Well
River
Cl- (mg L-1)
d
3rd Quartile
2nd Quartile
HCO3- (mg L-1)
e
Mg2+ (mg L-1)
f
Ca2+ (mg L-1)
05/15/12
05/30/12
06/15/12
06/30/12
07/16/12
07/31/12
08/16/12
08/31/12
5/15/12
5/30/12
6/14/12
6/29/12
7/14/12
7/29/12
8/13/12
8/28/12

Figure 20. Time series of water temperature and major ions. On box-and-whisker plots, the upper and lower bars represent the minimum and maximum measurement for that date. The shaded box represents the 25th to 50th percentile, hollow box represents the 50th to 75th percentile. a) Temperature increased steadily in the piezometers until mid-late July, after which it stabilized. Vegetated island shallow groundwater temperatures were relatively cooler than the non-vegetated for the entire study period. The deeper piezometers of each nest were also cooler than the shallow piezometer in the same nest. Groundwater temperatures were relatively stable throughout the study period. River water temperature fluctuated, and is likely influenced by the time of day temperature measurements were collected. b) Total dissolved solids increased over the summer in the vegetated and non-vegetated island (data shown collectively in box and whisker plots). River and monitoring well data do not show a temporal trend. c) Chloride concentration in the islands and monitoring well remained stable after an initial increase in June. d,e,f) Major carbonate system ions increased over the study period. The greatest increase was measured in HCO_3^- concentration, followed by Ca^{2+} and Mg^{2+}.

3.2 Temporal Trends in Carbonate System Major Ions

Samples from all three locations (shallow groundwater piezometers, river, deep groundwater monitoring well) exhibited Ca^{2+}-Na^+-HCO_3^- type water (see Appendix A for complete results). HCO_3^- and SO_4^{2-} dominated anion chemistry, as together the two ions contributed 84% of total anion molarity on average. Ca^{2+} and Na^+ together averaged 80% of cation molarity. Measured TDS ranged generally between 500 mg L^{-1} and 800 mg L^{-1} with a slight increasing trend over the summer (Fig. 20).

HCO_3^-, Ca^{2+}, and Mg^{2+} contributed the most to the TDS increase, as all three ions increased over the study period (Fig. 20). K^+ and Na^+ demonstrated temporal trends of a smaller scale, exhibiting a decreasing and increasing trend, respectively. HCO_3^- and Ca^{2+} also exhibited a strong correlation with temperature (Fig. 21). At the beginning of the study period, both calcite and dolomite were slightly undersaturated to nearly saturated in each of the piezometer locations. The saturation indices (SI, logarithm of the ratio between the ion activity product (IAP) and mineral solubility product (K_{sp})) for calcite and dolomite generally increased over summer, and were slightly supersaturated by the end of the study period (data not shown). Maximum calcite saturation indices ranged from 0.22 to 1.6 in the piezometers (<2 to >10 times saturation).

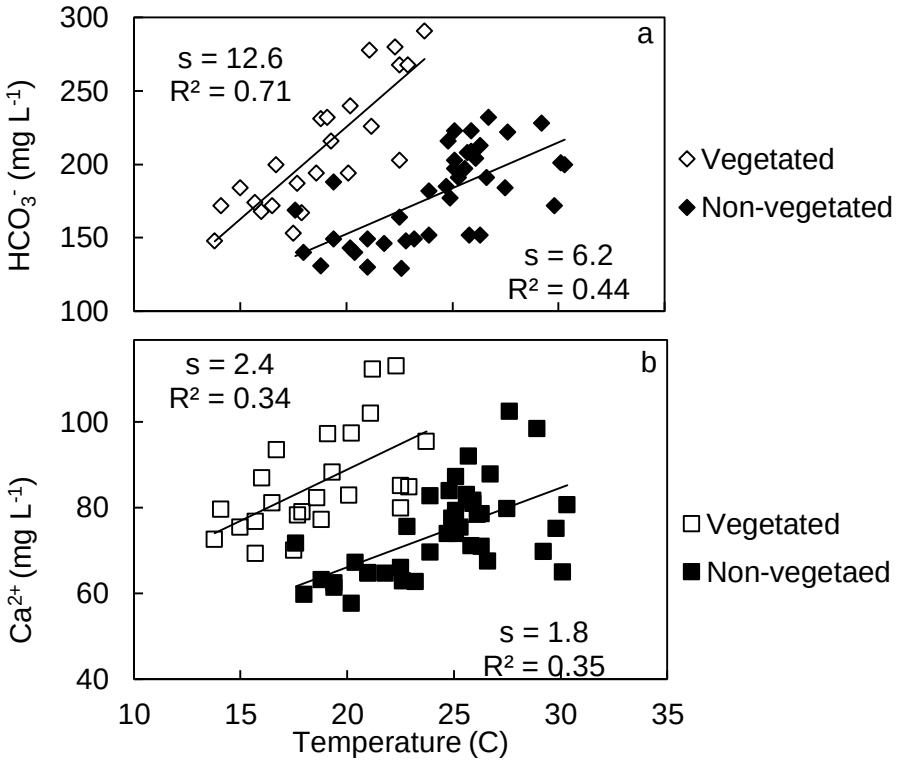

Figure 21. Both HCO_3^- and Ca^{2+} exhibit a correlation with temperature in each island. The highest slope ("s") and correlation is between HCO_3^- and temperature in the vegetated island. A one-way ANCOVA between the islands indicated the slope of this correlation is significantly different. However, outliers in the non-vegetated HCO_3^- data likely contribute to this difference. The slope of the Ca^{2+} and temperature correlation is not significant between the islands.

3.3 Shallow Groundwater Isotopic Composition

Figure 22 shows the isotopic composition of the shallow groundwater piezometers, deep groundwater monitoring well, and river. Samples collected from the river were among the heaviest, or most isotopically enriched. The deep groundwater monitoring well and select samples from the vegetated island were among the isotopically lightest samples. Linear regression indicates a slope of 6.1, which is slightly lower than the average local meteoric water line (LMWL) slope of 7.5 from two isotope measurement stations within 150 miles of the study area (Harvey and Welker, 2000; Harvey, 2001).

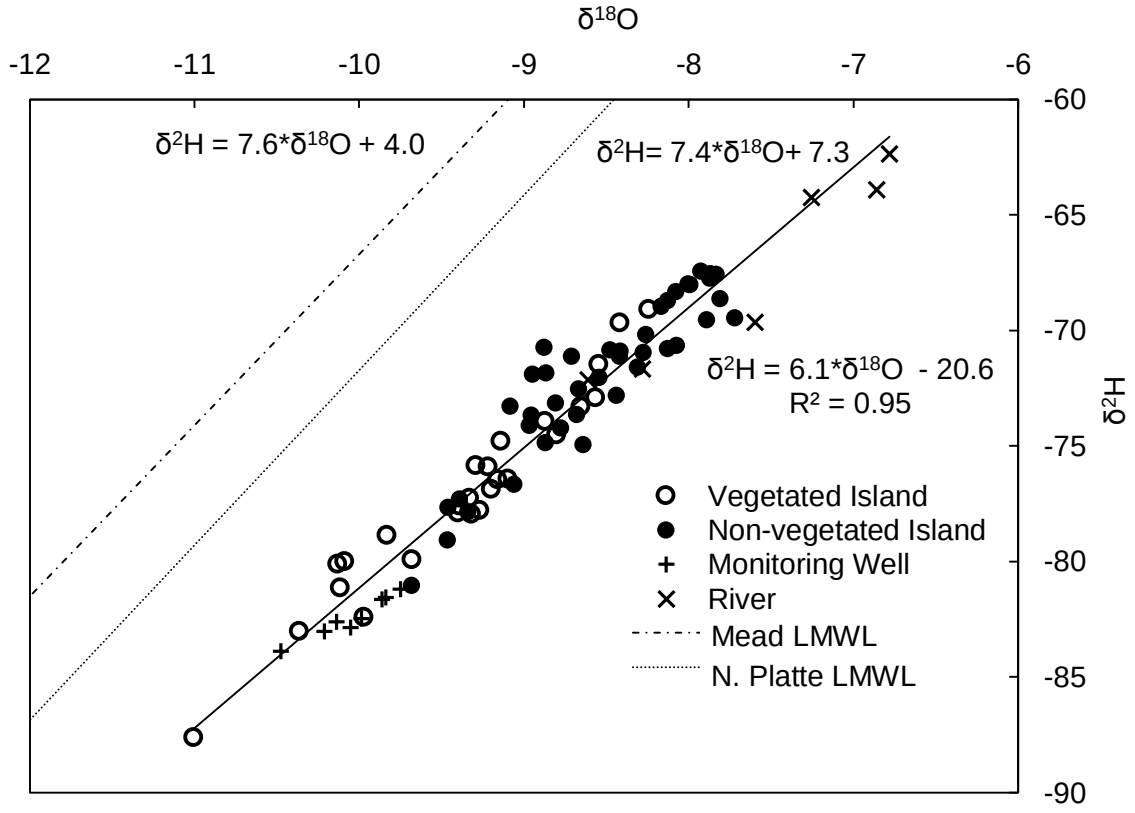

Figure 22. Stable isotopes of water for the islands, monitoring well, and river shown with the local meteoric water lines from Mead and North Platte, NE. The river water is the most isotopically enriched, while the monitoring well is generally the most depleted of all samples. Samples collected have a lower slope than the meteoric water, indicating evaporation after recharge.

4.0 DISCUSSION

Interactions between the carbonate system in shallow groundwater are complex given their sensitivity to many factors, including temperature, pH, dissolved gas concentrations, and sediment mineralogy. Furthermore, in a shallow fluvial system, all of these components can be additionally impacted by evaporation and ambient CO_2. In order to determine whether there were significant differences between the HCO_3^- or Ca^{2+} correlation with temperature between the islands, a one-way analysis of covariance (ANCOVA) was performed. The ANCOVA demonstrated that the slopes of the temperature/ HCO_3^- correlation between the vegetated and

non-vegetated islands were significantly different ($p<0.01$; Fig.21a). However, it should be noted that early-season low temperatures in the non-vegetated island are not representative of the broader temperature/HCO_3^- trend, but were included in this statistic. When these anomalous temperatures are removed from the dataset and the statistical analysis is repeated, there is no significant difference between the slopes ($p=0.05$). In addition, the difference in slope of the temperature/Ca^{2+} relationship between both islands was not significant ($p=0.49$). The ANCOVA test did demonstrate that the mean between the two islands was significantly different for both the temperature/alkalinity ($p<0.001$) and temperature/Ca^{2+} ($p<0.001$) correlations. Overall, these results indicate that the rate of change in HCO_3^- and Ca^{2+} with respect to temperature was not different between the two islands, but the absolute concentrations of both ions were significantly different over the study period.

4.1 Possible Explanations for Carbonate System Temporal Trends

4.1.1 Potential for Evaporative Concentration

One hypothesis for the observed increase in select major ions is that evaporation through the study period caused concentration of the dissolved species, a process referred to here as evapo-concentration. Stable isotopes as well as conservative tracers can be explored to determine the likelihood of evapo-concentration. Chloride is a common conservative tracer with high solubility, and temporal trends in chloride can be used to indicate evaporation from a water reservoir. Chloride data was collected from all piezometers and remained relatively stable over the entire study period (Fig. 20). This indicates that evaporation was not a cause for the increase in select ion concentrations, as chloride would demonstrate the same or greater concentration increase if evapo-concentration was occurring.

The lower slope of the stable isotope data relative to both LMWLs is an indication that the river water, shallow, and deep groundwater have been evaporated relative to precipitation.

However, this evaporation may have occurred at any time following precipitation and prior to recharge. Upstream from the study area, Bohlke et al. (2007) found the isotopic signature of the North Platte River and alluvial aquifer similarly exhibited a lower slope relative to precipitation, and interpreted this as due to evaporation from upstream reservoirs.

4.1.2 Progressive Groundwater Mixing

A second hypothesis for the TDS and alkalinity increase is mixing within the monitoring zone with groundwater that contains a higher concentration of HCO_3^- and Ca^{2+}. However, this hypothesis has several weaknesses, including the fact that only the carbonate-system major ions demonstrated temporal trends, while other major ions such as Cl^- and SO_4^- did not. In addition, the most likely means for mixing between groundwater and another geochemically distinct water would be in the hyporheic zone, as a result of groundwater mixing with river water. However, no water flowed in the channel for four weeks of the study, indicating no possible groundwater/surface water mixing at that time. In addition, vertical hydraulic gradients (Fig. 8) indicated that groundwater flow in the area contained a component of downward flow, even during the periods when water was flowing in the channel. Therefore, it seems unlikely that groundwater mixing led to the increase in TDS or alkalinity over summer 2012.

4.1.3 Increase in Soil Zone PCO_2

4.1.3.1 Geochemical Model of Soil CO_2 Impact on Shallow Groundwater Chemistry

After determining the low likelihood of evaporation or mixing as the cause for alkalinity increases in the shallow groundwater, the hypothesis that the temporal changes in major carbonate-system ion concentrations are related to the dissolution of CO_2 was tested. Thermodynamic equilibria calculations predict that as solution temperature increases, CO_2 solubility decreases, which subsequently leads to a decrease in HCO_3^- concentration (Eqn. 3.3). In

order for dissolution of CO_2 into groundwater to increase concurrently with increases in water temperature, there must be a source of CO_2 in either the saturated or unsaturated zone. We determined that the likelihood of significant CO_2 production in the saturated zone was low, given that dissolved O_2 concentrations indicated anaerobic conditions, and that concentration of the next most favorable electron acceptor—NO_3^-—was likely too low for significant organic matter oxidation to occur (Chapter 2). Therefore, our hypothesis was that CO_2 production in the soil zone impacted alkalinity at the water table and shallow groundwater.

To test this hypothesis, Phreeqc (Parkhurst and Appelo, 1999) was used to calculate the PCO_2 needed in the soil zone that, through equilibration with groundwater, would increase HCO_3^- by the amount measured in each piezometer. For the PCO_2 models, the input for each piezometer included concentrations of all major ions and pH measured in each piezometer at the beginning of the study period, as well as the temperature and calcite SI averaged from all sampling events at the piezometer. Following, 0.005 moles CO_2 were added to solution in a stepwise manner, simulating a gradual increase in PCO_2. At each step, new solution pH, ion, and CO_2 gas molarities were calculated. Also at each step, this output was used to calculate the equilibrium HCO_3^- concentration and PCO_2 in soil gas using Henry's Law and CO_2 molarity. At each incremental CO_2 addition, the process of a new output and calculated HCO_3^- and PCO_2 was repeated, until the HCO_3^- molarity of the output solution was equivalent to the HCO_3^- concentration measured at the last sampling event in each piezometer.

Henry's Law coefficients for CO_2 were calculated for each piezometer after Weiss (1974) to account for the different average temperatures measured at each piezometer. This adds some uncertainty to the model because solution temperatures were not constant throughout the summer, and the model is moderately sensitive to temperature. The model is also sensitive to calcite saturation, and saturation index specified in the model was estimated as the average saturation

index for all sampling events over the summer. Throughout the addition of CO_2 to solution, the solution pH was permitted to vary.

The results of the geochemical modeling for each piezometer are shown in Figure 23. The dashed line represents the predicted alkalinity for shallow groundwater in equilibrium with increasing soil PCO_2 and the water quality composition of samples from that piezometer at the beginning of the study. This model indicates that the measured change in alkalinity can be attributed to a reasonable increase in soil PCO_2, and that the shallow groundwater was close to being at equilibrium with increasing soil PCO_2 for most sampling events. This can possibly be attributed to the shallow water table, and subsequent rapid exchange between soil gas and the water table. Also, the range of PCO_2 needed for the given increase in HCO_3^- in each piezometer is reasonable for soil zone partial pressures (Brooke et al., 1983; Kiefer and Amey, 1992).

In order to determine the sensitivity of the model to water temperature, HCO_3^- evolution was modeled at the approximate minimum and maximum temperatures at piezometer AN8, which underwent the greatest temperature increase of 10 ºC over the 3 month period (Fig. 20). The temperature sensitivity indicated in Figure 24 is in response to the decreased solubility of calcite at higher temperatures. This figure indicates that some of the spread in the measured HCO_3^- data from off of the modeled equilibrium line may be attributable to the difference in the modeled temperature and the measured temperature at the time each sample was taken.

4.1.3.2 HCO_3^- Increase as a Result of Mineral Weathering or Carbonic Acid Dissociation

As shown in Eqns. 3.2 and 3.4, increased soil PCO_2 can lead to increased shallow groundwater alkalinity through 1) dissociation of carbonic acid, and 2) carbonate mineral weathering due to formation of carbonic acid. Major ion concentrations can be used to determine

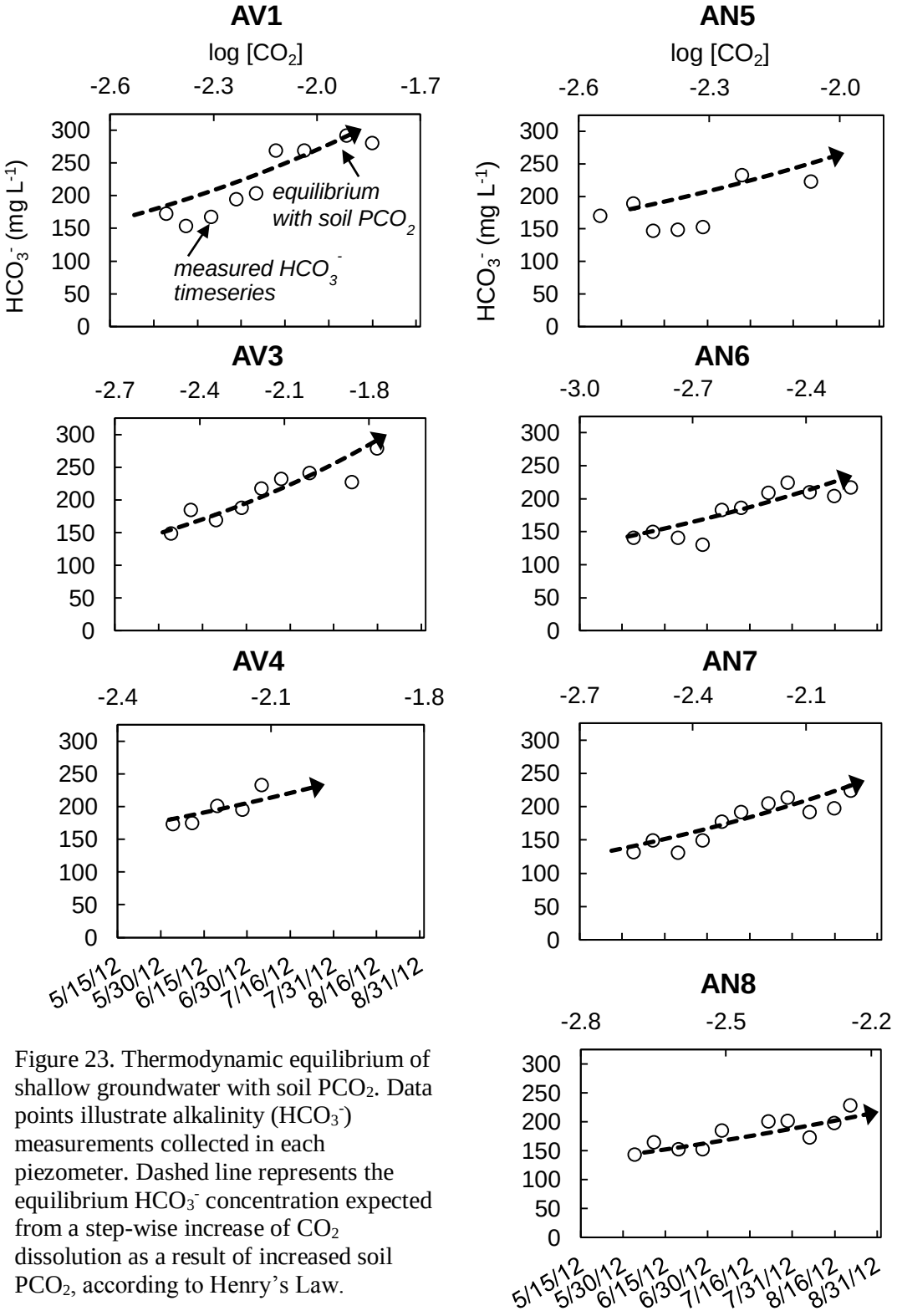

Figure 23. Thermodynamic equilibrium of shallow groundwater with soil PCO_2. Data points illustrate alkalinity (HCO_3^-) measurements collected in each piezometer. Dashed line represents the equilibrium HCO_3^- concentration expected from a step-wise increase of CO_2 dissolution as a result of increased soil PCO_2, according to Henry's Law.

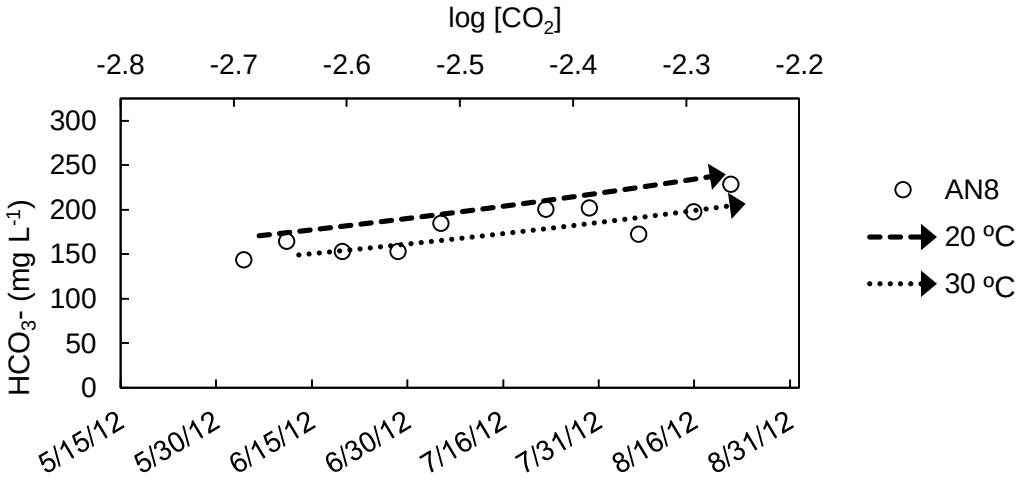

Figure 24. The equilibrium models are moderately sensitive to temperature. The difference in equilibrium CO_2 is shown here using the highest and lowest temperatures recorded in piezometer AN8, on the non-vegetated island. The difference can be attributed to lower calcite solubility at higher temperatures.

which process (or, a combination) contributed to the observed HCO_3^- increase. In pure dissociation of carbonic acid, only the concentration of HCO_3^- is expected to increase while the solution maintains a roughly neutral pH. However, through the dissolution of calcite or dolomite (Eqn. 3.4), Ca^{2+} and Mg^{2+} together increase in a 1:1 ratio with HCO_3^-. In this study, Ca^{2+} and Mg^{2+} concentrations increased slightly in most piezometers over the summer (Fig. 20), and Ca^{2+} demonstrated a weak correlation with temperature (Fig. 21b). These data, in conjunction with increasing solution saturation with respect to calcite (data not shown), suggest carbonate mineral weathering over the summer. Figure 25 shows the ratio of $Ca^{2+} + Mg^{2+}$: HCO_3^- to illustrate the relative changes in major carbonate ions. The slightly decreasing ratio of $Ca^{2+} + Mg^{2+}$: HCO_3^- over summer indicates that the increase in alkalinity only very slightly outpaced the combined increase in Ca^{2+} and Mg^{2+}. This gives evidence for a strong influence of carbonate mineral weathering on the HCO_3^- increase, with possibly a smaller influence of carbonic acid dissociation.

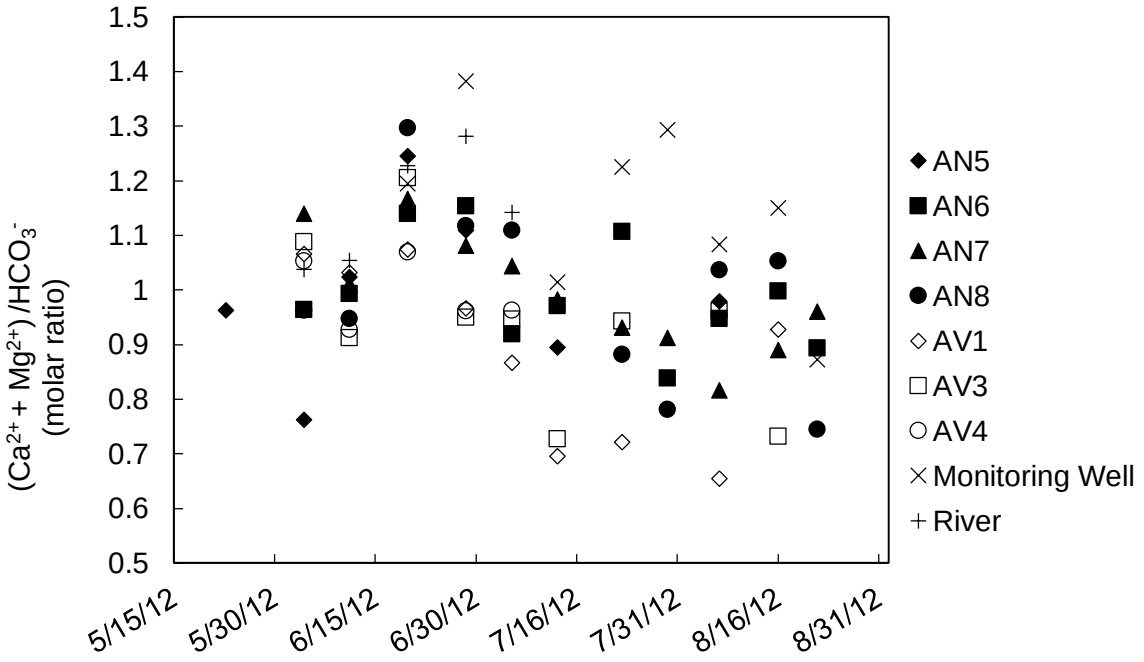

Figure 25. The molar ratio between carbonate system major cations and HCO_3^-. The slight decrease in the molar ratio suggests that Ca^{2+} and Mg^{2+} increased at a slightly higher rate than the increase in HCO_3^-, indicating that carbonate mineral weathering, rather than pure dissolution of H_2CO_3, likely contributed to the alkalinity increase over the summer.

Several other studies have found disequilibrium with respect to calcite in short residence-time flow regimes such as streams (Suarez, 1983; Tobias and Böhlke, 2011; Lauerwald et al., 2013) and long residence-time groundwater (Amrhein and Suarez, 1987; Suarez et al., 1992; Macpherson et al., 2008). Disequilibrium in these studies has been attributed to slow calcite or dolomite precipitation kinetics relative to organic matter mineralization (Reardon et al., 1979; Amrhein and Suarez, 1987), precipitation inhibition by dissolved organics or Mg^{2+} (Suarez, 1983), or a combination of both processes (Suarez et al., 1992). It is beyond the scope of this paper to determine the cause for disequilibrium with respect to calcite. However, it is plausible that the combined addition of HCO_3^- to groundwater from organic matter oxidation and mineral weathering led to supersaturated conditions at a faster rate than calcite precipitation.

4.2 Controls on Soil PCO_2

The results of the Phreeqc model support the hypothesis that increased soil PCO_2 over the summer can reasonably increase shallow groundwater alkalinity as seen in the piezometers. However, it is unclear whether temperature increase or water table decrease and drought conditions led to increased soil PCO_2. The positive correlation between bulk soil respiration and temperature is well established in the literature. However, the effects of changes in temperature, soil moisture, and ancillary soil respiration controls are interrelated and site-specific. The following discusses the general impacts of the two most significant controls to soil respiration, as well as a discussion of the difficulty in determining the relative contributions of root and microbial respiration to bulk soil respiration.

4.2.1 Temperature Effects on Soil Respiration

Soil respiration rates are positively correlated to soil temperature. Higher temperatures stimulate both primary productivity and microbial respiration, leading to increased soil respiration. However, without specifically measuring autotrophic or heterotrophic respiration, the temperature sensitivity of either cannot be assumed or determined for a given site (Kirschbaum, 2006). For example, Boone et al. (1998) concluded that autotrophic respiration combined with rhizosphere carbon oxidation, demonstrated a greater sensitivity to temperature than bulk soil. However, Kirschbaum (1995) found from a review of controlled studies of constant water content and similar substrate, that organic matter decomposition rates had a greater sensitivity than root respiration at low temperatures (<10 ºC), but that decomposition rates became similar to root respiration at higher temperatures (20-30 ºC).

4.2.2 Moisture Effects on Soil Respiration

In general, low water availability limits both primary productivity and microbial respiration. Similarly, saturation of the soil zone also inhibits microbial respiration, and has variable effects on NPP (Pumpanen et al., 2003). However, soil respiration in fine-grained soils has been found to be more sensitive to moisture content than sandy, well-drained soils (Kiefer and Amey, 1992). In addition, soil respiration in dry soils is less sensitive to temperature increases than in moist soils (Howard and Howard, 1993; Reichstein et al., 2002; Kirschbaum, 2006). Kirschbaum (1995) agreed that summer droughts will lead to a decrease in the organic decomposition contribution to soil respiration, leading to overall less soil respiration than may be predicted by temperature alone.

4.2.3 Autotrophic and Heterotrophic Contribution to Total Soil Respiration

Not only do autotrophic and heterotopic soil processes have different sensitivity to temperature, moisture, organic C availability, and ambient CO_2, but root respiration and microbial respiration seasonally may contribute a different fraction to total soil respiration. Root respiration may dominate in soils with low carbon availability or during the growing season when root density is high. Widén and Majdi (2001) and Hendry et al. (1999) found that the fraction of CO_2 produced by roots was greatest during the growing season, up to 62% and 74%, respectively. However, outside of the growing season when the root density is low, organic matter oxidation may dominate subsurface CO_2 production. Changing weather patterns or water storage may also impact the contribution of each process to total respiration. Pumpanen et al. (2003) concluded that the microbial fraction of soil respiration was impacted more by drought conditions than root respiration when each process contributes 50% of the soil carbon flux.

4.3 Mechanism for Increasing PCO_2 at Study Area

Soil respiration has been shown on many occasions to be sensitive to temperature (Andrews and Schlesinger, 2001; Karberg et al., 2005; Lauerwald et al., 2013), and has further been shown to greatly increase soil PCO_2 as well as lead to an increase in groundwater alkalinity (Appelo et al., 2002). The rate of increase in HCO_3^- as well as Ca^{2+} with temperature were similar between the islands (Fig. 21). This relationship suggests that both islands exhibited relatively the same temperature sensitivity, though the initial HCO_3^- and Ca^{2+} concentrations in the vegetated island were higher. Given that no significant root respiration likely occurred in the non-vegetated island, the similar rates between the two islands suggest that organic matter oxidation could have been the dominant mechanism for PCO_2 increase. Though increasing temperature is expected to greatly increase root respiration, (Ciais et al., 2005; Zeng and Qian, 2005), primary productivity can be expected to decline under drought conditions, thereby lowering actual root respiration rates compared to those expected purely from a temperature increase (Kirschbaum, 1995). However, without specific measurements of both heterotrophic and autotrophic respiration, it is impossible to know with certainty which process actually dominated CO_2 production in the subsurface at the study site. It is also plausible that the fraction each process contributed to total soil respiration fluctuated over the study period.

The increase in soil PCO_2 may also have been related to the declining water table. Water table decline in the study area increased the thickness of the unsaturated zone, thereby increasing the available area for aerobic microbial respiration (i.e. organic matter oxidation). Though temperature was likely the main factor in PCO_2 increase through oxidation of organic matter, it is plausible that the declining water table also led to a greater increase in soil PCO_2 than temperature alone may have caused if the water table had not declined.

5.0 CONCLUSION

Shallow groundwater (0.5-1 m) was monitored and compared to channel water and deep groundwater in a Midwestern USA parafluvial zone (Platte River, Nebraska). The monitoring period took place during the severe to extreme drought of 2012 which caused a 27-day period of no flow in the river. Piezometers slightly below the water table in one vegetated and one non-vegetated island were sampled on a weekly basis over a 3-month monitoring period. Groundwater temperatures within 1 m of the surface increased steadily for the first 8 weeks of sampling before generally stabilizing. Absolute temperatures and relative temperature increases were greatest in the non-vegetated island. Aqueous chemistry of the shallow groundwater also exhibited spatial and temporal trends. TDS increased in the shallow groundwater by approximately 20% over the 3-month period. The main contributing ions to this increase were HCO_3^- and Ca^{2+}. Stable isotopes, major ions, and thermodynamic equilibrium modeling suggested that HCO_3^- increases represented equilibration at the water table with increasing soil PCO_2, and subsequent carbonate mineral weathering due to formation of carbonic acid. These findings also support the hypothesis that the hydrochemical evolution of the shallow groundwater over the summer is in response to increased soil temperature and soil respiration in the river islands.

Numerous studies have shown that soil respiration is dominated by root (heterotrophic) respiration, and microbial (autotrophic) respiration from the decomposition of organic matter. The high correlation between temperature and HCO_3^- over the summer shows that the subsurface production of CO_2 was strongly controlled by increasing soil temperatures. However, both autotrophic and heterotrophic respiration are sensitive to temperature, as well as soil moisture and other interrelated factors. Without independent measurements of both processes, we cannot with certainty determine whether autotrophic or heterotrophic respiration had a greater contribution to overall soil respiration. However, because the rate of change in HCO_3^- and Ca^{2+} in each island is similar, it appears that both islands demonstrated approximately the same overall sensitivity of

soil respiration to temperature. It is reasonable to conclude that dry conditions hindered primary productivity in the vegetated island, such that organic matter oxidation in the non-vegetated island progressed at the same rate as organic matter oxidation, and possibly minimal root respiration, in the vegetated island.

6.0 REFERENCES

Amrhein, C., and Suarez, D.L., 1987, Calcite supersaturation in soils as a result of organic matter mineralization: Soil Science Society of America Journal, v. 51, p. 932-937.

Andrews, J.A., and Schlesinger, W.H., 2001, Soil CO_2 dynamics, acidification, and chemical weathering in a temperate forest with experimental CO_2 enrichment: Global Biogeochemical Cycles, v. 15, p. 149-162.

Appelo, C.A.J., Van Der Weide, M.J.J., Tournassat, C., and Charlet, L., 2002, Surface complexation of ferrous iron and carbonate on ferrihydrite and the mobilization of arsenic: Environmental Science and Technology, v. 36, p. 3096-3103.

Böhlke, J.K., Verstraeten, I.M., and Kraemer, T.F., 2007, Effects of surface-water irrigation on sources, fluxes, and residence times of water, nitrate, and uranium in an alluvial aquifer: Applied Geochemistry, v. 22, p. 152-174.

Bond-Lamberty, B., and Thomson, A., 2010, Temperature-associated increases in the global soil respiration record: Nature, v. 464, p. 579.

Boone, R.D., Nadelhoffer, K.J., Canary, J.D., and Kaye, J.P., 1998, Roots exert a strong influence on the temperature sensitivity of soil respiration: Nature, v. 396, p. 570-572.

Borken, W., Xu, Y.J., Brumme, R., and Lamersdorf, N., 1999, A climate change scenario for carbon dioxide and dissolved organic carbon fluxes from a temperate forest soil: Drought and rewetting effects: Soil Science Society of America Journal, v. 63, p. 1848-1855.

Brooke, G.A., Folkoff, M.E., and Box, E.O., 1983, A world model of soil carbon: Earth Surface Processes and Landforms, v. 8, p. 79-88.

Ciais, P., Reichstein, M., Viovy, N., et al., 2005, Europe-wide reduction in primary productivity caused by the heat and drought in 2003: Nature, v. 437, p. 529-533.

Cole, J.J., Prairie, Y.T., Caraco, N.F., et al., 2007, Plumbing the global carbon cycle: Integrating inland waters into the terrestrial carbon budget: Ecosystems, v. 10, p. 171-184.

Cornic, G., and Fresneau, C., 2002, Photosynthetic carbon reduction and carbon oxidation cycles are the main electron sinks for photosystem II activity during a mild drought: Annals of Botany, v. 89, p. 887-894.

Crossey, L.J., Karlstrom, K.E., Springer, A.E., Newell, D., Hilton, D.R., and Fischer, T., 2009, Degassing of mantle-derived CO_2 and He from springs in the southern Colorado Plateau region--Neotectonic connections and implications for groundwater systems: Geological Society of America Bulletin, v. 121, p. 1034-1053.

Drake, J.J., and Wigley, T.M.L., 1975, The effect of climate on the chemistry of carbonate groundwater: Water Resources Research, v. 11, p. 958-962.

Harvey, F.E., 2001, Use of NADP archive samples to determine the isotope composition of precipitation: Characterizing the meteoric input function for use in groundwater studies: Ground Water, v. 39, p. 380-390.

Harvey, F.E., and Welker, J.M., 2000, Stable isotopic composition of precipitation in the semi-arid north-central portion of the US Great Plains: Journal of Hydrology, v. 238, p. 90-109.

Hendry, M.J., Mendoza, C.A., Kirkland, R.A., and Lawrence, J.R., 1999, Quantification of transient CO_2 production in a sandy unsaturated zone: Water Resources Research, v. 35, p. 2189-2198.

Howard, D.M., and Howard, P.J.A., 1993, Relationships between CO_2 evolution, moisture-content and temperature for a range of soil types: Soil Biology & Biochemistry, v. 25, p. 1537-1546.

Jahangir, M.M.R., Johnston, P., Khalil, M.I., Hennessy, D., Humphreys, J., Fenton, O., and Richards, K.G., 2012, Groundwater: A pathway for terrestrial C and N losses and indirect greenhouse gas emissions: Agriculture, Ecosystems and Environment, v. 159, p. 40-48.

Jarvie, H.P., Neal, C., Smart, R., Owen, R., Fraser, D., Forbes, I., and Wade, A., 2001, Use of continuous water quality records for hydrograph separation and to assess short-term variability and extremes in acidity and dissolved carbon dioxide for the River Dee, Scotland: The Science of the Total Environment, v. 265, p. 85-98.

Karberg, N.J., Pregitzer, K.S., King, J.S., Friend, A.L., and Wood, J.R., 2005, Soil carbon dioxide partial pressure and dissolved inorganic carbonate chemistry under elevated carbon dioxide and ozone: Oecologia, v. 142, p. 296-306.

Kaushal, S.S., Likens, G.E., Utz, R.M., Pace, M.L., Grese, M., and Yepson, M., 2013, Increased river alkalinization in the eastern U.S.: Environmental Science and Technology, v. 47, p. 10302-10311.

Kessler, T.J., and Harvey, C.F., 2001, The global flux of carbon dioxide into groundwater: Geophysical Research Letters, v. 28, p. 279-282.

Kiefer, R.H., and Amey, R.G., 1992, Concentrations and Controls of Soil Carbon Dioxide in Sandy Soil in the North Carolina Coastal Plain: Cantena, v. 19, p.539-559.

Kirschbaum, M.U.F., 1995, The temperature dependence of soil organic matter decomposition, and the effect of global warming on soil organic C storage: Soil Biology and Biochemistry, v. 27, p. 753-760.

Kirschbaum, M.U.F., 2006, The temperature dependence of organic-matter decomposition—still a topic of debate: Soil Biology and Biochemistry, v. 38, p. 2510- 2518.

Lauerwald, R., Hartmann, J., Moosdorf, N., Kempe, S., and Raymond, P.A., 2013, What controls the spatial patterns of the riverine carbonate system? –A case study for North America: Chemical Geology, v. 337-338, p. 114-127.

Liu, Z., and Zhao, J., 1999, Contribution of carbonate rock weathering to the atmospheric CO_2 sink: Environmental Geology, v. 39, p. 1053-1058.

Liu, Z., Dreybrodt, W., and Wang, H., 2010, A new direction in effective accounting for the atmospheric CO_2 budget: Considering the combined action of carbonate dissolution, the global water cycle and photosynthetic uptake of DIC by aquatic organisms: Earth-Science Reviews, v. 99, p. 162-172.

Lloyd, J., and Taylor, J.A., 1994, On the temperature-dependence of soil respiration: Functional Ecology, v. 8, p. 315-323.

Macpherson, G.L., 2009, CO_2 distribution in groundwater and the impact of groundwater extraction on the global C cycle: Chemical Geology, v. 264, p. 328-336.

Macpherson, G.L., Roberts, J.A., Blair, J.M., Townsend, M.A., Fowle, D.A., and Beisner, K.R., 2008, Increasing shallow groundwater CO_2 and limestone weathering, Konza Prairie, USA: Geochimica et Cosmochimica Acta, v. 72, p. 5581-5599.

Medlyn, B.E., 2011, Comment on "Drought-induced reduction in global terrestrial net primary production from 2000-2009: Science, v. 333, p. 1093-d.

Meehl, G.A., and Tebaldi, C., 2004, More intense, more frequent, and longer lasting heat waves in the 21st Century: Science, v. 305, p. 994-997.

Naganawa, T., Kyuma, K., Yamaoto, H., Yamamoto, Y., Yokoi, H., and Tatsuyama, K., 1989, Measurement of soil respiration in the field: Influence of temperature, moisture level, and application of sewage sludge compost and agro-chemicals: Soil Science and Plant Nutrition, v. 35, p. 509-516.

Neal, C., Watts, C., Williams, R.J., Neal, M., Hill, L., and Wickham, H., 2002, Diurnal and longer term patterns in carbon dioxide and calcite saturation for the River Kennet, south-eastern England: The Science of the Total Environment, v. 282-283, p. 205-231.

Parkhurst, D.L., and Appelo, C.A.J., 1999, User's guide to PHREEQC (Version 2) -a computer program for speciation, batch-reaction, one-dimensional transport, and inverse geochemical calculations: Water Resources Investigations Report 99-4259, 312 p.

Pumpanen, J., Ilvesniemi, H., and Hari, P., 2003, A process-based model for predicting soil carbon dioxide efflux and concentration: Soil Science Society of America Journal, v. 67, p. 402-413.

Raymond, P.A., and Cole, J.J., 2003, Increase in the export of alkalinity from North America's Largest River: Science, v. 301, p. 88-91.

Reardon, E.J., Allison, G.B., and Fritz, P., 1979, Seasonal chemical and isotopic variations of soil CO_2 at Trout Creek, Ontario: Journal of Hydrology, v. 43, p. 335-371.

Reichstein, M., Tenhunen, J.D., Roupsard, O., et al., 2002, Severe drought effects on ecosystem CO_2 and H_2O fluxes at three Mediterranean evergreen sites: revision of current hypotheses?: Global Change Biology, v. 8, p. 999-1017.

Richey, J.E., Krusche, A.V., Johnson, M.S., da Cunha, H.B., and Ballester, M.V., 2009, The Role of Rivers in the Regional Carbon Balance: Amazonia and Global Change Geophysical Monograph Series 186, p. 489-504.

Suarez, D.L., 1983, Calcite supersaturation and precipitation kinetics in the Lower Colorado River, All-American Canal and East Highline Canal: Water Resources Research, v. 19, p. 653-661.

Suarez, D.L., Wood, J.D., and Ibrahim, I., 1992, Reevaluation of calcite supersaturation in soils: Soil Science Society of America Journal, v. 56, p. 1776-1784.

Tobias, C., and Böhlke, J.K., 2011, Biological and geochemical controls on diel dissolved inorganic carbon cycling in a low-order agricultural stream: Implications for reach scales and beyond: Chemical Geology, v. 283, p. 18-30.

Tsypin, M., and Macpherson, G.L., 2012, The effect of precipitation events on inorganic carbon in soil and shallow groundwater, Konza Prairie LTER Site, NE Kansas, USA: Applied Geochemistry, v. 27, p. 2356-2369.

Weiss, R.F., 1974, Carbon dioxide in water and seawater: the solubility of a non-ideal gas: Marine Chemistry, v. 2, p. 203-215.

Widén, B., and Majdi, H., 2001, Soil CO_2 efflux and root respiration at three sites in a mixed pine and spruce forest: seasonal and diurnal variation: Canadian Journal of Forest Research, v. 31, p. 786-796.

Worrall, F., and Lancaster, A., 2005, The release of CO_2 from riverwaters-the contribution of excess CO_2 from groundwater: Biogeochemistry, v. 76, p. 299-317.

Xie, X., Wang, Y., and Su, C., 2012, Hydrochemical and sediment biomarker evidence of the impact of organic matter biodegradation on arsenic mobilization in shallow aquifers of Datong Basin, China: Water Air and Soil Pollution, v. 223, p. 483-498.

Yan, J., Wang, Y.P., Zhou, G., Li, S., Yu, G., and Li, K., 2011, Carbon uptake by karsts in the Houzhai Basin, southwest China: Journal of Geophysical Research, v. 116, p. G04012.

Zeng, N., and Qian, H., 2005, Impact of 1998-2002 midlatitude drought and warming on terrestrial ecosystem and the global carbon cycle: Geophysical Research Letters, v. 32.

Zhao, M., and Running, S.W., 2010, Drought-induced reduction in global terrestrial net primary production from 2000 through 2009: Science, v. 329, p. 940-943.

SUMMARY AND CONCLUDING REMARKS

The objective of this study was to determine the impact of the summer 2012 drought on river and shallow groundwater chemistry and hydrogeology in the lower Platte River. Weekly water samples and sub-hourly water level data were collected. Water level data from nine river bed and fluvial island piezometers were used to develop a conceptual flow model of the study reach. This conceptual model indicated a steadily declining water table during the May through August study period, over which time the river recharged the alluvial aquifer before becoming dry in early July. In addition to the piezometers, multi-level samples were collected from a 15 m-deep borehole in the riparian zone. ^{3}H indicated that the oldest groundwater sampled, 15 m below the surface, recharged ~6 years prior to sampling, while at the water table, groundwater age is ~2 years. Vertical groundwater seepage estimates from the ^{3}H data and a modified temperature envelope method indicated the maximum component of downward flow is <10 mm d^{-1}. This is comparable to the overall water table decline measured in the piezometers, which averaged <17 mm d^{-1}.

These low-flow conditions are also hypothesized to have impacted nutrient cycling in the river bed sediments, including denitrification. Despite high (exceeding federal drinking standards) nitrate concentration in regional groundwater, all groundwater sampled during the study was well below drinking water standards. Lab microcosm experiments indicated that the island sediments have high denitrification potential, but appear to be carbon-limited, likely leading to low denitrification rates in the field. Intermediate denitrification products NO_2^- and N_2O were analyzed in the island and riparian pore water, but were below detection limits, indicating active denitrification was likely not occurring. However, $\delta Ar/N_2$ and $\delta^{15}N_2$ indicated that up to 17 mg L^{-1} NO_3-N may have been denitrified in groundwater flowing beneath the river bank, leading to excess N_2. Though the timing and location of denitrification relative to the study is unclear, it's reasonable to conclude that the low-flow conditions allowed for nearly complete denitrification of

groundwater prior to sampling at the study area. Though many studies have indicated that the hyporheic and riparian zones can be responsible for denitrification of high-nitrate groundwater, in this study it appears that groundwater denitrification occurs outside of the hyporheic and riparian zones. It is plausible that during high-flow conditions, organic carbon delivered by river water may increase in situ rates of island denitrification, assuming coincident increase in nitrate-loading to the river and shallow groundwater.

Seasonal increases in soil and shallow groundwater temperature were found to be highly correlated to groundwater DIC in both the vegetated and non-vegetated island. These increases occurred inspite of groundwater saturation with respect to carbonate minerals at the beginning of the study period. Thermodynamic equilibrium modeling indicated that groundwater DIC increases were in equilibrium with reasonable increases in soil zone PCO_2, and not likely a result of groundwater mixing or evaporative concentration. Soil zone CO_2 likely increased due to warmer temperatures stimulating organic matter oxidation rates. The declining water table also likely increased vadose zone thickness, thereby allowing for more additional aerobic respiration and CO_2 production. The DIC in groundwater has two possible sources related to increased soil CO_2: 1) Increasing PCO_2 in soil, through Henry's Law, increased HCO_3^- of ground water, and 2) the formation of carbonic acid in soil and groundwater increased weathering of carbonate minerals. Water quality data from the island pore water indicates that both of these processes likely impacted groundwater DIC, and outpaced the kinetics of carbonate mineral precipitation. This led to carbonate supersaturation by the end of the study period.

Future research may work to fill some of the data gaps identified by this study. A better understanding of the nitrate dynamics in the alluvial basin would be useful for better constraining the timing and location of denitrification relative to groundwater discharge at the river during time periods when the Platte River is gaining. It would also be informative to repeat this study during a high-flow period, to determine whether additional nitrate or carbon loading to the

surface water occurs, and if this increases denitrification rates in the island sediments. In addition, a long-term study of soil CO_2 and groundwater CO_2, including instrumentation to measure soil CO_2 concentration and possibly C-isotopes in the islands, may help to elucidate the mechanism for the increase in soil CO_2 and groundwater CO_2. High-resolution (at least weekly) sample collection of the course of a year or more may clarify whether the TDS increase measured in this study is seasonal, or more closely connected to extreme weather events, such as the 2012 drought. An annual study of riparian temperature profiles would also inform the modified temperature envelope method used in this study and help to constrain vertical groundwater flow rates.

APPENDIX A: ALL SAMPLES IONS AND STABLE ISOTOPE

Date	Piezometer	Temp (C)	O_2	TDS	pH	ORP	Alkalinity	δ^2H	$\delta^{18}O$	SO_4^-	Cl^-	Na^+	Ca^{2+}	K^+	Mg^{2+}	DOC
5/23	AN5	17.6	0.4	585	7.8	--	--	-77	-9.4	261	32	89	72	12	21	2.54
6/4	AN5	19.4	2.3	553	7.85	22	188	-71	-8.7	200	34	96	61	11	20	2.54
6/11	AN5	21.8	0	553	7.61	-53	146	-71	-8.3	202	32	84	65	12	20	--
6/20	AN5	22.8	0	624	7.59	-91	148	-70	-7.9	255	42	88	75	14	28	--
6/29	AN5	25.8	0	637	7.67	-101	152	-69	-7.8	253	39	88	71	15	24	--
7/13	AN5	26.7	0.1	663	7.53	--	232	-74	-8.7	292	29	68	88	18	29	--
8/7	AN5	27.6	--	741	7.58	66	222	-71	-8.5	298	42	81	102	14	24	--
6/4	AN6	18	0	533	7.77	45	140	-72	-8.9	226	33	75	60	11	18	2.29
6/11	AN6	19.4	0.1	553	7.68	3	149	-73	-9.1	242	27	63	62	13	21	--
6/20	AN6	20.4	0.1	559	7.69	-61	140	-69	-7.7	230	35	77	67	14	23	3.26
6/29	AN6	22.6	0.1	572	7.76	-38	129	-71	-8.1	207	34	74	63	14	21	--
7/6	AN6	23.9	0	598	7.71	-36	182	-77	-9.1	223	38	100	70	21	24	--
7/13	AN6	24.7	0.3	611	7.64	--	185	-79	-9.5	231	38	85	74	19	27	--
7/23	AN6	25.7	0.1	--	7.58	68	208	-78	-9.5	238	45	74	92	19	36	--
7/30	AN6	25.9	0.1	663	7.37	58	223	-73	-8.8	238	38	87	81	20	25	--
8/7	AN6	25.9	0.3	637	7.64	98	209	-70	-8.3	226	39	68	82	14	29	--
8/16	AN6	25.1	0	657	7.42	60	203	-69	-8.2	254	40	64	74	16	36	--
8/22	AN6	24.8	0.1	676	7.45	32	216	-68	-7.9	258	39	60	84	11	26	--
6/4	AN7	18.8	0.1	527	7.78	70	131	-72	-8.9	216	30	93	63	11	21	--
6/11	AN7	21	0	559	7.65	-21	149	-72	-8.3	233	33	74	65	13	21	--
6/20	AN7	21	0.1	559	7.71	89	130	-73	-8.7	212	33	86	65	12	21	3.48
6/29	AN7	23.2	0	579	7.68	-86	149	-74	-9.0	225	34	79	63	15	26	--
7/6	AN7	24.9	0.1	637	7.62	43	177	-81	-9.7	264	39	90	77	14	27	--
7/13	AN7	25.3	0.1	592	7.63	--	191	-75	-8.6	249	40	61	75	17	29	--
7/23	AN7	26.1	0.1	--	7.48	30	204	-75	-8.9	231	38	94	78	20	28	--
7/30	AN7	26.3	0.1	663	7.52	-25	213	-72	-8.5	234	39	68	78	12	30	--
8/7	AN7	26.6	0	624	7.61	7	191	-68	-8.0	221	39	56	67	10	21	--
8/16	AN7	25.6	0	657	7.41	-5	197	-69	-8.1	233	41	67	83	10	20	--
8/22	AN7	25.1	0.1	670	7.5	-34	223	-68	-7.9	256	81	89	87	13	32	--
6/4	AN8	20.2	0	520	7.7	-10	143	-71	-8.9	205	29	90	58	11	20	2.67
6/11	AN8	22.5	0.2	599	7.6	-35	164	-74	-9.0	244	20	83	66	13	22	--
6/20	AN8	23.9	0.1	657	7.54	-103	152	-71	-8.4	262	41	97	83	15	28	4.18
6/29	AN8	26.3	0.1	--	7.55	-78	152	-71	-8.1	241	37	90	71	14	25	--
7/6	AN8	27.5	2.2	650	7.6	-53	184	-78	-9.3	275	41	81	80	16	33	--

Date	Piezometer	Temp (C)	O_2	TDS	pH	ORP	Alkalinity	δ^2H	$\delta^{18}O$	SO_4^-	Cl^-	Na^+	Ca^{2+}	K^+	Mg^{2+}	DOC
7/13	AN8	28.9	--	585	7.96	--	--	-73	-8.4	240	38	63	98	17	31	--
7/23	AN8	30.3	--	--	7.82	99	200	-74	-8.8	223	39	81	81	14	21	--
7/30	AN8	30.1	--	650	8.02	73	201	-71	-8.4	232	39	53	65	10	23	--
8/7	AN8	29.8	--	611	7.73	85	172	-67	-7.9	221	38	70	75	10	26	--
8/16	AN8	25.1	--	663	7.69	13	197	-68	-8.1	247	40	67	79	15	35	--
8/22	AN8	29.2	--	663	8.04	60	228	-68	-7.8	249	39	63	70	11	25	--
5/23	AV1	15.7	0.4	791	7.9	96	--	-80	-9.7	250	38	76	77	12	26	2.32
6/4	AV1	16.5	0.1	631	7.67	51	172	-88	-11.0	226	39	88	81	17	24	2.32
6/11	AV1	17.5	0.6	611	7.69	103	153	-83	-10.4	267	38	83	70	11	20	--
6/20	AV1	17.9	0.1	605	7.65	-24	167	-82	-10.0	234	34	88	79	11	24	--
6/29	AV1	20.1	0.1	631	7.76	-48	194	-81	-10.1	235	34	92	83	12	25	--
7/6	AV1	22.5	0.1	611	7.69	-21	203	-75	-8.8	169	37	77	80	14	22	--
7/13	AV1	22.5	0.1	631	7.23	--	268	-73	-8.6	202	42	85	85	20	23	--
7/23	AV1	22.9	0.9	--	7.62	150	268	-73	-8.7	208	39	70	85	12	26	--
8/7	AV1	23.7	3.8	663	7.3	203	291	-71	-8.5	214	41	70	95	13	18	--
8/16	AV1	22.3	--	774	7.94	192	280	-70	-8.4	336	40	71	113	21	35	--
8/22	AV1	--	--	--	--	--	--	-69	-8.2	233	40	74	94	19	30	--
6/4	AV3	13.8	0.1	598	7.54	-113	148	-80	-10.1	218	40	83	73	14	20	3.03
6/11	AV3	15	0.2	579	7.62	-102	184	-77	-9.3	230	36	91	75	7.7	21	--
6/20	AV3	16	0.2	605	7.53	-120	168	-79	-9.8	224	25	83	87	10	28	3.87
6/29	AV3	17.7	0	605	7.8	-123	187	-76	-9.1	247	35	79	78	10	23	--
7/6	AV3	19.3	0.1	637	7.88	-110	216	-78	-9.3	229	38	83	88	13	28	--
7/13	AV3	18.8	0.1	605	7.58	--	231	-77	-9.2	218	36	51	77	8	20	--
7/23	AV3	20.2	--	--	7.68	79	240	-76	-9.2	278	38	68	97	18	31	--
8/7	AV3	21.2	--	735	7.68	184	226	-75	-9.1	303	38	76	112	16	18	--
8/16	AV3	21.1	--	676	7.89	192	278	-76	-9.3	243	36	69	102	13	19	--
6/4	AV4	14.1	0	618	7.41	-127	172	-78	-9.4	249	39	92	80	7.3	24	3.05
6/11	AV4	15.7	0.1	598	7.45	-119	174	-80	-10.1	261	33	79	69	8.6	22	--
6/20	AV4	16.7	0.1	676	7.27	-131	200	-78	-9.4	237	37	91	93	8.6	29	4.21
6/29	AV4	18.6	0.1	--	7.57	-118	194	-76	-9.2	242	36	85	82	8.3	24	--
7/6	AV4	19.1	0.1	657	7.73	-129	232	-78	-9.3	254	37	96	97	11	30	--
6/20	Gnd	12.2	0.6	566	7.52	-44	144	-84	-10.5	228	27	60	88	6.4	15	1.51
6/29	Gnd	12.8	0.2	579	7.62	-30	137	-81	-9.8	237	29	72	98	5.3	16	0.98
7/13	Gnd	13	0.3	540	7.82	--	165	-82	-9.9	229	30	42	86	3.3	15	1.94

Date	Piezometer	Temp (C)	O_2	TDS	pH	ORP	Alkalinity	δ^2H	$\delta^{18}O$	SO_4^-	Cl^-	Na^+	Ca^{2+}	K^+	Mg^{2+}	DOC
7/23	Gnd	13.4	0.3	--	8.08	-17	160	-82	-10.0	247	29	74	102	11	16	--
7/30	Gnd	13.2	0.3	546	8.21	25	144	-83	-10.1	256	29	51	97	3.8	15	--
8/7	Gnd	13.3	0.3	559	8.26	-29	168	-83	-10.1	228	29	43	92	6.1	16	--
8/16	Gnd	13.4	1.6	566	7.9	-49	168	-83	-10.2	231	29	50	97	6.6	18	--
8/22	Gnd	12.9	0.3	559	8.2	-35	184	-82	-9.8	228	29	40	83	3.0	14	--
5/23	River	22.8	7.2	403	8.6	75	--	--	--	--	--	--	--	--	--	--
6/4	River	33.1	13	559	8.68	102	151	-72	-8.28	217	33	75	64	17	24	3.41
6/11	River	26.5	9.5	599	8.53	162	149	-72	-8.61	280	13	85	64	17	24	--
6/20	River	21.2	9.2	592	8.4	113	143	-64	-7.25	241	39	88	70	18	27	3.8
6/29	River	34.8	8	572	8.79	41	115	-62	-6.78	230	38	85	55	15	25	--
7/6	River	30.4	9.3	572	8.56	130	133	-64	-6.86	247	40	91	59	13	25	--
8/7	River	33.6	9.6	566	8.73	89	148	-70	-7.59	225	38	84	82	11	6.8	--
9/13	River	23.4	7.4	494	8.33	7.6	--	--	--	--	--	--	--	--	--	--
9/13	PR 10	24.1	2.4	--	6.9	-44	244	-72	-7.91	525	43	107	198	20	54	--
9/13	PR 15	22.2	0.2	--	7.57	50	173	-69	-7.65	233	40	101	78	14	22	--
9/13	PR 20	19.6	0.2	--	7.91	74	183	-73	-8.57	232	40	93	86	13	20	--
9/13	PR 25*	16.5	0.3	--	7.79	59	175	-75	-9.07	228	38	96	101	5.5	17	--
9/13	PR 30	14	0.6	--	7.67	77	172	-70	-8.48	185	37	78	85	3.3	10	--
9/13	PR 35	13.3	0.2	--	7.72	91	180	-70	-8.61	209	38	100	100	4.0	11	--
9/12	PR 40	13	0.3	--	7.64	145	180	-75	-8.93	217	37	77	88	3.9	12	--
9/12	PR 45	13	0.4	--	7.7	159	184	-71	-8.46	216	36	87	104	5.2	17	--
9/12	PR 50	13	0.3	--	7.74	173	188	-66	-7.94	192	36	82	75	7.3	14	--

DATE	Piezometer	NO_3-N	NO_2^-	N_2O
5/23	AN5	0.04	n/d	--
6/4	AN5	n/d	n/d	--
6/11	AN5	n/d	n/d	--
6/20	AN5	0.04	n/d	--
6/29	AN5	n/d	n/d	n/d
7/13	AN5	0.04	--	--
8/7	AN5	0.87	n/d	--
6/4	AN6	0.14	n/d	--
6/11	AN6	--	n/d	--
6/20	AN6	n/d	n/d	--
6/29	AN6	n/d	n/d	n/d
7/6	AN6	--	n/d	n/d
7/13	AN6	n/d	n/d	--
7/23	AN6	0.15	n/d	--
7/30	AN6	n/d	--	--
8/7	AN6	n/d	n/d	--
8/16	AN6	0.32	n/d	--
8/22	AN6	n/d	n/d	--
6/4	AN7	0.60	n/d	--
6/11	AN7	n/d	n/d	--
6/20	AN7	n/d	n/d	--
6/29	AN7	n/d	n/d	n/d
7/6	AN7	n/d	n/d	n/d
7/13	AN7	0.18	n/d	--
7/23	AN7	0.05	n/d	--
7/30	AN7	n/d	--	--
8/7	AN7	n/d	n/d	--
8/16	AN7	0.06	n/d	--
8/22	AN7	0.04	n/d	--
6/4	AN8	0.08	n/d	--
6/11	AN8	n/d	n/d	--
6/20	AN8	n/d	n/d	--
6/29	AN8	n/d	n/d	n/d

7/6	AN8	--	n/d	n/d
Date	**Piezometer**	**NO_3-N**	**NO_2^-**	**N_2O**
7/13	AN8	n/d	n/d	--
7/23	AN8	0.04	n/d	--
7/30	AN8	0.06	--	--
v8/7	AN8	0.05	n/d	--
8/16	AN8	n/d	n/d	--
8/22	AN8	n/d	n/d	--
5/23	AV1	n/d	n/d	--
6/4	AV1	n/d	n/d	--
6/11	AV1	n/d	n/d	--
6/20	AV1	n/d	n/d	--
6/29	AV1	0.21	n/d	n/d
7/6	AV1	n/d	n/d	n/d
7/13	AV1	n/d	n/d	--
7/23	AV1	0.06	n/d	--
8/7	AV1	0.78	n/d	--
8/16	AV1	0.11	n/d	--
8/22	AV1	0.24	--	--
6/4	AV3	n/d	n/d	--
6/11	AV3	--	n/d	--
6/20	AV3	n/d	n/d	--
6/29	AV3	n/d	n/d	n/d
7/6	AV3	0.94	n/d	n/d
7/13	AV3	0.10	n/d	--
7/23	AV3	0.13	n/d	--
8/7	AV3	0.54	n/d	--
8/16	AV3	0.10	n/d	--
6/4	AV4	n/d	n/d	--
6/11	AV4	n/d	n/d	--
6/20	AV4	n/d	n/d	--
6/29	AV4	n/d	n/d	n/d
7/6	AV4	n/d	n/d	n/d
6/20	Gnd	n/d	n/d	--
6/29	Gnd	0.06	n/d	n/d

7/13	Gnd	n/d	n/d	--
DATE	Piezometer	NO_3-N	NO_2^-	N_2O
7/23	Gnd	0.18	n/d	--
7/30	Gnd	n/d	--	--
8/7	Gnd	n/d	n/d	--
8/16	Gnd	0.27	n/d	--
8/22	Gnd	0.06	n/d	--
5/23	River	--	n/d	--
6/4	River	0.42	n/d	--
6/11	River	0.03	n/d	--
6/20	River	0.16	n/d	--
6/29	River	--	n/d	n/d
7/6	River	n/d	n/d	n/d
8/7	River	0.05	n/d	--
9/13	PR 10	--	n/d	n/d
9/13	PR 15	0.07	n/d	n/d
9/13	PR 20	0.09	n/d	n/d
9/13	PR 25	0.30	n/d	n/d
9/13	PR 30	1.15	n/d	n/d
9/13	PR 35	1.22	n/d	n/d
9/12	PR 40	0.43	n/d	n/d
9/12	PR 45	0.32	n/d	n/d
9/12	PR 50	0.11	n/d	n/d

Units: O_2, TDS, Alkalinity, N_2O, DOC, and all ions are given in mg L^{-1}. Nitrate reported as NO_3^- concentration.
Isotopes are given in per mil (‰) ORP is given in mV
n/d indicates non-detect '- -' indicates no sample was collected

**Charge balance error of 10.4*

APPENDIX B: FIELD PHOTOS

Figure I. Photographs of the Platte River South Channel looking west near Doniphan, NE.

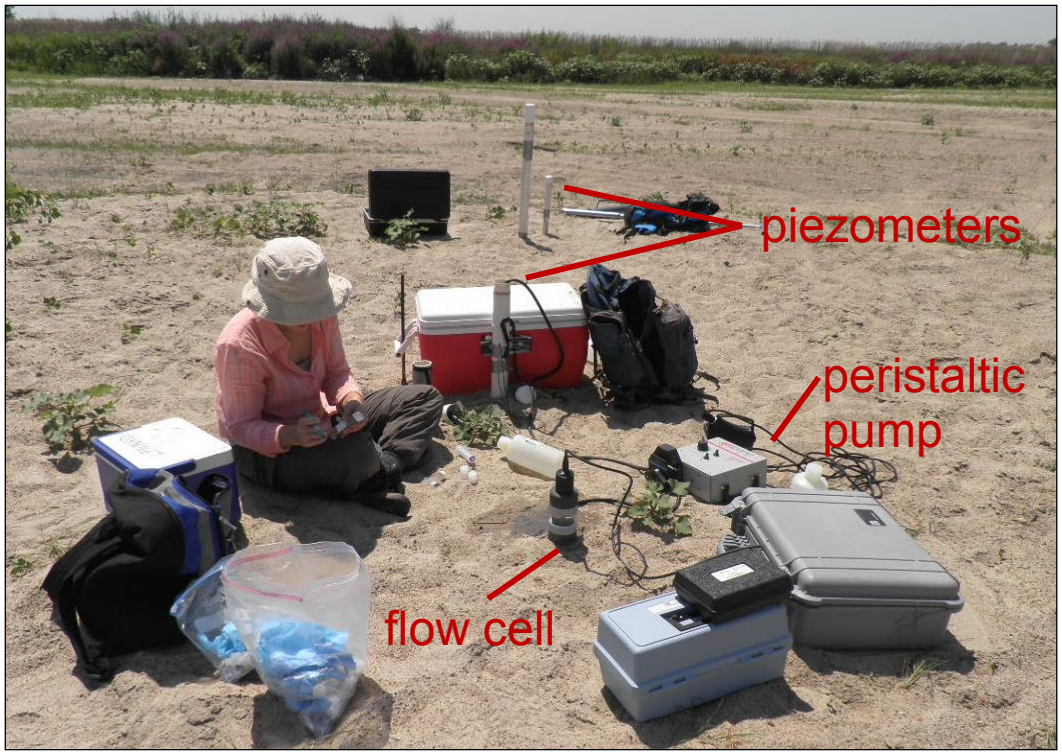

Figure II. Piezometers were constructed of 6 cm PVC and installed with a hand auger. A peristaltic pump and flow cell were used to maintain a closed sampling system.